

## EMPIR Project: '18SIB04 QuantumPascal'

**Deliverable D1:** '*Design guide for FP-based refractometry for pressure assessments with relative uncertainties of 500 ppm in the range 1 Pa - 1 kPa and 10 ppm in the range 1 kPa - 100 kPa*'

Organisation Name of Lead Partner for the Deliverable: 'UmU'

Due Date of the Deliverable: '31/08/2022'

Actual Submission Date of the Deliverable: '30/11/2022'

Update of cover page: '08/12/2022'

Acknowledgement: This project '18SIB04 QuantumPascal' has received funding from the EMPIR programme co-financed by the Participating States and from the European Union's Horizon 2020 research and innovation programme.



The EMPIR initiative is co-funded by the European Union's Horizon 2020 research and innovation programme and the EMPIR Participating States

# Fabry-Perot-cavity-based refractometry — A guide to its realization and implementation

Deliverable D1 in the EMPIR project 18SIB04, "QuantumPascal"

Tom Rubin<sup>1</sup>, Isak Silander<sup>2</sup>, Johan Zakrisson<sup>2</sup>, Clayton Forssén<sup>2,3</sup>, Martin Zelan<sup>3</sup>, André Kussicke<sup>1</sup>, Zaccaria Silvestri<sup>4</sup>, Jean-Pierre Wallerand<sup>4</sup>, Sergio Molto González<sup>5</sup>, Carmen Garcia-Izquierdo<sup>5</sup>, Janez Setina<sup>6</sup>, and Ove Axner<sup>2</sup>

<sup>1</sup>Physikalisch-Technische Bundesanstalt (PTB), Abbestr 2-12, Berlin, Germany

<sup>2</sup>Department of Physics, Umeå University, SE-901 87 Umeå, Sweden

<sup>3</sup>Measurement Science and Technology, RISE Research Institutes of Sweden, SE-501 15 Borås, Sweden

<sup>4</sup>Conservatoire national des arts et métiers (Cnam), LNE-Cnam, 61 rue du Landy, Saint-Denis, France

<sup>5</sup>Centro Español de Metrología (CEM), Tres Cantos, Spain

<sup>6</sup>Institute of Metals and Technology, Ljubljana, Slovenia

---

**Abstract** The present report constitutes the D1 report addressed to EURAMET of the first work package "Pressure measurements based on Fabry-Pérot cavity based refractometry" of the EMPIR 18SIB04 "QuantumPascal" project, titled "Towards quantum-based realisations of the pascal". Its aim is to, based on four guides, viz. those on Cavity deformation from A1.1.4, Temperature control and assessment from A1.2.3, Gas permeation from A1.3.4, and Gas modulation methodologies from A1.4.3, provide a "Design guide for FP-based refractometry for pressure assessments with relative uncertainties of 500 ppm in the range 1 Pa – 1 kPa and 10 ppm in the range 1 kPa - 100 kPa". Based on the four guides, the report adequately presents the outcome of the "QuantumPascal" project within the aforementioned areas. Significant progress has been achieved within all of these areas. Regarding cavity deformation, a novel methodology for assessment of the cavity deformation that, for the case when pure gases are used, can provide such an accurate assessment that the deformation only contributes to the uncertainty in the assessment of pressure down on the 1 - 2 ppm level. Several systems have been realized that can provide assessments of the gas temperature with such low uncertainty that are well below the requirement for obtaining the benchmark conditions. Studies of gas permeability have been made that clearly provide recommendations for which cavity spacer materials are suitable and which should be avoided. The Gas Modulation Refractometry (GAMOR) methodology has been further developed so as to make possible assessments of important characterization parameters with low uncertainty and to allow for the realization of refractometers with a short-term precision down to the  $10^{-8}$  level and an uncertainty close to the benchmarks. It has also allowed for the construction of a transportable system that has been used in other work packages. The guide also provides an updated theoretical model of Fabry-Pérot (FP) refractometry that includes effects of frequency shifts, mode jumps, cavity deformation, mirror penetration depth, and the Gouy phase. It also provides a set of recommendations for the realization of FP cavity based refractometry.

---

## Contents

<b>1</b>	<b>Introduction</b>	<b>6</b>
<b>2</b>	<b>Theory</b>	<b>7</b>
2.1	Assessment of refractivity	7
2.1.1	General expression for the refractivity assessed from a single FP cavity	7
2.1.1.1	Round trip resonance condition for the phase	7
2.1.1.2	Cavity mode frequencies	7
2.1.1.3	Assessment of refractivity — In the presence of mode jumps	8
2.1.1.4	For the case with nitrogen — A simplified non-recursive expression	8
2.1.1.5	A yet simpler formulation of the expression for the refractivity	9
2.1.1.6	For the case when the mirrors are not used around their center frequency	9
2.1.1.7	Physical interpretation of the refractivity-normalized relative elongation, $\varepsilon'$ — A representative of the relative influence on the assessed refractivity	9
2.1.2	Dual-FP-cavity refractometry	9
2.2	Molar Density	10
2.3	Pressure	10
2.4	Molecular Data for nitrogen	10
<b>3</b>	<b>Pressure-induced cavity deformation in Fabry-Perot refractometry</b>	<b>10</b>
3.1	Benchmarks for the cavity deformations	11
3.2	Simulations	12
3.2.1	Initial scrutiny	12
3.2.2	Basic dependencies	12
3.2.3	Net zero deformation dual FP cavity (DFPC) systems	12
3.2.4	Simulations of existing cavities	13
3.2.4.1	Simulations of closed dual FP cavity (DFPC) systems realized in Zerodur and Invar spacers at UmU and RISE	13
3.2.4.1.1	A closed DFPC system realized in a Zerodur spacer at UmU	13
3.2.4.1.2	Closed DFPC systems realized in Invar spacers at UmU and RISE	13
3.2.4.2	Simulation of a closed single FPC system realized in a Zerodur spacer at PTB	14
3.2.4.3	Simulations of a multi-cavity system based on sapphire components at PTB	14
3.2.4.4	Simulation of an open single FPC system realized in a Zerodur spacer at CNAM	15
3.2.4.5	Simulation of a single FPC system at CEM	15
3.2.5	Conclusive remarks regarding deformations assessed by simulations	16
3.2.5.1	Deformations assessed by simulations	16
3.2.5.2	Uncertainties in the simulated amounts of distortions	17
3.3	Experimental characterizations	17
3.3.1	Experimentally assessed deformation of the Invar-based DFPC refractometers at UmU and RISE	17
3.3.1.1	Development of a novel robust and disturbance-resistant methodology for assessment of cavity deformation	17
3.3.1.2	Assessment of the pressure-induced deformation of the stationary Invar-based DFPC cavity (the SOP) at UmU	18
3.3.1.3	Assessment of the pressure-induced deformation of the transportable Invar-based DFPC cavity (the TOP) at RISE	18
3.3.2	Experimentally assessed deformation of the Zerodur-based single FP-cavity refractometer at PTB	19

3.3.3	Experimentally assessed deformation of the new Zerodur-based single FP-cavity refractometer at CNAM . . . . .	19
3.3.4	Experimentally assessed deformation of the single FPC system realized at CEM . . . . .	19
<b>4</b>	<b>Temperature control and assessment</b>	<b>20</b>
4.1	Design and realization of FPC-based refractometer systems that can provide highly stable and homogeneous temperature conditions . . . . .	20
4.1.1	Design and construction of FPC-based refractometry systems that can provide highly stable and homogeneous temperature conditions . . . . .	20
4.1.1.1	Systems constructed by UmU and RISE . . . . .	20
4.1.1.1.1	The first system . . . . .	20
4.1.1.1.2	The second system . . . . .	21
4.1.1.1.3	The third system . . . . .	21
4.1.1.2	System constructed by PTB . . . . .	21
4.1.1.3	System constructed by CNAM . . . . .	22
4.1.1.4	System constructed by CEM . . . . .	23
4.1.2	Scrutiny of the thermodynamic effects that originate from the filling and evacuation of gas (so called <b>pV</b> -work) in FPC-based refractometers . . . . .	24
4.1.2.1	Scrutiny of the thermodynamic effects that originate from <b>pV</b> -work in an Invar-based DFPC refractometer using the GAMOR methodology . . . . .	24
4.1.2.1.1	Studies of gas dynamic behaviors . . . . .	24
4.1.2.1.2	Studies of transfer of heat in the system . . . . .	24
4.1.2.1.3	Estimates of upper limits . . . . .	25
4.1.2.1.4	Experimental verification of predicted thermodynamic properties . . . . .	25
4.1.2.1.5	Long term effects . . . . .	25
4.1.2.1.6	Conclusions . . . . .	26
4.1.2.2	Scrutiny of the thermodynamic effects that originate from the filling and evacuation of gas in a Zerodur-based FPC refractometer . . . . .	26
4.2	Development, implementation, and investigation of various methods for temperature assessment of FPC-based refractometry system . . . . .	26
4.2.1	Systems constructed by UmU and RISE . . . . .	26
4.2.1.1	The first system . . . . .	26
4.2.1.2	The second system . . . . .	26
4.2.1.3	The third system . . . . .	27
4.2.2	System constructed by PTB . . . . .	27
4.2.3	System constructed by CNAM . . . . .	28
4.2.4	System constructed by CEM . . . . .	28
<b>5</b>	<b>Permeation of gas into various cavity spacer material</b>	<b>29</b>
5.1	Introduction . . . . .	29
5.2	Approach . . . . .	29
5.3	Experimental assessments and conclusions . . . . .	29
<b>6</b>	<b>Scrutiny and implementation of gas modulation in FPC-based refractometry (GAMOR)</b>	<b>29</b>
6.1	Commonly occurring limitations of refractometry - Disturbances . . . . .	29
6.1.1	Conventional means to reduce the influence of disturbances in refractometry . . . . .	30
6.1.2	A novel means to reduce the influence of disturbances — Gas Modulation Refractometry (GAMOR) . . . . .	31
6.2	Content of the present section . . . . .	31

6.3	Procedure for autonomous assessment of refractivity from assessed shifts in laser frequencies and mode jumps by use of the GAMOR methodology . . . . .	32
6.4	Theoretical analysis and explication of the ability of the GAMOR methodology to mitigate the influence of disturbances . . . . .	33
6.4.1	Ability of the GAMOR methodology to mitigate the influence of fluctuations . . . . .	33
6.4.2	Ability of the GAMOR methodology to mitigate the influence of drifts . . . . .	35
6.4.2.1	Qualitative description . . . . .	36
6.4.2.2	Quantitative analysis . . . . .	37
6.5	A note on the uncertainty in assessments of refractivity . . . . .	38
6.6	Experimental Setup . . . . .	38
6.6.1	GAMOR instrumentation - General realization . . . . .	38
6.6.2	The Invar-based DFPC system . . . . .	39
6.6.2.1	Advantages of constructing a FPC system made of Invar . . . . .	39
6.6.2.2	The refractometry system . . . . .	40
6.6.2.3	The gas handling system . . . . .	41
6.7	A cycle-resolved illustration of the operation and performance of the GAMOR methodology . .	41
6.8	Achievements of GAMOR . . . . .	43
6.8.1	Experimental verification of the predicted abilities of the GAMOR methodology to mitigate the influence of disturbances . . . . .	43
6.8.1.1	Verification of the predicted ability of GAMOR to reduce the influence of fluctuations . . . . .	43
6.8.1.2	Verification of the predicted ability of GAMOR to reduce the influence of drifts . . . . .	44
6.8.2	Demonstration of the ability of the GAMOR methodology to improve on precision . . . . .	45
6.8.2.1	Ability of GAMOR to reduce the influence of drifts from a non-temperature stabilized system . . . . .	45
6.8.2.2	An alternative realization of GAMOR — Gas-equilibration GAMOR (GEq-GAMOR) . . . . .	46
6.8.2.3	Assessment of the precision of the Invar-based DFPC system utilizing the GAMOR methodology . . . . .	46
6.8.2.4	Short-term performance of two Invar-based DFPC GAMOR systems for assessment of pressure . . . . .	49
6.8.3	Demonstration of the ability of GAMOR-based refractometer systems to provide low uncertainty assessments . . . . .	49
6.8.3.1	The influence of thermodynamic effects ( $pV$ -work) on the assessments and the ability to assess gas temperature accurately . . . . .	50
6.8.3.2	Development of a Ga fixed-temperature cell for accurate assessment of temperature. . . . .	51
6.8.3.3	Development of a disturbance-resistant methodology for assessment of cavity deformation . . . . .	51
6.8.3.4	Development of a methodology for accurate in-situ assessment of the penetration depth of mirrors comprising a QWS of type H . . . . .	52
6.8.3.5	Assessment of the uncertainty of the stationary and the transportable Invar-based FPC optical Pascals — the SOP and the TOP — for assessment of pressure . . . . .	52
6.8.4	Realization of transportable refractometer systems based on the GAMOR methodology . . . . .	53
6.9	A recipe on how to construct a GAMOR-based FPC refractometry system suitable for high precision and low uncertainty assessments . . . . .	54

<b>7</b>	<b>Conclusions</b>	<b>56</b>
7.1	Pressure-induced cavity deformation in FP-based refractometry . . . . .	56
7.1.1	Deformation assessed by simulations . . . . .	56
7.1.2	Development of a novel disturbance-resistant methodology for assessment of cavity deformation . . . . .	57
7.1.3	Deformation assessed by experimental means . . . . .	57
7.2	Temperature control and assessment . . . . .	57
7.3	Permeation of gas into cavity spacer materials . . . . .	58
7.4	Gas modulation in FPC-based refractometry — the GAMOR methodology . . . . .	58
7.5	Assessment of the performance of FPC-based refractometry developed within the QuantumPascal project . . . . .	59
<b>8</b>	<b>Recommendations</b>	<b>60</b>
8.1	Pressure-induced cavity deformation in FP-based refractometry . . . . .	60
8.2	Temperature control and assessment . . . . .	60
8.3	Gas permeability . . . . .	60
8.4	Gas modulation in FPC-based refractometry — the GAMOR methodology . . . . .	61
8.5	Realization and implementation of state-of-the-art FPC-based refractometers . . . . .	61
	<b>References</b>	<b>61</b>
	<b>Appendix</b>	<b>67</b>
A.	Derivation of expressions for the refractivity in FP-based refractometry in the presence of mirrors comprising a QWS of type H and the Gouy phase . . . . .	67
A.1.	For working ranges centred on the mirror center frequency . . . . .	67
A.2.	For working ranges not centred on the mirror center frequency . . . . .	69
A.3.	Comparison with previously used nomenclature . . . . .	69
B.	Nomenclature and definitions of drifts . . . . .	71

## 1 Introduction

In the SI-system of units, the pascal is defined as the force per unit area. In practice, it is realized with mechanical devices such as piston gauges (also known as pressure balances) and liquid manometers both of which measure force per area. However, a drawback is that they suffer from practical and environmental limitations (the latter contains toxic mercury). In addition, their performance has remained essentially unchanged over the past few decades [1–6].

By the revision of the SI system in May 2019, in which the uncertainty of the Boltzmann constant was eliminated [7, 8], possibilities opened up for the realization of photon-based standards, in particular those based on refractometry. Since refractometry can be used to assess not only refractivity but also, by the use of the Lorentz-Lorenz equation and an equation of state, molar density and pressure, such techniques have the potential of replacing current mechanical standards of the unit for gas pressure, the pascal [9].

The most sensitive refractometers are based on Fabry-Perot (FP) cavities in which a laser is used to probe the frequency of a longitudinal mode [10–16]. Since frequency is the entity that can be assessed with highest accuracy in our society [17–19], FPC-based refractometry has a great potential for accurate assessment of pressure [9, 20–28].

However, even if it is simple in theory to realize FPC-based instrumentation, it is not trivial in practice to construct them and to carry out high-accuracy pressure assessments.

One reason for this is that the cavities are subjected to pressure-induced deformation when they are exposed to gas that will change their lengths. Without taking this effect into consideration properly, pressure assessments can be adversely affected, up to the permille range. It is therefore of importance to accurately assess the amount of deformation in FP-cavities used for refractometry.

Another reason is that, as the pressure of a gas depends not only on its density but also, through an equation of state, on its temperature, it is necessary to perform highly accurate assessments of the gas temperature. Hence, to be able to develop refractometry into a quantum based primary pressure standard, it is of importance to be able to accurately assess also the temperature of the gas.

Moreover, assessments can be affected by the fi-

nite permeability of gas in the cavity spacer material. If being too large, this can adversely affecting assessment, both by altering the length of the cavity and giving rise to gas impurities [29]. This implies that it is of importance to have accurate knowledge about the amount of permeability of various gases (primarily He) in various types of cavity spacer materials, so that cavities, if possible, can be constructed by low gas-permeability materials.

Finally, refractometry assessments are (both knowingly and unknowingly) affected by various types of disturbances (drifts, fluctuations, and noise). To mitigate the influence of such, the gas modulation refractometry (GAMOR) methodology has been developed. This methodology has repeatedly proven an ability to mitigate the influence of existing disturbances [26]. To be able to develop refractometry into an as highly-precise and sturdy method as possible, it is of importance to characterize the GAMOR methodology regarding its abilities and means of implementation.

The EMPIR 18SIB04 "QuantumPascal" project, titled "*Towards quantum-based realisations of the pascal*", was initiated 2019 with the overall aim to develop novel quantum-based pressure standards based on optical, microwave and dielectric methods and to assess their potential with the aim of replacing the existing mechanical based pressure standards [30]. Its first work package, WP1, has been devoted to "*Pressure measurements based on Fabry-Pérot cavity based refractometry*". The main aim of this work package has been to investigate the three most prominent factors that limit the use of FP cavity-based refractometry techniques for the assessment of gas density and pressure (cavity deformation, temperature control and assessment, and gas permeation), and the ability of one specific gas modulation methodology (GAMOR) to mitigate the influence of disturbances (drifts and fluctuations), with the goal of developing instrumentation for pressure measurement with a target relative uncertainty of 500 ppm in the 1 Pa - 1 kPa range and 10 ppm in the 1 kPa - 100 kPa range.

This guide regarding "*Fabry-Perot-cavity-based refractometry — A guide to its realization and implementation*" is based on the four guides;

- (i) "*Pressure-induced cavity deformation in Fabry-Perot refractometry assessed by the use of simulations and experimental characterizations*" [31];

- (ii) "Development of methods for control and assessment of the temperature of the gas in Fabry-Perot cavities" [32];
- (iii) "Guide: Information about permeation of gas into various cavity spacer materials" [33]; and
- (iv) "Gas modulated Fabry-Perot-cavity-based refractometry (GAMOR) — Guide to its basic features, performance, and implementation" [34],

that have been written as parts of the activities A1.1.4, A1.2.3, A1.3.4, and A1.4.3 within the tasks 1.1 ("Fabry-Perot cavity deformation"), 1.2 ("Temperature control and assessment"), 1.3 ("Gas permeation"), and 1.4 ("Gas modulation methodologies") of the first work package of the QuantumPascal project, respectively.

To provide a background to the recommendations of how to realize and implement FP-based refractometry instrumentation with performance at the, or beyond, the state of the art given at the end of this guide, the results of these four tasks are shortly summarized in the sections 3, 4, 5, and 6 of this guide, respectively.

However, before these are presented, which thus constitute the main part of this guide, a short summarizing description of how refractivity can be assessed in terms of shifts of frequencies of laser light and mode jumps, how molar density is assessed in terms of refractivity and molecular properties, and how pressure is assessed from molar density and temperature, is shortly summarized in section 2.

Finally, this guide provides the relevant conclusions from the four guides in section 7, followed by a set of recommendations for how to best pursue FP-based refractometry in section 8.

## 2 Theory

### 2.1 Assessment of refractivity

Refractivity is, in general, assessed as a change between two situations, with and without gas in a cavity (henceforth implicitly assumed to be the measurement cavity), in terms of a change in the frequency of laser light that is locked to a mode of the cavity.

### 2.1.1 General expression for the refractivity assessed from a single FP cavity

#### 2.1.1.1 Round trip resonance condition for the phase

When the penetration depth from mirrors and the Gouy phase are taken into account, the frequency of a given mode in an FP cavity can be obtained by the use of a round-trip resonance condition for the phase of the light. As is shown in Appendix A, following Koks and van Exter [35], such a condition for the  $m^{\text{th}}$   $TEM_{00}$  mode of a FP cavity with DBR mirrors can be written as

$$2k_{in}(L_0 + \delta L) + \phi_1 + \phi_2 - 2\Theta_G = 2\pi m, \quad (1)$$

where  $k_{in}$  is the wave vector of the light in the cavity,  $L_0$  the distance between the front facets of the two DBRs coatings of the mirrors when the cavity is empty,  $\delta L$  the pressure induced cavity deformation,  $\phi_1$  and  $\phi_2$  the reflection phases of the two DBR equipped mirrors,  $\Theta_G$  the (single pass) Gouy phase, and  $m$  an integer, representing the number of the longitudinal mode the laser addresses, defined by Eq. (1).<sup>1</sup>

#### 2.1.1.2 Cavity mode frequencies

As is shown in Silander et al. [38] as well as in Appendix A, for the case with mirror coatings comprising a QWS of type H, and for the case when the working ranges are centred on the mirror center frequency, the frequency of the mode of the cavity the laser addresses in the absence and in the presence of gas (when addressing the  $m_0^{\text{th}}$  and the  $m^{\text{th}}$  modes, respectively),  $\nu_0$  and  $\nu$ , can be written as

$$\nu_0 = \frac{cm_0 \left( 1 + \frac{\Theta_G}{\pi m_0} + \frac{\gamma_c}{m_0} \right)}{2(L_0 + 2L_{\tau,c})} \quad (2)$$

and

$$\nu = \frac{cm \left( 1 + \frac{\Theta_G}{\pi m} + \frac{\gamma_c}{m} \right)}{2n(L_0 + \delta L + 2L_{\tau,c})}, \quad (3)$$

<sup>1</sup>When the effect of the mirror penetration depth and the Gouy phase are neglected, as has been the case in some situations when specific features of the technique have been under scrutiny [36, 26, 27, 37], it is customary to view the resonance condition as a condition on the number of wavelengths the light experiences under a round trip, as  $2n(L_0 + \delta L) = q\lambda$ , where  $q$  is the number of wavelengths the light experiences in a round trip in the cavity.

respectively, where we have introduced  $\gamma_c$  and  $L_{\tau,c}$ , two purely material-dependent but index-of-refraction-independent parameters, which, on the mirror center frequency,  $\nu_c$ , are given by  $2\tau_c \nu_c/n$  and  $c\gamma_c/(4\nu_c)$ , respectively, where, in turn,  $\tau_c$  is the group delay (GD), which represents the time delay a narrow-band light pulse experiences upon reflection.<sup>2</sup> For the case when an ideal QWS is considered,  $\gamma_c$  is given by  $(n_H - n_L)^{-1}$  [35, 38]. It can be noticed that  $L_{\tau,c}$  represents the frequency penetration depth of a single mirror ( $2L_{\tau,c}$  thus represents the elongation of the length of the cavity experienced by the light during scans due to the penetration of light into the mirror coatings).

### 2.1.1.3 Assessment of refractivity — In the presence of mode jumps

For sufficiently large changes in pressure in the cavity, the frequency of the laser cannot follow that of a given cavity mode, whereby it needs to make a mode jump. This implies that  $m$  might differ from  $m_0$ . Denoting this difference  $\Delta m$ , and, by defining the shift in the frequency of the laser that takes place when the gas is let into the cavity,  $\Delta \nu$ , as  $\nu_0 - \nu$ , as is shown in the same Appendix as well as in Silander et al. [38], when the working range is centered on the mirror center frequency, it is possible to express, with a minimum of approximations (on the  $10^{-9}$  to low  $10^{-8}$  level), the refractivity in term of measurable quantities and material parameters as<sup>3</sup>

<sup>2</sup>Equation (3) shows that when the mirror penetration depth and the Gouy phase are neglected, as was done in some previous works in which specific features of the technique were scrutinized (as, e.g., in [26, 27, 36, 37]), it is adequate to express the frequency of the cavity mode addressed in a simpler form, viz. as

$$\nu = \frac{cq}{2n(L_0 + \delta L)}. \quad (4)$$

<sup>3</sup>Irrespective of whether refractometry is performed unmodulated or modulated, it is based on the same fundamental principle; it measures the change in refractivity with and without gas in a cavity, as a change in the frequency of laser light that is locked to a mode of the cavity. Although there are more than one description of how to relate refractivity to shifts of mode (or laser) frequencies, mode jumps, and entities such as cavity deformations and mirror penetration depths in the literature, they all provide appropriate assessments of refractivity. However, since the most recent development of refractometry includes the use of modulated methodologies, we have here chosen to provide a description that is suitable also for such methodologies.

$$n - 1 = \frac{\frac{\Delta \nu}{\nu_0} \left(1 + \frac{\Theta_G}{\pi m_0} + \frac{\gamma_c}{m_0}\right) + \frac{\Delta m}{m_0}}{1 - \frac{\Delta \nu}{\nu_0} \left(1 + \frac{\Theta_G}{\pi m_0} + \frac{\gamma_c}{m_0}\right) + \frac{\Theta_G}{\pi m_0} + n\epsilon'}, \quad (5)$$

where we have introduced  $\epsilon'$  as the refractivity-normalized relative elongation of the length of the cavity due to the presence of the gas, defined as  $\frac{\delta L}{L'} \frac{1}{n-1}$ , where  $L'$  is the length of the cavity mode addressed experienced by the light in vacuum, given by  $L_0 + 2L_{\tau,c}$ .<sup>4,5</sup>

Since the  $n\epsilon'$  product in the expression above has a weak dependence on refractivity, both through the  $n$  and the  $\epsilon'$  entities, Eq. (5) constitutes an expression that has a weak recursivity.<sup>6</sup>

### 2.1.1.4 For the case with nitrogen — A simplified non-recursive expression

However, as is shown in Silander et al. [38] as well as in Appendix A, when when nitrogen is addressed and when the relative elongation is assumed to be linear with pressure, i.e. when  $\frac{\delta L}{L'}$  can be considered to be given by  $\kappa P$  where  $\kappa$  is the pressure-

<sup>4</sup>It can be noticed that the deformation dependence of Eq. (5) agrees with that of Eq. (2) in Egan and Stone [21]; series expanding Eq. (5) in terms of the distortion ( $n\epsilon'$ ) and making use of the definition of  $\epsilon'$  gives

$$n - 1 = \frac{\frac{\Delta \nu}{\nu_0} \left(1 + \frac{\Theta_G}{\pi m_0} + \frac{\gamma_c}{m_0}\right) + \frac{\Delta m}{m_0}}{1 - \frac{\Delta \nu}{\nu_0} \left(1 + \frac{\Theta_G}{\pi m_0} + \frac{\gamma_c}{m_0}\right) + \frac{\Theta_G}{\pi m_0}} - n \frac{\delta L}{L'}. \quad (6)$$

This indicates that the  $\epsilon'$ -concept is a fully analogous alternative to the  $\frac{\delta L}{L'}$ -concept to describe the influence of cavity distortion in refractometry.

<sup>5</sup>Equation (5) shows that when the mirror penetration depth and the Gouy phase are neglected, it is adequate, as was done in some works dealing with the GAMOR methodology in which specific features of the technique were scrutinized, e.g. [36, 26, 27, 37], for the case when the gas pressure and the cavity deformation are restricted so that  $(n-1)\epsilon'$  is negligible with respect to unity, to express the refractivity as

$$n - 1 = \frac{\frac{\Delta \nu}{\nu_0} + \frac{\Delta m}{m_0}}{1 - \frac{\Delta \nu}{\nu_0} + \epsilon}, \quad (7)$$

where  $\epsilon$  is defined as  $\frac{\delta L}{L'} \frac{1}{n-1}$ .

<sup>6</sup>Although this is a recursive equation in  $n-1$ , the recursivity is, in general, very weak; the  $(n-1)\epsilon'$  term in the denominator, which is the part of the  $n\epsilon'$  term that carries the recursivity, seldom contributes to the assessed refractivity by more than a few times  $10^{-6}$  on a relative scale. This implies that it is sufficient to utilize, in Eq. (5), in a recursive manner, a first order estimate of  $n-1$  with solely one to two significant digits for the  $(n-1)\epsilon'$  term to obtain a relevant value for  $n-1$ .

normalized relative deformation [which thus is defined as  $(\Delta L/L)/P$ ] and  $P$  is the pressure of the gas, the weak  $(n-1)$ -dependencies of the  $n$  and the  $\varepsilon'$  entities cancel. In this case, Eq. (5) can be expressed in a simpler manner, without any recursivity, as

$$n - 1 = \frac{\frac{\Delta \nu}{\nu_0} \left(1 + \frac{\Theta_G}{\pi m_0} + \frac{\gamma_c}{m_0}\right) + \frac{\Delta m}{m_0}}{1 - \frac{\Delta \nu}{\nu_0} \left(1 + \frac{\Theta_G}{\pi m_0} + \frac{\gamma_c}{m_0}\right) + \frac{\Theta_G}{\pi m_0} + \varepsilon'_0}, \quad (8)$$

where  $\varepsilon'_0$  is given by  $\kappa RT \frac{2}{3A_R}$ , where  $R$ ,  $T$ , and  $A_R$  denote the ideal gas constant, the temperature, and the dynamic molar polarizability, respectively [26, 37].

### 2.1.1.5 A yet simpler formulation of the expression for the refractivity

Although Eq. (8) is fully adequate under the aforementioned conditions (i.e. when the relative elongation is linear with pressure and when nitrogen is addressed), and irrespective of whether any modulated methodology is used or not, it can, by defining an "effective" empty cavity frequency,  $\nu'_0$ , given by  $\nu_0 / (1 + \frac{\Theta_G}{\pi m_0} + \frac{\gamma_c}{m_0})$ , be written in a more succinct form, viz. as

$$n - 1 = \frac{\overline{\Delta \nu} + \overline{\Delta m}}{1 - \overline{\Delta \nu} + \frac{\Theta_G}{\pi m_0} + \varepsilon'_0}, \quad (9)$$

where  $\overline{\Delta \nu}$  is defined as  $\Delta \nu / \nu'_0$  and where  $\overline{\Delta m}$  is a short hand notation for  $\frac{\Delta m}{m_0}$ , that is more suitable when gas modulation, in which assessments often are performed in a real-time manner, is applied.<sup>7</sup>

Since this expression has much resemblance with the simpler type of expression previously used when specific features of the technique were scrutinized and when the influence of penetration depth and the Gouy phase were neglected [26, 27, 36], presented by Eq. (7) in footnote 6 above, this shows that even

<sup>7</sup>This shows that the presence of mirror penetration depth and the Gouy phase can be seen as a shift of the empty cavity laser frequency (transforming  $\nu_0$  to  $\nu'_0$ ) and that the Gouy phase additionally provides a contribution the expression for the refractivity that is similar to that of the cavity deformation [ $\varepsilon$  in Eq. (7) in footnote 6 represents  $\frac{\Theta_G}{\pi m_0} + \varepsilon'_0$  in Eq. (9)]. It also shows that the quantum number  $q$ , which, as is shown in Eq. (4) in footnote 2, commonly is used when the mirror penetration depth and the Gouy phase are neglected, is related to  $m$ , which, according to Eq. (1), is the relevant mode number in the presence of the aforementioned concepts, by  $q = m + \frac{\Theta_G}{\pi} + n\gamma_c$ .

when the penetration depth and the Gouy phase are taken into account, it is possible, with a few simple redefinitions of entities, to make use of the simpler type of expression.

### 2.1.1.6 For the case when the mirrors are not used around their center frequency

As is shown in Silander et al. [38] as well as in Appendix A, when the mirrors are not used around their center frequency, the cavity mode frequencies and refractivity given above, i.e. the Eqs. (2), (3), and (7) - (9), can be used as long as the  $L_{\tau,c}$  and  $\gamma_c$  are replaced by  $L_{\tau,s}$  and  $\gamma'_s$ , which are given in terms of  $\tau_s(n)$ , the GD at the center frequency of the light, and  $\Delta \nu_{cs}$ , which represents the frequency difference between the mirror center frequency and the center of the working range, given by  $\nu_c - \nu_s$ .

### 2.1.1.7 Physical interpretation of the refractivity-normalized relative elongation, $\varepsilon'$ — A representative of the relative influence on the assessed refractivity

It can finally be concluded that Eq. (5) shows, after a series expansion in terms of  $n\varepsilon'$ ,<sup>8</sup> that the refractivity-normalized relative elongation,  $\varepsilon'$ , is a measure of the *relative* influence of the assessed refractivity due to deformation, while Eq. (6) shows that the relative elongation,  $\Delta L/L$ , represents the corresponding *absolute* influence in refractivity. This implies that a system with an  $\varepsilon'$  of  $10^{-4}$  is influenced by deformation on the 100 ppm level.

This also implies the important fact that its uncertainty, i.e.  $\delta \varepsilon'$ , represents the relative uncertainty in the assessment of refractivity and pressure; a system with an uncertainty in  $\varepsilon'$  of  $1 \times 10^{-5}$  represents a relative uncertainty in refractivity and pressure of 10 ppm.

## 2.1.2 Dual-FP-cavity refractometry

As was alluded to above, for improved performance, refractometry is often implemented in dual-FP-cavity

<sup>8</sup>which implies that Eq. (5) can be written as

$$n - 1 = \frac{\frac{\Delta \nu}{\nu_0} \left(1 + \frac{\Theta_G}{\pi m_0} + \frac{\gamma_c}{m_0}\right) + \frac{\Delta m}{m_0}}{1 - \frac{\Delta \nu}{\nu_0} \left(1 + \frac{\Theta_G}{\pi m_0} + \frac{\gamma_c}{m_0}\right) + \frac{\Theta_G}{\pi m_0}} (1 - n\varepsilon'), \quad (10)$$

(DFPC) systems. This implies that the change in refractivity, in practice, is assessed as a shift in the beat frequency between the frequencies of two lasers, one addressing the measurement cavity, and one probing the reference cavity when gas is let into (or evacuated from) the measurement cavity [26, 37, 39–41].

In this case, each laser is locked to its own cavity. The shift in the frequency of the measurement cavity is then assessed as a shift in the beat frequency between the two laser frequencies,  $f$ , given by  $|\nu_r - \nu_m|$ , where  $\nu_r$  and  $\nu_m$  are the frequencies of the measurement and reference lasers (addressing the measurement and reference cavities), respectively. This implies that Eq. (9) can, instead of being expressed in terms of the shift of the frequency of the measurement cavity,  $\Delta\nu$ , alternatively be expressed in terms of the shift of the beat frequency,  $\Delta f$ , which is given by the difference in the beat frequencies when measurement cavity is empty and filled with gas, respectively, i.e. as  $f^{(0)} - f^{(g)}$ , and any possible change in the number of the mode addressed in the reference cavity.

## 2.2 Molar Density

For pressures up to one atmosphere, the molar density can be calculated by assessing the refractive index and using the extended Lorentz–Lorenz equation as

$$\rho = \frac{2}{3A_R}(n-1)[1 + b_{n-1}(n-1)], \quad (11)$$

where  $b_{n-1}$  is given by  $-(1 + 4B_R/A_R^2)/6$ , where, in turn,  $B_R$  is the second refractivity virial coefficient in the Lorentz–Lorenz equation [27, 36, 42].

## 2.3 Pressure

The molar density can then be used to assess, by use of an equation of state, the pressure, e.g. as

$$P = RT\rho[1 + B_\rho(T)\rho], \quad (12)$$

where  $B_\rho(T)$  is the second density virial coefficient.

For more detailed descriptions of the Lorentz–Lorenz equation and the equation of state, and, for expressions valid for higher pressures (when higher order virial coefficients need to be included), the reader is referred to the literature, e.g. [9, 22, 27, 36, 42–45].

## 2.4 Molecular Data for nitrogen

The most frequently addressed gas has so far been nitrogen. Table 1 provides information about the relevant gas constants for nitrogen,  $A_R$ ,  $b_{n-1}$ , and  $B_\rho$ , at 302.91 K and 1550.14 nm, which represent the conditions under which the most accurate assessments with the Invar-based DFPC refractometry system utilizing the GAMOR methodology described below have been performed (see below) [46]. Data for nitrogen at other temperatures and wavelengths, for higher pressures (i.e. higher order virial coefficients) for other gases are given in the literature [47].

**Table 1. Gas coefficients for N<sub>2</sub> at 302.91 K and 1550.14 nm.**

Coef.	Value (k = 2)	Reference
$A_R$	$4.396549(34) \times 10^{-6} \text{ m}^3/\text{mol}$	[45, 46]
$b_{n-1}$	$-0.195(7)$	[23, 46]
$B_\rho$	$-4.00(24) \times 10^{-6} \text{ m}^3/\text{mol}$	[45, 46]

## 3 Pressure-induced cavity deformation in Fabry-Perot refractometry

As was alluded to above, and as has been described in some detail in the guide "Pressure-induced cavity deformation in Fabry-Perot refractometry assessed by the use of simulations and experimental characterizations" [31], the first task of the first work package of the "QuantumPascal" project was devoted to "Fabry-Perot cavity deformation".

One way to assess the amount of deformation in FP-cavities used for refractometry is to use simulations, preferably using the finite element method (FEM). By simulating a cavity spacer system with a given set of geometric and material parameters, and comparing the situations with and without gas in the cavity, the pressure-induced deformation of the cavity can be estimated.

Another means to assess the amount of cavity deformation comprises experimental characterizations. Since the refractive index of helium can be calculated accurately from first principles, and its value differs from that of most other gases by almost one order of magnitude, often advocated experimental

methods for assessment of cavity deformation are based on the use of this gas.

In the simplest form, originally proposed by Stone and Stejskal [20], helium gas is addressed at a known pressure and the deformation is assessed in terms of the difference between the measured and the theoretically predicted refractivity.

An alternative means is to utilize a detection methodology in which the influence of distortion is automatically canceled. Such a technique, also originally proposed by Stone and Stejskal [20], is to utilize two gases; rather than tracking the change in refractive index as the cavity is evacuated (i.e. to a situation for which  $n = 1$ ), one should instead assess the change in refractivity when the gas addressed is replaced by helium at the same pressure.

A variation of this technique, denoted the "two-gas method", was proposed by Egan et al. [45]. In this methodology, the deformation is assessed by performing measurements of the refractivity of two gases with different (but known) refractivity at the same pressure assessed by the use of an evaluation model that does not take deformation into account [45]. Since the two measurements are affected by a common error, given by the deformation, and the ratio of the refractivity of the two gases are known, the deformation can be unequivocally deduced.

Although all these approaches look straightforward, it is far from trivial to utilize any of them if deformation is to be assessed by the accuracy that is needed to obtain low uncertainty assessments of pressure. Simulations are often limited by either the finite accuracies by which the system can be modelled or various material properties are known (or both). Regarding the experimental methods, some of them require that the empty cavity optical length has been accurately assessed while others require low uncertainty assessments of two dissimilar gases. Irrespective of which method that is used, they are all affected by (and often limited by) drifts, gas impurities, and outgassing.

There are two ways around this. One is to create FP cavities with a minimum of (or even no) deformation. The justification for this is that, the smaller the deformation is, the less relative accuracy it needs to be determined with if cavity deformation should not contribute more than a given amount to the uncertainty of an assessment of refractivity (or pressure). A disadvantage of this is that the cavities design might become complex (in some cases so com-

plex that they might not be able to be realized practically).

Another is to develop and utilize detection methodologies that are less affected by the disturbances that limit them. An advantage of this is that a larger variety of cavities can be assessed with respect to their deformation.

The main aim of this task has been to assess pressure-induced cavity deformation in various types of FP-based refractometers by the use of simulations and experimental characterizations sufficiently well so they do not significantly affect the uncertainties of pressure assessments and, if possible, to propose cavity designs that exhibit a minimum amount of deformation.

As is further discussed below, to be able to accurately characterize cavities with respect to deformation by experimental means, a novel disturbance-resistant characterization methodology that has proven to be able to assess deformation with such high accuracy that it solely marginally contribute to the uncertainty of subsequent assessments of pressures of nitrogen has been developed [46]. This has decreased the immediate need for design and construction of FP-cavities with a minimum of distortion, wherefore the work in this work package has been focused upon the characterization of existing FP-cavities with respect to pressure-induced deformation based on both FEM-based simulations and experimental characterizations.

### 3.1 Benchmarks for the cavity deformations

A necessary prerequisite for an assessment of pressure with the targeted (relative) uncertainty of 10 ppm is that also the refractivity needs to be assessed with (at least) the same (relative) uncertainty.<sup>9</sup> As was alluded to in section 2.1.1.7 above, to achieve this, the refractivity-normalized relative elongation of the cavity, i.e.  $\epsilon'$ , needs to be assessed with an (absolute) uncertainty of (at least)  $1 \times 10^{-5}$ .

As is described in some detail in the guide "*Pressure-induced cavity deformation in Fabry-Perot*"

<sup>9</sup>Note that this is not a sufficient conditions, since also entities such as the molar polarizability, the virial coefficients, and the assessment of temperature can have associated uncertainties. However, since the latter entities was not addressed in Task 1.1 of the "QuantumPascal" project, the assessment of the cavity deformations was solely focused on the requirements to reach the necessary prerequisites.

refractometry assessed by the use of simulations and experimental characterizations" [31], this corresponds, for nitrogen, to a pressure-normalized relative deformation of the cavity, i.e.  $\kappa$ , of  $2.7 \times 10^{-14} \text{ Pa}^{-1}$ .

Since these two requirements, i.e. the refractivity-normalized relative deformation,  $\epsilon'$ , of  $1 \times 10^{-5}$  and the pressure-normalized relative deformation,  $\kappa$ , of  $2.7 \times 10^{-14} \text{ Pa}^{-1}$ , represent the targeted value of the deformation assessments in this Task, they have, for simplicity, been denoted the "benchmarks".

### 3.2 Simulations

#### 3.2.1 Initial scrutiny

The initial activity within task 1.1, referred to as A.1.1.1, dealt with simulations of the pressure-induced deformation of a given FP-cavity using various versions of two types of software, COMSOL Multiphysics® and ANSYS Workbench [48]. The main aim of this activity was to certify that all partners were using adequate modeling tools in a proper manner.

It was demonstrated, by four participants of the project, that simulations of the deformation could be performed adequately by the use of dissimilar software and versions of those, with such small discrepancies that the 95% confidence interval of the simulated pressure-induced axial deformation only would contribute to a sub-ppm discrepancy in refractivity assessments of  $\text{N}_2$  [48].

#### 3.2.2 Basic dependencies

To gain a basic understanding of the concept of cavity deformation, simulations of a single closed cavity<sup>10</sup> were performed with particular regard to the dependence on three parameters, viz. the radius  $r$  of the bore of the cavity; the thickness  $d$  of the mirror substrate (which is also the sealing plate of the cavity); and the length  $L$  of the cavity.

As has been described in some detail in the guide "Pressure-induced cavity deformation in Fabry-Perot refractometry assessed by the use of simulations and experimental characterizations" [31], it was found that the deformation mainly has a quadratic dependence on the radius of the measurement cavity, a

<sup>10</sup>The concept of "closed cavity" refers to a system that solely fills the cavity with gas, not the space outside the spacer.

strong dependence on the thickness of the mirrors for mirror thickness smaller than the diameter of the cavity but a weak one for thickness larger than the bore, and, for all but the shortest cavity lengths, a proportional dependence on the length of the cavity.

For the case with mirrors pressed into the spacer material, which so far has been the case for the Invar-based system at UmU and at RISE, it was found that the deformation is virtually independent of the cavity diameter. In this case, it was the width of interaction area between the rim of the mirror and the spacer that had the strongest influence on the deformation.

#### 3.2.3 Net zero deformation dual FP cavity (DFPC) systems

UmU and PTB investigated, by use of simulations, possible means to create single FP-cavity systems with no (or a minimum of) net cavity deformation [based on a balancing of the pressures (in reality the forces) created by the gas inside and outside the cavity]. To obtain a zero net cavity deformation in DFPC systems, the simulations strove for equal pressure-induced length changes of the measuring and reference cavities. Possible means to realize such systems were identified and investigated.

The simulations indicated though that the designs become rather complex. One such example, realized in a sapphire-based system, is shown in Fig. 1.

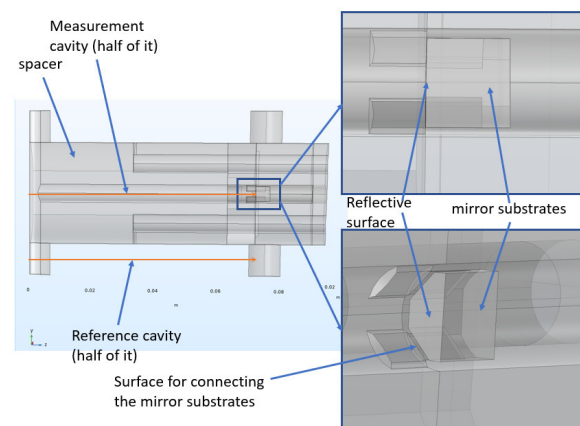


**Figure 1.** An example of a possible net zero deformation DFPC system.

It was concluded that such designs cannot be implemented at a reasonable cost due to complex struc-

tures and stringent manufacturing tolerances. Since the results of the experimental characterizations using the two-gas method (see below) were successful, the work on the zero deformation cavities was discontinued.

### 3.2.4 Simulations of existing cavities

Three partners of the QuantumPascal project, UmU, PTB, and CNAM, were then simulating different types of cavities with varying geometries made from the presently most commonly used spacer materials (Zerodur, Invar, and sapphire), representing cavity systems in which experimental characterizations were subsequently performed (or were planned to be performed). All simulations addressed the deformation caused by nitrogen gas.

#### 3.2.4.1 Simulations of closed dual FP cavity (DFPC) systems realized in Zerodur and Invar spacers at UmU and RISE

The longitudinal pressure-induced deformation of two different (existing) cavity spacer systems comprising dual Fabry-Perot cavities (DFPC) used with the GAMOR methodology were simulated by UmU with respect to the influence of some macroscopic entities of the cavity spacer block and the mirrors.<sup>11, 12</sup> One of the spacers, used in early works with the GAMOR methodology, was made of Zerodur [26, 27], while the other, which has been used in the more recent activities, was made of Invar [37–39, 49–52].

##### 3.2.4.1.1 A closed DFPC system realized in a Zerodur spacer at UmU

The two cavities in the Zerodur spacer consisted of 6.1 mm wide 190 mm long bores, separated by 50 mm. In the simulations, the mirrors were, for simplicity, assumed to be flat and mounted by optical contacting on each side of the bores. The longitudinal displacements of the center points of the mirror surfaces were assessed for each cavity separately, as well as for their difference, when the measurement cavity was exposed to a pressure of 100 kPa [53].

<sup>11</sup>Primarily the diameter of the cavities, the thickness of the mirrors, and the distance between the cavities, the latter to assess the conditions under which there is a cross-talk between the different cavities bored in the same material.

<sup>12</sup>Details of the simulations are given in the guide "Pressure-induced cavity deformation in Fabry-Perot refractometry assessed by the use of simulations and experimental characterizations" [31].

The simulations provided a net pressure-normalized relative deformation,  $\kappa$ , of  $0.76(2) \times 10^{-12} \text{ Pa}^{-1}$ , corresponding to a refractivity-normalized relative deformation,  $\varepsilon'$ , of  $2.8(1) \times 10^{-4}$ , where the uncertainty comes from the uncertainty in the material parameters, i.e. the Young's modulus and the Poisson ratio [53].

This implies that the uncertainties in the relative deformations, which for the pressure-normalized relative deformation was estimated to  $2 \times 10^{-14} \text{ Pa}^{-1}$ , are just within the required benchmark (which, for the pressure-normalized relative deformation, is  $2.7 \times 10^{-14} \text{ Pa}^{-1}$ ).

##### 3.2.4.1.2 Closed DFPC systems realized in Invar spacers at UmU and RISE

The second system characterized was a closed DFPC system made of Invar, shown in Fig. 2. This system comprises two 148 mm long and 6 mm wide cavities, separated by 25 mm. The spacer was made from an Invar rod with a diameter of 60 mm. Each cavity consists of two  $\varnothing 12.7$  mm highly reflective (99.997%) plano-concave mirrors.<sup>13</sup> Each mirror is placed in a 6 mm deep clearance hole in the spacer, drilled concentrically with the cavities. To allow for maintenance (exchange of mirrors), the mirrors were held in place by the use of O-rings, which, in turn, were pressed in by two back plates, mounted on each side of the spacer [49].

This mirror mounting differs markedly from the more commonly ones, based on optical contacting. Since the mirrors, which are curved with a radius of 500 mm, are pressed onto the Invar spacer, only their outer rim will physically be in contact with and be pressed into the spacer by the compression of the O-rings. Since the limit of plastic deformation is lower for Invar than glass, the spacer will plastically deform to form a contact area between the mirror and spacer. It was found that the width of this contact area plays the main role in how much deformation the cavity experiences.

A challenge for simulations is though that, since the contact area is small, its size and form will be affected by the roughness of the surface. This implies that it non-trivial to accurately estimate this areas by simulations.

<sup>13</sup>This reflectivity and mirror separation result in a finesse of  $10^4$  and, for the wavelength used, an FSR of 1 GHz.

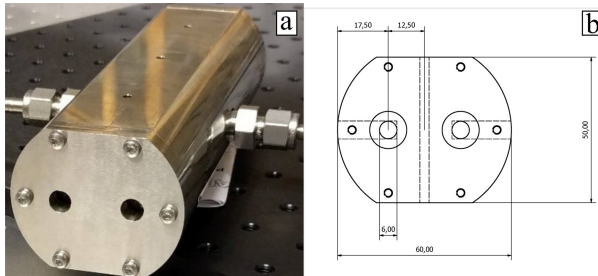


**Figure 2.** Panel (a): The Invar cavity assembly before being equipped with temperature probes and mounted inside the aluminium oven. The plates screwed into the spacer at its short ends press the mirrors, via O-rings, onto the spacer. Panel (b): A schematic drawing of the cavity assembly. Units in mm. Reproduced with permission from Ref. [52].

The simulations indicated that, for a wide (but possible) range of widths of the contact area, ranging from 2 to 8  $\mu\text{m}$ , the net pressure-normalized relative deformation of the two cavities, i.e.  $\kappa$ , range from  $7.8 \times 10^{-12} \text{ Pa}^{-1}$  to  $6.7 \times 10^{-12} \text{ Pa}^{-1}$ , which correspond to a net refractivity-normalized relative difference in length,  $\varepsilon'$ , ranging from  $2.9 \times 10^{-3}$  to  $2.5 \times 10^{-3}$ .

This implies that the uncertainty in the contact area gives rise to significant uncertainty in the simulated deformation that, for the pressure-normalized relative deformation, can be as large as  $10^{-12} \text{ Pa}^{-1}$ , which corresponds to an associated net refractivity-normalized relative deformation well into the  $10^{-4}$  range.<sup>14</sup>

Since these uncertainties are far above the benchmarks (which are  $2.7 \times 10^{-14} \text{ Pa}^{-1}$  and  $1 \times 10^{-5}$ , respectively), this indicates that it is not possible, by the use of simulations, to estimate the deformation of this system with such accuracy that it allows for assessments of pressure with the targeted uncertainty of 10 ppm. As is further discussed below, this system was therefore instead thoroughly characterized by the novel experimental characterization methodology developed.

<sup>14</sup>This argument is also strengthened by a further analysis of the simulation, which shows that almost all deformation occurs in close proximity of the contact surface [53].

### 3.2.4.2 Simulation of a closed single FPC system realized in a Zerodur spacer at PTB

PTB has simulated the pressure-induced deformation of a single closed FP cavity comprising a Zerodur-based spacer and two dichroic mirrors made from fused silica. The 3D model is based on the real system used at PTB. The spacer has a length of 100 mm, an outer diameter of 40 mm, and a cavity bore diameter of 10 mm. The mirrors, which are glued to the spacer with Torr seal®, have a diameter of 15 mm and a thickness of 6.7 mm. The outer gas pressure was set to 100 kPa while the inner gas pressure was varied between 0 Pa and 100 kPa.<sup>15</sup>

The simulations indicated that the pressure-normalized relative deformation of the Zerodur-based cavity,  $\kappa$ , is  $2.6(1) \times 10^{-12} \text{ Pa}^{-1}$ , which corresponds to a refractivity-normalized relative deformation,  $\varepsilon'$ , of  $9.6(4) \times 10^{-4}$ , where the uncertainties mainly originates from the glue.

This indicates that the uncertainties in the pressure- and refractivity-normalized relative deformations, which were estimated to  $10 \times 10^{-14} \text{ Pa}^{-1}$  and  $4 \times 10^{-5}$ , respectively, are a few times larger than the benchmarks. This implies that it is not possible to assess the deformation of this type of cavity by simulations with such a low uncertainty that it allows for an assessment of pressure of the targeted 10 ppm.

### 3.2.4.3 Simulations of a multi-cavity system based on sapphire components at PTB

PTB has also modeled a setup with one measurement cavity in the center and several reference cavities outside of the FP-spacer.<sup>16</sup> Here, the spacer, the mirror substrates, and the connectors were all made from sapphire. The outer diameter of the spacer was 37 mm and the diameter of the bore was 5.7 mm. Its length was 100 mm. The mirror substrates have a thickness of 8 mm and a diameter of 50 mm.

The simulations indicated that the net pressure-normalized relative deformation was one order of magnitude smaller than that for the Zerodur-based FP-cavity, viz.  $0.20(2) \times 10^{-12} \text{ Pa}^{-1}$ , which corre-

<sup>15</sup>Details of the simulations are given in the guide "Pressure-induced cavity deformation in Fabry-Perot refractometry assessed by the use of simulations and experimental characterizations" [31].

<sup>16</sup>As above, details of the simulations are given in the guide "Pressure-induced cavity deformation in Fabry-Perot refractometry assessed by the use of simulations and experimental characterizations" [31].

sponds to a refractivity-normalized relative deformation of  $7.4(7) \times 10^{-5}$ .

This implies that the relative uncertainties of the pressure- and refractivity-normalized relative deformations were estimated to be  $2 \times 10^{-14} \text{ Pa}^{-1}$  and  $0.7 \times 10^{-5}$ , barely within the benchmarks.

### 3.2.4.4 Simulation of an open single FPC system realized in a Zerodur spacer at CNAM

CNAM has modeled the deformation of a recently constructed open cavity bored in a Zerodur spacer with bonded silica mirrors.<sup>17</sup> The cavity system has been made from a 50 mm-squared block of Zerodur in which holes were bored according to Fig 3, viz. with two 12.5 mm diameter holes for the two mirrors, two 10 mm diameter holes for the gas filling, and two 10 mm radius holes for temperature measurements (as close as possible to the gas).

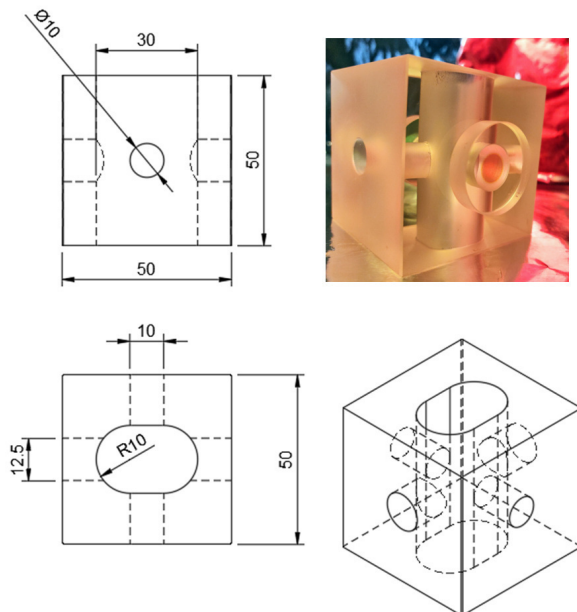


**Figure 3.** Drawing and picture of the novel CNAM FP-based cavity composed to a Zerodur 50 mm-squared spacer and two mirrors in fused silica mounted by optical contacting.

To simplify the modelling of this system, the cavity was considered to have flat mirrors mounted to

<sup>17</sup>As above, details of the simulations are given in the guide "Pressure-induced cavity deformation in Fabry-Perot refractometry assessed by the use of simulations and experimental characterizations" [31].

the cavity spacer by optical contacting. The simulations indicated that the pressure-normalized relative deformation of the novel cavity,  $\kappa$ , is  $-6.85(3) \times 10^{-12} \text{ Pa}^{-1}$ , which corresponds to a refractivity-normalized relative deformation of  $2.56(1) \times 10^{-3}$ .

This implies that the uncertainties in the pressure- and refractivity-normalized relative deformations were estimated to be  $3 \times 10^{-14} \text{ Pa}^{-1}$  and  $1.1 \times 10^{-5}$ , respectively, which are just above the corresponding  $2.7 \times 10^{-14} \text{ Pa}^{-1}$  and  $1 \times 10^{-5}$  benchmarks.

### 3.2.4.5 Simulation of a single FPC system at CEM

CEM has addressed the deformation of a single FPC system realized in Ohara's NEXCERA CD107 with mirrors made of ClearCeram-Z (CCZ) Regular.

NEXCERA™ is an ultra-low thermal expansion ceramic with a cordierite base (2MgO-2Al<sub>2</sub>O<sub>3</sub>-5SiO<sub>2</sub>). It has a number of properties that makes it appealing for FP-based refractometry.<sup>18</sup>

Initially, a study of the optimum geometry of the spacer was made and, based on that geometry, a study of different materials was made. The final design is shown in Fig 4.

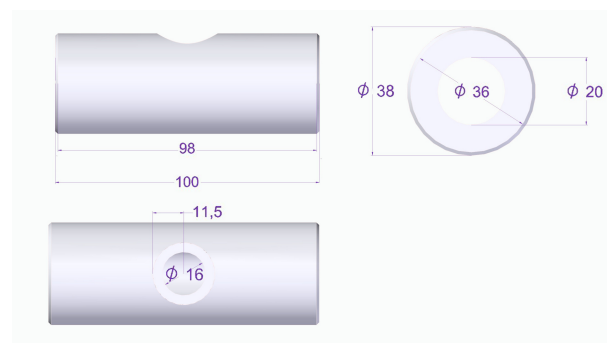


**Figure 4.** Cavity geometry of the FP system simulated by CEM. Dimensions are in mm.

The deformation simulations were made under assumption that the cavity was made by Zerodur. The results of the mirror deformation are shown in

<sup>18</sup>NEXCERA™ has a (near) zero thermal expansion coefficient at temperatures close to room temperature; a high aging and thermal stability; and a high stiffness; about 50% higher than general low thermal expansion glass. Since it is a pore-less material, it can be given a mirror finish by lapping and polishing and it can be sintered with near net shapes, enabling manufacturing of complex shapes at low cost.

Fig. 5 where R1 is mirror one and R2 is mirror 2. The light is introduced in the cavity through the R1 mirror, which implies that it needs a certain degree of transmission. The multiple reflections that take place between R2 and R1 give rise to the various cavity modes.

Figure 5 shows that although the configuration of two mirrors made of NEXCERA has the lowest deformation, it has been found that this configuration cannot be used as a FP-cavity since NEXCERA does not provide sufficient transmission of light. Under specific treatment it could be used as a highly reflective mirror but not as a FP-mirror with adequate transmission. An optimal configuration could be by making R2 of NEXCERA and R1 of another material. Figure 5 shows that the configuration with R1 made of CCZ presents a lower deformation than the other configurations [Ultra Low Expansion Glass (ULE) and Zerodur 38 mm].

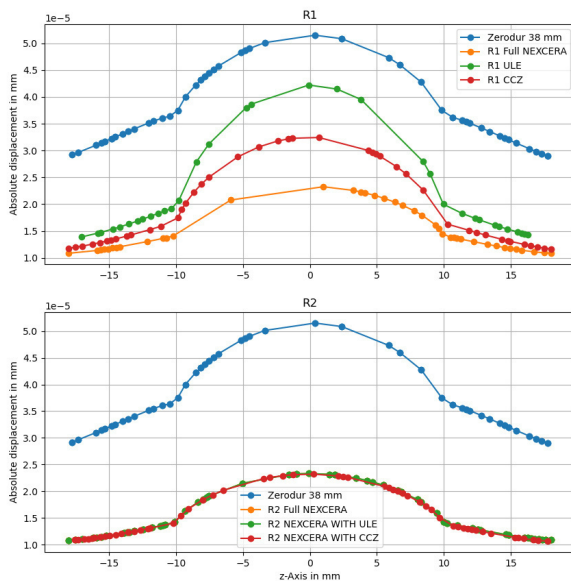


**Figure 5. Simulations by CEM of absolute mirror deformations for different mirror configurations.**

Figure 5 shows that although the configuration of two mirrors made of NEXCERA has the lowest deformation, it was found that this configuration cannot be used as a FP-cavity since NEXCERA does not provide sufficient transmission of light. Under specific treatment it could be used as a highly reflective mirror but not as a mirror with adequate transmission. An working configuration could be made through by

selecting R2 of NEXCERA and R1 made of another material. Figure 5 shows that the configuration with R1 made of CCZ presents a lower deformation than the other configurations (Ultra Low Expansion Glass (ULE) and Zerodur 38 mm).

### 3.2.5 Conclusive remarks regarding deformations assessed by simulations

#### 3.2.5.1 Deformations assessed by simulations

These simulations thus indicate that the net pressure-normalized relative deformations for the types of systems addressed ranged from  $0.20(2) \times 10^{-12} \text{ Pa}^{-1}$ , which was achieved for the closed multi-cavity system based on sapphire components at PTB,<sup>19</sup> up to  $(-6.85(3) \times 10^{-12} \text{ Pa}^{-1}$ , which was obtained for the open single FPC system realized in a Zerodur spacer at CNAM, and to values in the  $6.7 \times 10^{-12} \text{ Pa}^{-1}$  to  $7.8 \times 10^{-12} \text{ Pa}^{-1}$  range for the closed DFPC systems realized in Invar spacers at UmU and RISE. The corresponding values of the refractivity-normalized relative deformations range similarly from  $7.5 \times 10^{-5}$  to  $290 \times 10^{-5}$ . This implies that the amount of deformation of the systems addressed differ roughly by a factor of 35.

This shows that FP-systems, although being well design in many respect, still can exhibit a large variety of deformations, that in this case will contribute to the assessment of refractivity (and thereby pressure) on a level ranging from 75 ppm to 2.9 ‰.

The reason for this spread in deformation is that the systems are configured dissimilarly. The smallest deformation was obtained for the sapphire system. This originates mainly from the fact that sapphire has an exceptionally large Young's modulus. The deformation in this system was found to be about a third of a that of the DPFC Zerodur based system realized at UmU, which, in turn, was found to have about a third of the deformation of the DFPC system based on Zerodur at PTB. The reason for this was attributed to the fact that the former of these was considering a system with mirrors mounted by optical contacting, while the latter one utilized glue. The latter one was again found to have only a third

<sup>19</sup>Via  $0.76(2) \times 10^{-12} \text{ Pa}^{-1}$ , which was obtained for the closed DFPC system realized in a Zerodur spacer with mirrors mounted by optical contacting at UmU, and  $2.6(1) \times 10^{-12} \text{ Pa}^{-1}$ , which was obtained for the closed single FPC system realized in a Zerodur spacer with mirrors mounted by glue at PTB,

of the deformation of the open single cavity system based on Zerodur at CNAM. The reason for this is attributed to the fact that while the PTB system was a closed one, the CNAM system was open.<sup>20</sup>

### 3.2.5.2 Uncertainties in the simulated amounts of distortions

Although it is advisory to realize and utilize systems that have small amounts of deformation, not all systems with small deformation provide the most advantageous conditions. Those are instead produced by the systems whose deformation can be assessed with the smallest uncertainty.<sup>21</sup>

Based on the  $1 \times 10^{-5}$  benchmark for the uncertainty of  $\varepsilon'$ , it could be concluded that two of the simulations could provide deformations with uncertainties that are below this benchmark, viz. the DFPC Zerodur system at UmU and the multi-cavity sapphire system at PTB, which reported uncertainties in  $\varepsilon'$  of  $0.7 \times 10^{-5}$ , while one, the Zerodur spacer system at CNAM, provided a deformation whose uncertainty is more or less equal to the benchmarks (with an uncertainty in  $\varepsilon'$  of  $1.1 \times 10^{-5}$ ).

The simulation of the Zerodur system at PTB, which incorporated glued mirrors, provided an uncertainty that was four times above the benchmark. The reason for this was mainly attributed to glue used for the mounting of the mirrors.

The simulations for the Invar system, which suffers from a poor modelling of the mirror mounting, in turn, ended up with one order of magnitude larger uncertainty than the glued Zerodur system at PTB. This was mainly attributed to the uncertainty in the geometrical parameters of the spacer-to-mirror interface (the rim) caused by a difficulty to, in the presence of the pertinent surface roughness, sufficiently accurately model and assess the plastic deformation of the spacer material.

This implies that, although it is possible to model most types of system by the use of simulation programs, the accuracy by which the simulations can predict the deformation is often either marginally

<sup>20</sup>Which implies that the gas pressure could act on the entire short-end of the cavity spacer (and not only on the part of the mirror to which the gas in the cavity is exposed).

<sup>21</sup>It was concluded in section 2.1.1 above that the (absolute) uncertainty in the assessed refractivity-normalized relative deformation, i.e.  $\delta\varepsilon'$ , represents the relative contribution to the uncertainty of the overall pressure assessment from the deformation, i.e.  $\delta P/P$ .

sufficient or insufficient to allow for assessment of pressure with the targeted overall uncertainty of 10 ppm. The simulations are either limited by the uncertainty in the material parameters used, e.g. the Young's modulus and the Poisson ratio, which often are in the percent to permille range, or by the ability to model the system appropriately in the simulation program. While the former is particularly the case for systems that utilize glue for the mounting of the mirrors, the latter prevails for those with mirrors mounted to metal spacers by a press-on approach that provides plastic deformation of the spacer. This implies that it is not suitable to rely on simulations for assessing the deformation of these types of systems.

It can also be concluded that, for the other types of system, a deformation-characterization based solely on simulations will only seldom, preferably when the deformation is small, and then presumably only barely, provide characterizations that allow for assessments of pressures with the targeted relative uncertainty of 10 ppm.

## 3.3 Experimental characterizations

UmU, CNAM, PTB, RISE, and CEM have then (within activity A1.1.3) experimentally characterized one of their cavities with respect to cavity distortion.

### 3.3.1 Experimentally assessed deformation of the Invar-based DFPC refractometers at UmU and RISE

#### 3.3.1.1 Development of a novel robust and disturbance-resistant methodology for assessment of cavity deformation

Despite the fact that the two-gas method proposed by Egan et al. does not require accurate knowledge of the pressure — it is sufficient if it is constant [45] — it potentially opens up for disturbances from a number of physical processes, e.g. drifts, gas leakages, and outgassing, that can reduce the accuracy of the assessed cavity deformation. To mitigate these disturbances, Zakrisson et al. developed, within this QuantumPascal project, a robust and disturbance-resistant method based to two gases for assessment of deformation that is not affected to the same extent of these types of disturbances [46].

The novel methodology, which is further described in section 6.8.3.3 below, is based on scrutinizing the difference between two pressures — one provided by an external pressure reference system [in our case a dead weight piston gauge (DWPG), also referred to as a pressure balance, RUSKA] and the other being the pressure assessed by the refractometer evaluating the data by use of a model that does not incorporate cavity deformation — at a series of (set) pressures, for two gases with dissimilar refractivity, He and N<sub>2</sub>. For best performance, the methodology was carried out by use of the GAMOR methodology.

A thorough mathematical description of the procedure served as a basis for an evaluation of the basic properties and features of the procedure. It was found that the cavity deformation assessments are independent of systematic pressure-independent (i.e. constant) errors in both the reference pressure and the assessment of gas temperature. In addition, since the GAMOR methodology is used, the assessments are immune to linear drifts and has a significantly reduced sensitivity to gas leakages and outgassing into the system [54]. Thus, this provided a robust assessment of cavity deformation with small amounts of uncertainties [46].

This methodology was applied to the assessment of deformation, first in the stationary Invar-based DFPC refractometer at UmU (the SOP), and later also in the transportable system (the TOP) at RISE.

### 3.3.1.2 Assessment of the pressure-induced deformation of the stationary Invar-based DFPC cavity (the SOP) at UmU

It was found that this procedure provided deformation values of the stationary Invar-based DFPC cavity (the SOP) at UmU with significantly lower uncertainty than the simulated ones; while the simulations provided pressure-normalized relative deformations ranging from  $7.8 \times 10^{-12} \text{ Pa}^{-1}$  to  $6.7 \times 10^{-12} \text{ Pa}^{-1}$ , which correspond to a refractivity-normalized relative deformation,  $\epsilon'$ , in the  $2.9 \times 10^{-3}$  to  $2.5 \times 10^{-3}$  range [53], the experimental assessment of the deformation in the SOP system provided, in a first characterization, for pressures up to 16 kPa, and when the molar polarizability of N<sub>2</sub> was traced to a mechanical pressure standard, a pressure-normalized relative deformation of  $5.258(6) \times 10^{-6} \text{ Pa}^{-1}$ , which corresponds to a refractivity-normalized relative de-

formation of  $1.963(2) \times 10^{-3}$  [46].<sup>22</sup>

At a later instant, however, when the SOP had been refurbished and upgraded, it was found that the deformation was slightly different, viz.  $1.972(1) \times 10^{-3}$  [37].<sup>23</sup> Although not yet confirmed, the change in deformation between these two instants was attributed to either the remounting of the cavity mirrors or contamination of the He gas. The improvement in uncertainty (which did not comprise any possible contamination of the He gas) was attributed to an improved temperature assessment.

It was concluded that when a high-precision (sub-ppm) refractometer (which often can be obtained when the GAMOR methodology is used) is characterized according to the procedure developed, and under the condition that high purity gases are used, the uncertainty in the deformation contributes to the uncertainty in the assessment of pressure of nitrogen to a level of 1 or 2 ppm, which presently solely represents a fraction of the relative uncertainty of its molar polarizability. This implies, in practice, that, as long as gas purity can be sustained, cavity deformation is presently not a limiting factor in FP-based refractometer assessments of pressure of nitrogen.

### 3.3.1.3 Assessment of the pressure-induced deformation of the transportable Invar-based DFPC cavity (the TOP) at RISE

Regarding the transportable Invar-based system at RISE (the TOP), which is described in some detail in section 6.8.4 below, the same experimental characterization, [37], provided, for pressures up to 16 kPa, a refractivity-normalized cavity deformation of  $1.927(1) \times 10^{-3}$ .

Despite the slightly dissimilar values of the assessed pressure-induced cavity distortion of the two Invar-based systems,<sup>24</sup> their uncertainties, which

<sup>22</sup>For the case when the molar polarizability of N<sub>2</sub> was traced to a thermodynamic pressure standard, the corresponding values became  $5.258(12) \times 10^{-12}$  and  $1.963(4) \times 10^{-3}$ , respectively.

<sup>23</sup>For the case when the molar polarizability of N<sub>2</sub> was traced to a thermodynamic pressure standard, the corresponding value becomes  $1.963(2) \times 10^{-3}$ .

<sup>24</sup>It is relevant to point out though that although the cavity design and construction of the SOP and the TOP are virtually identical, the experimentally assessed deformations still differ outside their uncertainties. As was alluded to above, the cause of this has been attributed to the unconventional mirror-mounting, which, to provide a good seal, incorporate a plastic deformation of parts of the Invar spacer. Although this might be a sturdy and well work-

thus both were  $1 \times 10^{-6}$ , were found to be significantly below the targeted benchmark. This implies that when the systems are otherwise well-characterized, these deformation assessments are accurate enough to allow for assessments of pressure well within the targeted relative uncertainty of 10 ppm.

It should also be noticed that these deformation values differ significantly from the simulated ones (as given in section 3.2.4.1.2); while the simulations provided a refractivity-normalized relative deformation,  $\epsilon'$ , in the  $2.9 \times 10^{-3}$  to  $2.5 \times 10^{-3}$  range, the experimental assessments of the deformation provided, for pressures up to 16 kPa and for the two systems, refractivity-normalized relative deformations of  $1.972(1) \times 10^{-3}$  and  $1.927(1) \times 10^{-3}$  [37]. As was alluded to above, the main reason for this is attributed to a difficulty to properly assess the shape and minuscule size of the contact area between the curved mirror and the spacer.

Umu and RISE have also made a preliminary characterization of the Invar-based cavity system used in the TOP [37, 39] with regard to deformation up to 100 kPa by the use of a traceable pressure balance (Ruska 2365A-754) [55]. Although the response of this characterization was looking ostensibly linear on a pressure-vs-pressure plot, it was found that the response of the TOP vs. that of the pressure balance was weakly non-linear. A fit to the data provided a response of the refractometer of the form  $(a + bP + cP^2)$ , where  $a = -0.614$  Pa,  $b = 1.0021$ , and  $c = 1.52 \times 10^{-9}$  Pa<sup>-1</sup> [55].

The deviation of the  $b$  parameter from unity was mainly attributed to the fact that the refractometer was evaluated with the deformation parameter set to 0. Likewise, the non-linearity was attributed to a weak second order pressure dependence of the relative deformation ( $\Delta L/L$ ) caused by the mounting of the mirrors to the cavity spacer [55]. This non-linearity has not clearly been seen before when pressure up to a few tens of kPa has been considered, as was the case in [37] and [46]. Possible means to mitigate this non-linearity will be specifically addressed in future works.

---

ing mirror mounting for any given system, this clearly demonstrates the need of experimental assessment of the deformation (rather than assessment by simulations).

### 3.3.2 Experimentally assessed deformation of the Zerodur-based single FP-cavity refractometer at PTB

PTB has performed an experimental characterization of the pressure induced deformation of the single cavity Zerodur-based FP-system utilizing mirrors based on fused silica fixed by resin glue (Torr seal®) that was simulated above, utilizing the two-gas method with He and N<sub>2</sub> developed by Zakrisson et al. [46].

In this experiment, different gas pressures were realized at a constant temperature of 23.256(10) °C. The reference pressure sensors (type Mensor 'CPT9000') were calibrated directly in PTB's vacuum laboratory. The experimentally determined refractivity-normalized pressure induced deformation,  $\epsilon'$ , was determined to  $1.0(2) \times 10^{-3}$ .

### 3.3.3 Experimentally assessed deformation of the new Zerodur-based single FP-cavity refractometer at CNAM

The new Zerodur-based single FP cavity refractometer at CNAM has been subjected to a first preliminary characterization of the deformation. In this, the pressure-normalized relative deformation,  $\kappa$ , was assessed to  $-6.70(2) \times 10^{-12}$  Pa<sup>-1</sup>, which differ from the simulated value solely by 2 %.

This implies that the pressure-normalized relative deformation so far has been estimated with an uncertainty of  $2 \times 10^{-14}$  Pa<sup>-1</sup>, which is a slightly smaller than the targeted  $2.7 \times 10^{-14}$  Pa<sup>-1</sup> benchmark.

It should be emphasised though that, for a full characterization of the system, additional work is needed to complement the preliminary assessment. Work along these lines will be pursued in the closest future.

### 3.3.4 Experimentally assessed deformation of the single FPC system realized at CEM

CEM is presently in the process of finishing the assembly of the experiment. Results of this task cannot therefore be provided here; they will be reported when the system assembly is completed.

## 4 Temperature control and assessment

As was alluded to above, the second task of the first work package of the "QuantumPascal" project was devoted to "Temperature control and assessment". The main aim of this task has been to develop methods for accurately assessment of the temperature of the gas in FP-cavities.<sup>25</sup>

As is described in some detail in the guide "Development of methods for control and assessment of the temperature of the gas in Fabry-Perot cavities" [32], this has been performed within two activities; The first, pursued as Activity A1.2.1, presented in section 4.1 below, is concerned with the development of means to stabilising the temperature and minimising its gradients in the spacer material, while the second, performed within A1.2.2, presented in section 4.2, deals with the developments of methods for absolute and traceable temperature determinations.

### 4.1 Design and realization of FPC-based refractometer systems that can provide highly stable and homogeneous temperature conditions

The A1.2.1 activity, which is concerned with the "design and construction of FPC-based refractometer systems that can provide highly stable and homogeneous temperature conditions", comprises two parts.

The first one, presented in section 4.1.1 below, addresses the design and construction of FPC-based refractometry system(s) that can provide highly stable and homogeneous temperature conditions.

The second one, presented in section 4.1.2, is devoted to the thermodynamic effects that take place when gas is let into a FPC cavity, commonly referred to as  $pV$ -work. In particular, the influence of introducing a gas at a temperature dissimilar to that of the cavity (walls) should be estimated both experimentally and theoretically and the conditions under which this effect might influence the temperature determination should be assessed.

<sup>25</sup>As the gas molecules make frequent collisions with the walls of the cavity, the gas temperature is, to a first order approximation, primarily given by the temperature of the cavity walls.

### 4.1.1 Design and construction of FPC-based refractometry systems that can provide highly stable and homogeneous temperature conditions

In the first part of Activity 1.2.1, the participants (PTB, UmU, CNAM, CEM, and RISE) should together design and construct (at least) one FPC-based refractometry system that can provide highly stable and homogeneous temperature conditions and thereby enable an assessment of temperature in A1.2.2 with an accuracy below 3 mK. The system(s) should be well characterised with respect to temperature gradients using both FEM calculations and a minimum of two calibrated temperature sensors.

#### 4.1.1.1 Systems constructed by UmU and RISE

UmU and RISE have realised and investigated the performance of several systems for temperature assessment and control of the cavity spacer, all comprising an Invar-based DFPC, displayed in Fig. (2) above, using the GAMOR methodology, based on classical thermistors.

As presented in Silander et al. [49], the systems developed and scrutinized have typically utilized three Pt-100 sensors mounted in holes drilled in the cavity block, situated between the two cavities. This provides the possibility to detect temperature gradients along the spacer, which, if necessary, could be taken into account.

To stabilize the temperature of the spacer (i.e. to mitigate the effect of temperature fluctuations from the surrounding), the DFPC was placed inside a temperature stabilized aluminum enclosure, referred to as the "oven".

##### 4.1.1.1.1 The first system

In an early (the first) realization of the system, four Peltier elements were mounted below the oven and one under the cavity spacer. The temperature was then repeatedly measured by the Pt-100 sensors, while a feedback-loop was actively stabilizing the temperature of the cavity spacer by use of the Peltier elements. It was found that under typical measurement conditions, and within a measurement campaign (comprising 24 hours), the temperature of the cavity spacer could be stabilized to within 0.2 mK [49].

#### 4.1.1.1.2 The second system

In the second system, to improve on the accuracy of the system (as is further discussed in section 4.2.1 below), as shown in Fig. (6), a gallium fixed point cell was developed and implemented [50]. The temperature of the cavity was measured using a thermocouple type  $T$ , where the tip of one of its wires was situated in the gallium in the fixed-point cell while the other wire was wrapped around the cavity spacer inside the oven. The signal from the thermocouple was measured using a nano-voltmeter [50].

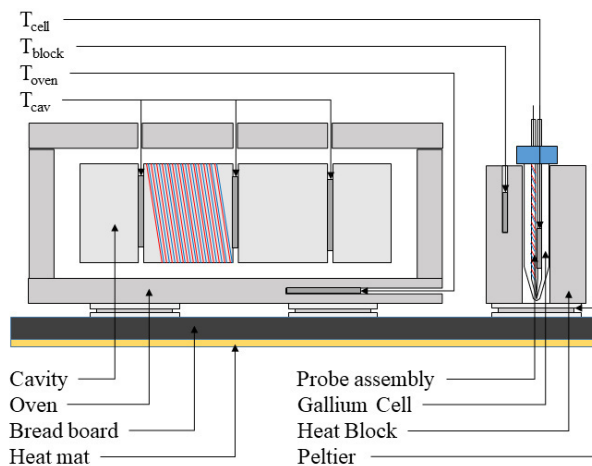


**Figure 6. Schematic illustration of the temperature control system of the second realization. The temperatures of the cavity assembly (left) and the gallium fixed-point cell (right) are controlled by separate proportional-integrating-differential (PID) controllers. Reproduced with permission from Ref. [50]**

In this realization, the temperature of the DFPC was increased to 29.76 °C. To avoid temperature gradients, e.g., from tubes, disturbing the DFPC, the oven and the gallium cell were contained in a temperature controlled enclosure. This enclosure was controlled by a separate proportional-integrating-differential (PID) controller, keeping the temperature close to the melting point of gallium. Again, four Peltier elements additionally stabilized the oven<sup>26</sup>. Both the oven and the gallium fixed point cell were controlled by separate PID con-

<sup>26</sup>in this case, the Peltier element directly under the spacer was removed since it was considered to cause temperature gradients in the spacer.

trollers.

The stability of the system was investigated by monitoring the difference between the measured temperatures using the thermocouple and the Pt-100 sensors in the spacer. It was found that during 13 hours of a melting cycle of the gallium cell, the  $2\sigma$  noise was estimated to  $\pm 220 \mu\text{K}$ , similar to what was found for the first system. Since the assessment of the stability of the measurement module was found to represent  $80 \mu\text{K}$ , the combined stability of the fixed-point cell and thermocouple measurement can be assumed to be slightly below  $220 \mu\text{K}$ .

#### 4.1.1.1.3 The third system

The third and last system that was developed, located in the same stabilized enclosure as described above, is based on a balanced bridge using two Pt-100 sensors. The two Pt-100 sensors are balanced with two sets of low temperature drift resistors to give a zero output voltage at the gallium melting point. To reduce the effect of stray offset voltages (including drifts), homodyne detection was used by utilizing a lock-in amplifier modulating the supply voltage to the bridge and performing detection at the same frequency (40 Hz). The system is presently under further development and characterization, but preliminary assessments have shown an improved performance.

#### 4.1.1.2 System constructed by PTB

PTB has implemented a regulation of the ambient air temperature within the laboratory by three commercial water cooled systems comprising fans and radiators ( $P2P = 1 \text{ K}$ ). This system uses: double polystyrene enclosure (simulated damping of temperature variations by a factor of 20000 for temperature oscillations with a 12 minutes period or faster); a liquid-based thermostat (PolyScience 15L Refrigerated/heated Circulator ( $P2P = 10 \text{ mK}$ )); a thermometer (PT100 metal-based to track fast temperature changes which cannot be resolved by the SPRTs from Ludwig Schneider Physics 1000); and custom made aluminium based vacuum chamber (Vacom).

The assessments of the temperature of the FP-refractometer realized at PTB was performed as described in section 4.2.2, i.e., by the use of four calibrated SPRTs (FLUKE type 5686-B). Two of the SPRTs can be probed simultaneously by a precision thermometry bridge (Isotech type mircoK 70).

The temperature stabilization was realized via the ultra-precise thermal bath (Kambic OB200) including a custom designed pump upgrade to circulate the thermalizing liquid. The set temperature was chosen to be 23 °C or 296.150 K. It was found though that the temperature measured with the SPRTs was 238 mK lower than the set temperature. This was expected since the tubing of the circulating liquid is affected by the room temperature.

Figure 7 shows the assessed temperature of a 140 h measurement campaign. After the first four days (at about 96 h), the pumping speed was lowered, which additionally increased the temperature offset to 239 mK. This could though be detected equally with both SPRTs; in fact, their difference (shown in the lower panel representing also the gradient in the system) remained constantly zero within the uncertainties, which are 300 and 350  $\mu$ K ( $k=1$ ), respectively, for the two SPRTs with respect to the calibrations performed by PTB's temperature laboratory. The standard deviation of this difference was 7  $\mu$ K for the running mean (3 h) while the peak to peak variation was 40  $\mu$ K.

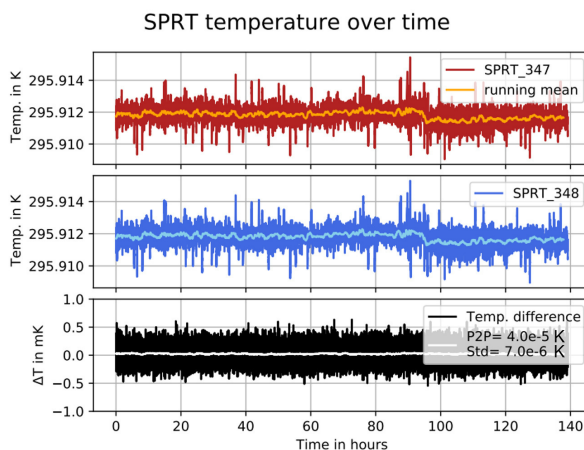


**Figure 7.** Stabilized temperature measured with SPRTs (FLUKE type 5686-B) in combination with a precision thermometry bridge (Isotech type mircoK 70). The set temperature was 23 °C. After four days the pumping speed of the thermalizing liquid was lowered, producing a 1 mK temperature change within the setup.

The measuring volume is located inside an aluminum-based vacuum chamber between both SPRTs. Accordingly, it is assumed that only the mea-

suring gas and the laser radiation will be able to influence the temperature of the refractometer. However, the simulations and experiments regarding the influence of  $pV$ -work on a refractometer presented in section 6.8.3.1 above indicate that these influences are negligible when a well chosen design, comprising with small gas volumes and correspondingly good thermal conduction and heat capacity of the gas, is utilized.

#### 4.1.1.3 System constructed by CNAM

Before the initiation of this EMPIR project, CNAM developed a FP-refractometer for determination of refractive index of air. However, it was found that that system could not guarantee adequately long term temperature stability and homogeneity conditions. To improve on that, CNAM decided to realise and investigate a new, more compact, absolute refractometer, working at 532 nm, that has the advantage of being more stable and have better temperature homogeneity. The main part of the refractometer, shown in Fig. 8, is composed of a 50 mm-squared single Fabry-Perot resonator (two silica mirrors and a spacer made in Zerodur) and an enclosure in copper working alternatively under vacuum and with gas.

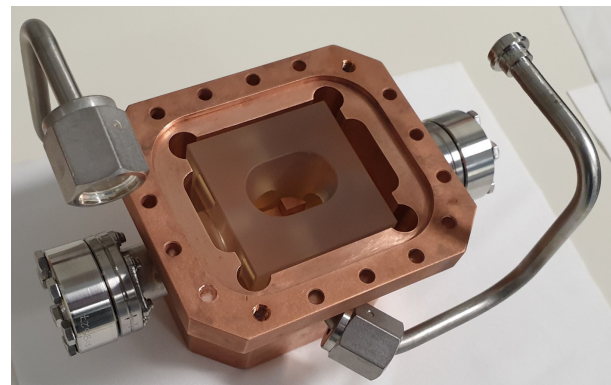


**Figure 8.** Picture of the open CNAM refractometer: the 50 mm-squared single Fabry-Perot resonator (with its two silica mirrors and a spacer made in Zerodur) residing inside the copper enclosure.

Gas temperature is measured by a calibrated Standard Platinum Resistance Thermometer (SPRT) sensor placed inside the copper enclosure (see Fig. 9) on the top part. When the system is correctly regulated and stabilized, we assume that the mea-

sured temperature is the gas temperature inside the Fabry-Perot resonator.

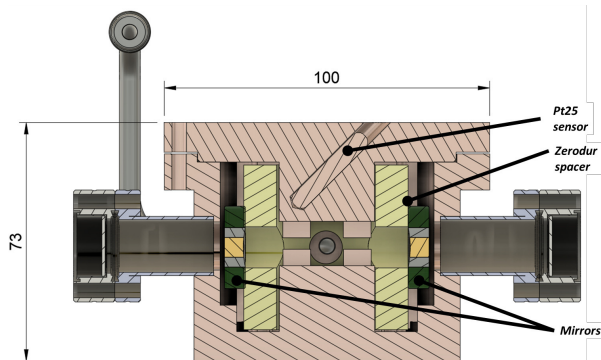


**Figure 9.** Sectional view of the CNAM refractometer.

To insure a temperature stability of less than 1 mK, the CNAM refractometer is composed of 4 enclosures shown in Fig. (10): enclosure 1 in expanded polystyrene; enclosure 2 in steel; enclosure 3 in copper; and enclosure 4 in copper.

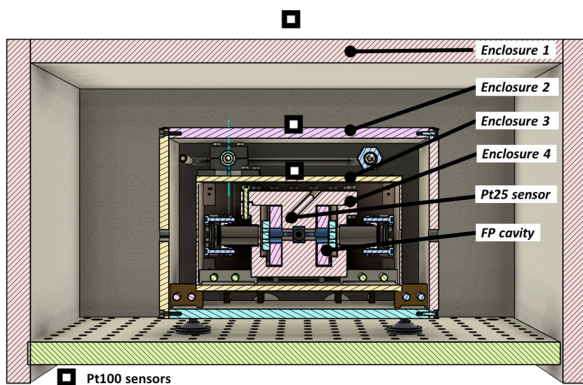


**Figure 10.** Sectional view of Cnam refractometer with its 4 enclosures. Enclosure 1 in expanded polystyrene, enclosure 2 in steel, enclosure 3 in copper and enclosure 4 for gas and vacuum in copper.

to which is added a stand-alone Arduino-based temperature regulation system including several flexible thermofolios heaters and ( $\pm 1$  mK) Pt-100 sensors: two thermofolios coupled to one Pt-100 sensor are positioned on lateral sides in Enclosure 2 while one thermofoil coupled to one Pt-100 sensor is positioned on the top of Enclosure 4.

In addition, to reach the best uncertainties in thermodynamic temperature measurements ( $< 1$  mK), the temperature regulation was designed to operate at the gallium melting point ( $29.76$  °C). In the presence of a variation of the laboratory temperature of  $\pm 100$  mK, with the temperature in Enclosure 2 varying  $\pm 50$  mK, and with the temperature of Enclosure 3 varying  $\pm 10$  mK, the temperature variation inside the FP-cavity (in Enclosure 4, shown in Fig. 11) was, over a period of 1 week, found to be better than  $\pm 1$  mK both under vacuum conditions and with gas in the cavity.

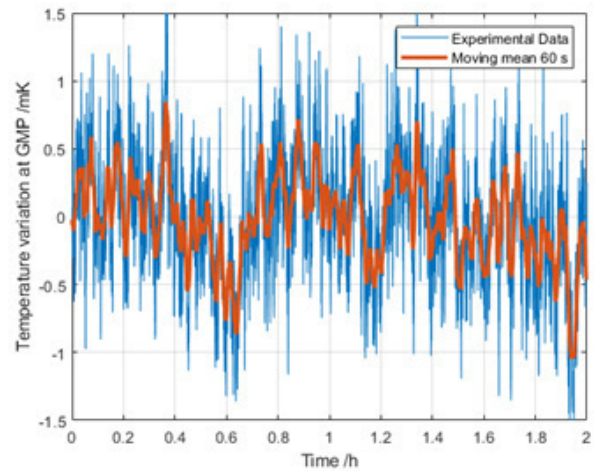


**Figure 11.** Variation of the temperature inside the regulated refractometer around the gallium melting point.

#### 4.1.1.4 System constructed by CEM

CEM has designed, realised, and investigated the performance of a system for temperature assessment and control based on classical Pt-100. As is shown in Fig. 12, the system comprises several temperature control steps. The first one regulates the temperature to  $\pm 0.1$  K, the second to  $\pm 0.01$  K and the third one to  $\pm 0.001$  K. Also, a gas reservoir with a temperature regulation steps (that reduces the temperature difference between the cavity and the gas) was added to thermalize the gases that are introduced into the cavities. The last steps for the FP-cavities and the gas reservoir are copper sleeves. All the system is controlled by the same device and it is possible to set different objective temperatures. The system is not fully assembled yet but the various control loops

have been checked.

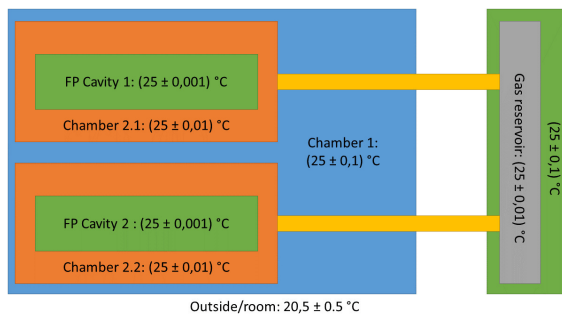


**Figure 12.** The main principles of temperature stabilization of the FPC-system at CEM.

#### 4.1.2 Scrutiny of the thermodynamic effects that originate from the filling and evacuation of gas (so called *pV*-work) in FPC-based refractometers

In the second part of Activity 1.2.1, the participants should scrutinize the thermodynamic effects that originate from the filling and evacuation of gas in FPC-based refractometer (so called *pV*-work).

##### 4.1.2.1 Scrutiny of the thermodynamic effects that originate from *pV*-work in an Invar-based DFPC refractometer using the GAMOR methodology

In this part of Activity 1.2.1, PTB, UmU, and RISE jointly scrutinized the thermodynamic effects that originate from the filling and evacuation of gas in an Invar-based DFPC refractometer when used with the GAMOR methodology [52].

The first (and main) part of the investigation dealt with simulations, first regarding gas dynamics, and then concerned with of transfer of heat in the system (primarily the cavity spacer). These simulations, of which some were made as parametric studies, predicted a number of "characteristic" thermodynamic behaviors of the refractometer. Those that provided opportunities for experimental verification were then, in the second part of the investigation, verified through experimental studies [52].

##### 4.1.2.1.1 Studies of gas dynamic behaviors

Simulations of gas dynamics showed, among other things, primarily due to the facts that the system is "closed"<sup>27</sup> and that each cavity has been manufactured with a narrow bore<sup>28</sup>, that the equilibration of pressure in the cavity when nitrogen is let in takes place on a time scale of *tens milliseconds* [52].

The simulations also showed, primarily to the second fact above, that the gas will adopt the temperature of the cavity wall on a time scale of less than a couple of seconds [52].

This implies that, within the longer of these two time scales, i.e., within a couple of seconds, there is an equilibrium in both pressure and temperature in the cavity, and, due to the latter, also a thermal equilibrium with the cavity walls [52].

##### 4.1.2.1.2 Studies of transfer of heat in the system

Regarding transfer of heat in the system (between the cavity walls and the rest of the cavity), it was found that, by virtue of a combination of a number of carefully selected design entities<sup>29</sup> (a small cavity volume<sup>30</sup>, a spacer material with high heat capacitance<sup>31</sup>, a high thermal conductivity<sup>32</sup>, no regions that are connected with low thermal conductance, i.e. no heat islands<sup>33</sup>, and a continuous as-

<sup>27</sup>The notation that the cavity system is "closed" implies that the gas does not fill a volume surrounding the spacer as is the case for an "open" system; instead it fills only one of the cavities. This restricts the amount of gas being transferred into the refractometer in a single gas filling cycle

<sup>28</sup>Each cavity has been manufactured with a bore with a radius of 3 mm.

<sup>29</sup>The design entities are further discussed in some detail in section 6.6.2.1.

<sup>30</sup>The fact that each cavity has been manufactured with a narrow bore with a radius of 3 mm implies that each filling of gas brings in only a small volume of gas (with a spacer length of 148 mm, < 5 cm<sup>3</sup>), and thereby, when 100 kPa is addressed, only a small amount of energy (< 0.5 J)

<sup>31</sup>The high volumetric heat capacity implies that a given amount of energy supplied to the spacer (from the gas) only provides a small temperature increase in the spacer material

<sup>32</sup>Invar has a high thermal conductivity, being ca. twice as large as that for many types of glasses.

<sup>33</sup>The system was constructed without any regions that are connected with low thermal conductance, referred to as heat islands. This implies that any possible small temperature inhomogeneity created by the filling or evacuation of gas will rapidly spread in the system (significantly faster than in systems with cavity spacers made of glass materials, with larger gas volumes or with heat islands) so as to make the temperature of the DFPC-system homogeneous in a short time, which is a prerequisite for an accurate assessment of the temperature of the gas

assessment of temperature of the cavity spacer<sup>34</sup>), the Invar-based DFPC system is not significantly affected by *pV*-work when the GAMOR methodology is applied<sup>35</sup>. Simulations show that 10 s after the filling all temperature gradients in the system are well into the sub-mK range [52].

#### 4.1.2.1.3 Estimates of upper limits

The analysis given in the study indicated that an upper limit for the influence of *pV*-work on the Invar-based DFPC system using 100 s long gas modulation cycles is 0.5 mK/100 kPa (or 1.8 ppm/100 kPa) (and even smaller when 200 s long cycles are used<sup>36</sup>) [52].

#### 4.1.2.1.4 Experimental verification of predicted thermodynamic properties

Experiments performed at pressures up to 30 kPa support the finding from the simulations that refractivity assessments initiated 40 s after the initiation of the gas filling are not significantly affected by the *pV*-work. As an example of this, Fig. (13) displays, by a pair of panels, the 100 s long filling part of a 200 s long modulation cycle from a pressure of 30.7 kPa.

The top panel shows the pressure settling process of the system as assessed by the refractometer. The colored curves represent ten consecutive gas fillings, while the solid black curve represents their average. The initial (15 - 20 s) parts of the data, which are out of scale, represent the combined effect of settling of the piston gauge (regulating the pressure) and filling of the cavity. The dashed lines represent  $\pm 3$  ppm, which correspond to a variation (drift) of the temperature of  $\pm 1$  mK.

Additional experimental investigations performed up to 100 kPa by Rubin et al. [56] indicated that the upper limits assessed by the simulations

<sup>34</sup>Since the gas takes the temperature of the cavity wall within seconds, pressure assessments are only influenced by the *difference* between the temperature of the cavity walls and that(those) of the cavity spacer at the position(s) of the sensors. It was found that, under normal conditions (for pressures up to 100 kPa and when the gas modulation periods are 100 or 200 s), this difference will, when the refractivity assessments are made, be minute, well into the sub-mK range.

<sup>35</sup>GAMOR is typically performed utilizing repeated gas fillings and emptying cycles with duration of either 100 or 200 s [26].

<sup>36</sup>When 200 s long gas modulation cycles are used, the corresponding upper limit is 0.4 mK/100 kPa (corresponding to 1.3 ppm/100 kPa).

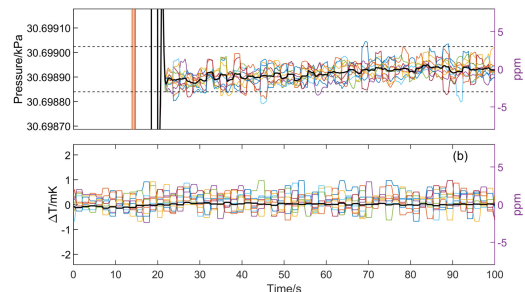


**Figure 13.** The upper panel displays, by the coloured curves, the gas filling part (0 - 100 s) of 10 individual consecutive gas modulation cycles (each with a total modulation time of 200 s) for a pressure of 30.7 kPa. The black curve shows the mean of the ten individual coloured curves. The dashed black curves represent  $\pm 3$  ppm deviations from the measured pressure. The lower panel illustrates, by the colored curves, the mean temperature of the three Pt-100 sensors in the cavity spacer during the same 10 cycles in terms of the average temperature of 100 consecutive temperature assessments of the three Pt-100 sensors. The black curve depicts the mean of 100 consecutive temperature assessments normalized to their individual averages. Reproduced with permission from Ref. [50]

in Rubin et al. [52] indeed are upper limits for the thermodynamic effects in the system and that the actual effects are markedly smaller, typically about a third of the predicted upper limits.

#### 4.1.2.1.5 Long term effects

Although the upper limits for the inter-cycle thermodynamic effect scrutinized above were found to be small (up to 0.5 mK/100 kPa), it can be concluded that to assess the long term effect of gas modulation on the assessment of pressure, the effect of both the filling and an evacuation of the gas should be taken into account.

Since it can be surmised that, when gas is evacuated from the cavity during the second part of the modulation cycle, a similar amount of energy is removed from the system as the filling brings in, giving rise to a temperature decrease of the system that is similar in magnitude to that caused when the gas was filled. The net supply of energy to

the cavity from the gas filling and emptying process (and thereby the long term effects) on the system is therefore practically negligible<sup>37</sup>.

#### 4.1.2.1.6 Conclusions

All this show clearly that thermodynamic effects (i.e.  $pV$ -work) will not be a limiting factor when the Invar-based DFPC GAMOR system is used for assessments of pressure or as a primary pressure standard up to atmospheric pressures [30, 52].

#### 4.1.2.2 Scrutiny of the thermodynamic effects that originate from the filling and evacuation of gas in a Zerodur-based FPC refractometer

CNAM has not performed any simulations of the thermodynamic effects that originate from the filling and evacuation of gas in their Zerodur-based FPC refractometers. CNAM refractometer uses an active temperature regulation inside as close as possible to the cavity. Initial tests have shown that filling and evacuation of gas from vacuum to 100 kPa and back-again, resulted in a temperature change of  $\pm 10$  mK. Since the subsequent stabilisation time was about 20-30 min, it was not possible to make use of as fast gas filling and evacuation cycles as typically is used in the GAMOR technique.

Since the temperature regulation is affected by the fast changes of pressure, a procedure was developed to minimize these effects by using a flowmeter or manual dosing valves in order fill or evacuate gas with a reduced flow rate (of about 5-10 ml/min). By this, CNAM was able to perform vacuum to 100 kPa and 100 kPa to vacuum cycles in 5 min with a maximum variation of temperature of  $\pm 0.5$  mK although the gas is at room temperature.

<sup>37</sup>In the most recent study by Rubin et al. [56], evidence for a small long-term net energy deposit to the cavity was found. This was attributed to the fact that the thermodynamic effects of the filling and the emptying processes onto the cavity spacer do not fully cancel each other; some of the energy is deposited in tubes and valve just outside the cavity spacer, the net effect of an entire gas modulation cycle<sup>38</sup> was estimated to be well into the sub-ppm range. Since this is counter acted by the temperature regulation processes of the cavity spacer (described in section 2.1.1), this will not lead to any pile up effects of temperature after an extended period of gas modulations.

## 4.2 Development, implementation, and investigation of various methods for temperature assessment of FPC-based refractometry system

In this activity, denoted A1.2.2 in the QuantumPascal project, the various partners should develop, implement, and scrutinize at least 3 methods for temperature assessment and control using the cavity-based refractometry systems addressed in either of the activities A1.1.3 or A1.2.1.

Systems for temperature assessment based on either classical thermistors or the gallium melting point (or a combination of the two) should be scrutinised. The feasibility of high-resolution photonic thermometry for temperature regulation/control, which is based on the temperature dependent frequency shift of birefringent spacers, should also be investigated.

To enable the assessment of pressure with a relative uncertainty of 10 ppm in the kPa range, the goal was that at least one of the systems should enable traceable gas temperature assessments with a precision below 1 mK ( $< 3 \times 10^{-6}$ ) and an uncertainty below 3 mK ( $< 1 \times 10^{-5}$ ).

### 4.2.1 Systems constructed by UmU and RISE

UmU and RISE have realised and investigated the performance of the same three systems as was described in section 4.1.1.1 above (i.e. based on classical thermistors and/or a combination of a thermocouple and a gallium fixed-point cell) for their ability to assess the temperature.

#### 4.2.1.1 The first system

In the first realization, which was mainly constructed and evaluated to assess the temperature stability of the regulation system, the Pt-100 sensors were not calibrated. Hence, the assessments relied on their standard uncertainty. This implies that the temperature measurement system had an uncertainty of 200 mK.

#### 4.2.1.2 The second system

In the second realization, in which the temperature of the cavity was measured using a combination of a thermocouple and a gallium cell, the extended uncertainty of the temperature assessment was esti-

mated to  $\pm 1.2$  mK, mainly originating from the uncertainty of the nano-voltmeter. Since this corresponds to a relative uncertainty of the temperature of 4 ppm, it contributes to an assessment of pressure by the same amount.

#### 4.2.1.3 The third system

As was alluded to above, the third realization is based on a balanced and modulated bridge using two Pt-100 sensors. The modulation of the supply voltage of the bridge was generated by the internal frequency generator in a lock-in amplifier (with an amplitude of 0.1 V). The output signal of the bridge, which represents the amplitude of the voltage response of the bridge and is directly related to the resistance of the two Pt-100 sensors, where the latter, in turn, is a measure of the temperature, was then detected by the same lock-in amplifier by homodyne detection. The output of the lock-in amplifier provided, after a calibration using the gallium cell, an accurate assessment of the temperature of the sensors around the melting point of gallium.

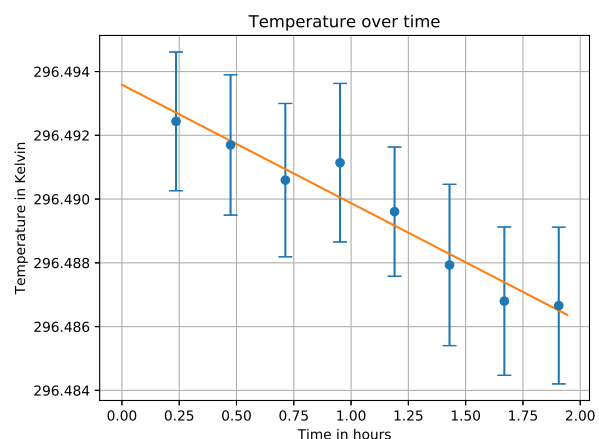
This realization provides a low noise level and high precision that makes it possible to measure the temperature variations in the spacer that originates from the filling and evacuation of the measurement cavity when 100 kPa of nitrogen was assessed by the GAMOR methodology utilizing a cycle time of 200 s [56]. It was found that the measured intra-cycle temperature variations were lower than  $\pm 0.2$  mK, which was several times lower than the upper limits predicted by simulations performed by Rubin et al. [52].

#### 4.2.2 System constructed by PTB

The assessments of the temperature of the FP-refractometer realized at PTB was performed by the use of four calibrated SPRTs (FLUKE type 5686-B). Two of these SPRTs can be probed simultaneously by a precision thermometry bridge (Isotech type mircoK 70). They have a Standard uncertainty for the temperature assessment of  $300 \mu\text{K}$  to  $350 \mu\text{K}$  (not considering gradients in the system).

As an alternative to assessing the temperature by the use of sensors, it was investigated to which extent it is possible to assess the temperature of the spacer in terms of a beat signal from measurement of the optical length of the spacer, addressing it by light at a position where there is no cavity bore.

Figure (14) illustrates the temperature inside the aluminum vacuum chamber assessed by a Pt-100 sensor over a period of two hours. The decreasing trend originates from an induced change in temperature to test the features of the sapphire-based spacer as a thermometer.



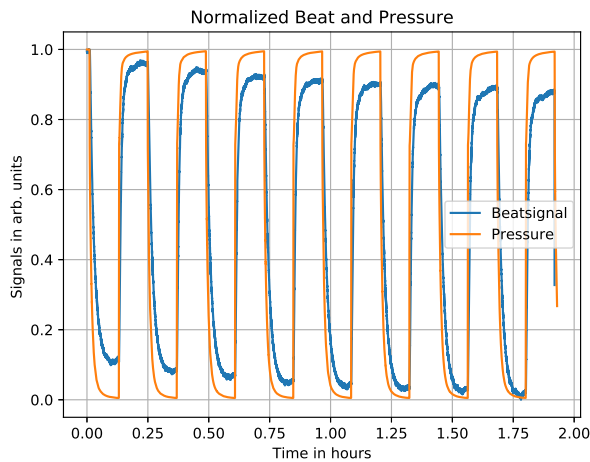
**Figure 14.** Temperature change in the PTB system to be assessed by the change in optical path length inside the sapphire-based spacer.

Figure (15) illustrates the corresponding beat signal between the frequency standard (iodine-stabilized HeNe lasers), acting as a reference, and the red diode laser (DLC Pro Toptica) locked to the optical path length of the long axis of the sapphire-based spacer<sup>39</sup> when the pressure was periodically modulated from 0 Pa to 89.6 kPa. As a consequence of this, the length of the spacer was then altered both as a response to the pressure-induced deformation of the spacer and the change in temperature due to the cooling performed by the gas.

While the major part of the modulation of the beat is caused by the gas pressure compressing the spacer, the declining trend of the beat, which in this case is about a tenth of the alteration of the length due to the pressure, represents the response of the decreasing temperature (it amounts to ca. 1 GHz/mK). This shows that the change in beat frequency can be used as a means to assess the temperature.

The next step will be the attachment of HR coated substrates to increase the finesse and decrease the

<sup>39</sup>Hence, the laser was locked to the pure spacer by the use of its natural reflections on the front and back.



**Figure 15.** Periodic pressure modulation from 0 pa to 89.6 kPa (normalized signal in orange) to change the temperature of the sapphire spacer as shown in Fig. 14 and the corresponding beat signal (normalized signal in blue). The declining trend of the beat represents the decreasing temperature (with about 1 GHz/mK), while the about ten times stronger modulation of the beat is caused by the gas pressure compressing the spacer.

noise of the beat signal. A measured change of this beat of 1 kHz will then correspond to a change in temperature of the spacer in the order of 1  $\mu$ K. The temperature of a spacer with good heat conductivity correlates strongly with the gas temperature as show in the  $pV$ -work section.

#### 4.2.3 System constructed by CNAM

CNAM has realised and investigated a system for temperature regulation based on the gallium melting point. As described in previous sections, the entire CNAM system has been designed to operate at the gallium melting point in order to reach the best uncertainties in thermodynamic temperature measurements ( $< 1$  mK). A high-performance Standard Platinum Resistance Thermometer (SPRT) with a nominal resistance of 25.5 ohms (Fluke Calibration model 5686-B) was placed on the top part of the refractometer in copper (see Fig. 9). Ideally, a second SPRT sensor would be needed at the bottom part. The sensor is about 2 mm of the internal surface of the copper. Temperature measurements are per-

formed with this SPRT and a 8.5 digits multimeter (Keithley model 2002) in 4 wires ohmmeter mode. The whole set-up has been calibrated at the gallium melting point and at the triple water point with an uncertainty of 0.7 mK by the LNE-CNAM temperature group. Because high-fragility (handling and shocks) and possible drifts of this sensor, calibration should be performed regularly. Thus, at the design stage of the refractometer, the possibility to easily remove with care the temperature sensor has been planned. The system realised by CNAM enables traceable gas temperature determination with a precision below 1 mK ( $< 3 \times 10^{-6}$ ) and an uncertainty below 3 mK ( $< 1 \times 10^{-5}$ ), in order to enable the assessment of pressure with a relative uncertainty of 10 ppm in the kPa range.

#### 4.2.4 System constructed by CEM

AS is shown in Fig. 16, CEM has realised and investigated the performance of a system for temperature assessment and control based on classical thermistors.

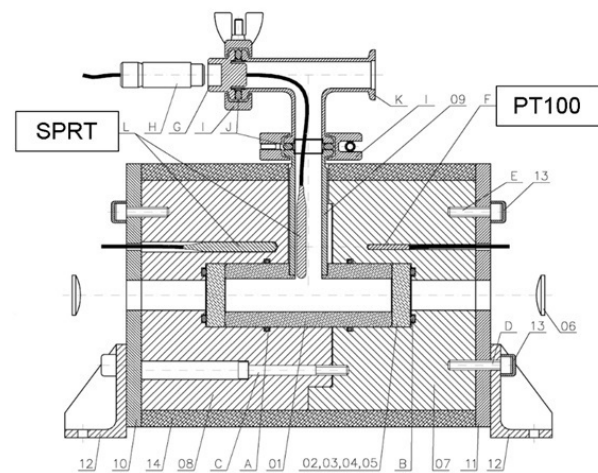


**Figure 16.** Schematic depiction of the FP-baser refractometer system at CEM.

The system uses PT-100 as probes to the temperature control and SPRT as probes of the temperature assessment. As it is explained in section 4.1.1.4 above, the system has different temperature control steps; each step has one PT-100 probe to read the temperature in that step.

For the temperature assessment two SPRT probes are placed in the last step. One inside the copper sleeve and another in contact with the gas. Moreover, with this system the difference between the gas temperature and the copper sleeve can be derived and then the temperature system could be optimized for reducing this difference.

## 5 Permeation of gas into various cavity spacer material

### 5.1 Introduction

As is described in some detail in the guide "*Guide: Information about permeation of gas into various cavity spacer materials*" [33], since permeation of gas in the cavity spacer material can adversely affect both the purity and the pressure of the gas as well as, potentially, the physical length of the cavity, Task 1.3 of the QuantumPascal project has addressed the permeation of gas into the cavity spacer material.

Since different cavity materials provide dissimilar gas permeation, this phenomenon needs to be assessed for various spacer materials. As is described in some detail in the Guide about this, [33], the focus of the study was on three materials, viz. ULE-glass, Zerodur, and sapphire.

### 5.2 Approach

Since gas diffusion in solids is a relatively slow process (equilibrium takes weeks under best conditions, otherwise months or even years are needed) in terms of the frequency scale of gas pressure changes in the devices that were developed, e.g. in the QuantumPascal project, equilibrium conditions will be rare. This requires a modelling of the dynamics of the gas transport in the material. However, such modelling can be performed only when diffusion constants and the permeability of the gas in the materials are known. The work performed within Task 1.3 of the QuantumPascal project has therefore, to a large extent, been devoted to assessment of such diffusion constants.

Such experimental assessments of permeability and outgassing have been performed both at the Institute of Metals and Technology (IMT) in Ljubljana, and at the Physikalisch-Technische Bundesanstalt (PTB), in Berlin. At PTB, a new apparatus was developed for simultaneous determination of the out-

gassing rates of different material samples at well-defined different temperatures in each case.

### 5.3 Experimental assessments and conclusions

It was clearly established in the Guide [33] that there are measurable effects of He diffusion in different types of glass. Hence, when FP cavities are made of glass, and is exposed to He for a certain period of time, the He will diffuse into the walls of the cavity. After subsequent evacuation and filling with another measurement gas, He will diffuse out of the cavity walls (outgassing) which will contaminate the measurement gas.

The assessments showed that the permeability effect is significantly higher in ULE-glass than in Zerodur. For example, it was found that the diffusion constant,  $D$ , for He in Zerodur is almost 3 orders of magnitude lower than in ULE-glass, and that the permeation coefficient  $K$  is more than 4 orders of magnitude lower in Zerodur than in ULE-glass. He solubility of He in Zerodur is almost 30 times lower than in ULE-glass. Therefore, the influence of absorbed He on the spacer length is expected to be significantly higher in ULE-glass than in Zerodur. To minimize disturbing effects of He gas diffusion in optical cavity walls (e.g. contamination of other gases by He outgassing and drifts of cavity length), Zerodur is the preferred glass material.

Finally, it was concluded that there is a negligible diffusion of any gas in metals near room temperature (effects of  $H_2$  diffusion are too small to be considered). It was also found that there is practically no diffusion of He in sapphire. This implies that the best in this respect is to use metals or sapphire, since there is virtually no permeation of He near room temperature in these materials.

## 6 Scrutiny and implementation of gas modulation in FPC-based refractometry (GAMOR)

### 6.1 Commonly occurring limitations of refractometry - Disturbances

As was alluded to above, and as has been described in some detail in the guide "*Gas modulated Fabry-Perot-cavity-based refractometry (GAMOR) — Guide*

to its basic features, performance, and implementation" [34], although it is simple in theory to realize FPC-based instrumentation and to perform low uncertainty refractivity assessments, it is not trivial in practice to carry them out with low uncertainty. One reason is that FPCs often are (knowingly or unknowingly) exposed to a variety of disturbances on different time scales, for simplicity here referred to as<sup>40</sup>

- high-frequency disturbances ( $f \geq 0.1$  Hz), denoted *noise*;
- low-frequency periodic disturbances ( $10 \mu\text{Hz} \leq f \leq 0.1$  Hz), referred to as *fluctuations*; and
- monotonic (or ultra-low frequency) disturbances ( $f \leq 10 \mu\text{Hz}$ ), termed *drifts*.

While noise can originate from a number of sources, e.g. electronics, fast vibrations, and turbulence, fluctuations can be caused by slow air pressure variations, slow vibrations (e.g. from motions of air damped optical tables or buildings), slow disturbances of the central supply of power, and temperature regulation processes in electronics. Drifts can originate from a number of sources, not least from changes of the length of the cavity, e.g. from thermal expansion, aging, relaxations, and diffusion of gas into the material that can change its length in a slow but unpredicted manner. Irrespective of whether the disturbances can be monitored and identified or not, all of them can severely affect the ability to perform adequate (high precision or low uncertainty) measurements [20, 22, 29, 57, 58].

The high sensitivity to disturbances was early recognized as a practical limitation of FPC-based interferometry for high-accuracy assessment of pressure and realization of the pascal. For example, a disturbance that causes a change in the length the cavity of 1 pm, a percent-sized fraction of the "size" of

an individual atom, gives rise to, for a 15 cm long cavity, a change in the frequency of the cavity mode addressed that corresponds to an alteration in the assessed pressure of 2 mPa. It was therefore widely recognized that the realization of refractometry systems requires an exceptional mechanical and thermal stability. This implies, for example, that it is far from trivial to assess refractivity with low uncertainty by assessing  $L_0$  and  $L$  in two separate assessments.

A number of procedures to reduce the influence of disturbances and thereby alleviate some of the above-mentioned limitations have therefore been developed and implemented over the years.

### 6.1.1 Conventional means to reduce the influence of disturbances in refractometry

One means to reduce the influence of disturbances is to base FPC-based refractometry on DFPCs in which the two cavities are simultaneously addressed by two laser fields and the change in mode frequency of the cavity in which gas is let is assessed as the change in the beat frequency between the two cavities [12, 21–23, 29, 36, 58–61]. An advantage of this is that any change in length of the cavity spacer (into which both cavities are bored) that affects both cavities similarly does not affect the assessment. However, since the lengths of two cavities also can fluctuate dissimilarly over time, DFPC-based refractometry will still be affected by disturbances, although often to a lesser extent [22].

Another means to alleviate the limitations are to construct the FPC of low thermal expansion glass, e.g., ULE glass [22, 23] or Zerodur [10, 13, 14, 20, 21, 24, 58–60, 62–64], place it in a highly temperature stabilized environment (a combined gas and vacuum chamber) [22], and let the system relax and equilibrate for long time periods after each gas filling or emptying process [22]. However, several of these actions are cumbersome to realize; they often give rise to complex systems that are meticulously stabilized.

Although such types of actions frequently are taken, assessments of refractivity are still often limited by residual amounts of disturbances. This limits the performance and thereby the applicability of FPC-based refractometry, in particular when low pressures are assessed. It also limits the use of the

<sup>40</sup>There are no strict limits between the various types of disturbances. We have here defined noise as periodic disturbances whose frequencies are above 0.1 Hz, since this corresponds to the inverse of the time period over which consecutive data points typically are averaged, in this work denoted  $1/t_{avg}$ . Drifts are defined as monotonic disturbances or periodic disturbances whose frequencies are below the inverse of the time between the assessments of refractivity in the presence and absence of gas in conventional refractometry. Since this time is assumed to be in the order of  $10^5$  s, drifts are here defined as the disturbances whose frequencies are below  $10 \mu\text{Hz}$ . Fluctuations, finally, are characterized as disturbances whose frequencies are between these two.

technology outside well-regulated laboratories.

### 6.1.2 A novel means to reduce the influence of disturbances — Gas Modulation Refractometry (GAMOR)

It is alternatively possible to utilize a methodology that can reduce the *influence* of disturbances on the assessment of refractivity. As is described in some detail in the guide "*Gas modulated Fabry-Perot-cavity-based refractometry (GAMOR) — Guide to its basic features, performance, and implementation*" [34], one such is gas modulation refractometry (GAMOR). This methodology is built upon two principles, here referred to as two cornerstones; viz.,

- (i) the refractivity of the gas in the measurement cavity is assessed by a frequent referencing of filled measurement cavity beat frequencies to evacuated cavity beat frequencies; and
- (ii) the evacuated measurement cavity beat frequency at the time of the assessment of the filled measurement cavity beat frequency is estimated by use of an interpolation between two evacuated measurement cavity beat frequency assessments, one performed directly before and one directly after the filled cavity assessments.

Molar density and pressure are then assessed by convectional means; as is indicted by the Eqs. (11) and (12), by the use of the Lorentz-Lorenz expression and an equation of state, respectively.

By this, as is illustrated below, the GAMOR methodology mitigates swiftly and conveniently the influence of various types of disturbances in refractometry systems, not only those from changes in length of the cavity (e.g. caused by drifts in the temperature of the cavity spacer), but also several of those that have other origins (e.g. those from gas leakages and outgassing) [26, 27, 36, 54, 65].

## 6.2 Content of the present section

This section of the guide about FP-based refractometry, which deals with a "*Scrutiny and implementation of gas modulation in FPC-based refractometry (GAMOR)*" and is based on the guide "*Gas modulated Fabry-Perot-cavity-based refractometry (GAMOR) —*

*Guide to its basic features, performance, and implementation*" [34],<sup>41</sup> first provides (in section 6.3) expressions for assessment of refractivity in FPC-based refractometry in DFPC-based systems that, based on the general expressions for refractivity given in section 2.1 above, are suitable for the automated pressure assessments that are performed as a part of the GAMOR methodology.

It then describes (in section 6.4) the basic principles of the GAMOR methodology by separately providing explanations and descriptions of the ability of the GAMOR methodology to mitigate the influence of fluctuations and drifts.

It thereafter provides (in section 6.6) a short depiction of the most commonly used instrumentation for GAMOR-based refractometry, viz. an Invar-based DFPC system.

By use of some typical cycle-resolved data, it then gives (in section 6.7) an illustration of the operation and performance of the GAMOR methodology in practice.

Thereafter, it provides (in section 6.8) an overview of the most important and extraordinary achievements of the GAMOR methodology; in particular it provides (in section 6.8.1) verification of the theoretical predictions regarding its ability to mitigate the influence of fluctuations and drifts and it illustrates (in section 6.8.2) the extraordinary/exquisite precision it has achieved under various conditions. After reporting on some concepts of importance for the ability of GAMOR-based refractometry performed in an Invar-based DFPC to provide low uncertainty assessments in section 6.8.3 — its low susceptibility to thermodynamic effects, so called *pV*-work (in section 6.8.3.1), its ability to assess the gas temperature (in section 6.8.3.2), and its ability to accurately assess cavity deformation (in section 6.8.3.3) and penetration depth of mirrors comprising QWS coatings of type (in section 6.8.3.4) — this guide reports (in section 6.8.3.5) on the extended uncertainty the methodology so far has achieved.

<sup>41</sup>The present section is based upon scientific papers published during the last few years, to some extent dealing with the predecessor to the GAMOR methodology (Drift-free or Fast switching DFPC-based refractometry [36, 58, 60]), but mainly referring to papers addressing the GAMOR methodology, of which a few were published before the QuantumPascal project [26, 27, 65] while a majority of them have been published as a part of it [30, 37–41, 46, 49–52, 54–56, 65, 66].

It then provides (in section 6.8.4) a demonstration of its ability to realize transportable systems. Finally, it gives (in section 6.9)) a practical recipe of how to implement the GAMOR methodology in refractometry.

### 6.3 Procedure for autonomous assessment of refractivity from assessed shifts in laser frequencies and mode jumps by use of the GAMOR methodology

Section 2 provided appropriate expressions for assessments of refractivity, molar density, and pressure from a variety of measured or calculated entities.<sup>42</sup> Although these expressions give adequate estimates of the refractivity in the ideal case, since the evacuated and the filled measurement cavity beat frequencies [i.e. the  $f^{(0)}$  and the  $f^{(g)}$ ] cannot be assessed simultaneously, the assessed refractivity will irrefutably be affected by the presence of various types of disturbances that the system can be exposed to, predominantly fluctuations [65] and drifts [54]. To mitigate the effect of such types of disturbances, as was alluded to in section 6.1.2 above, the GAMOR methodology incorporates a process in which the evacuated measurement cavity beat frequency is, for each gas modulation cycle, not assessed at a single instant; it is instead estimated for all time instants of the modulation cycle by the use of a linear interpolation between two evacuated measurement cavity beat frequency assessments performed in rapid succession — one performed directly prior to when the measurement cavity is filled with gas, and another directly after the cavity has been evacuated. By this, the evacuated measurement cavity beat frequency can be estimated at all times during a modulation cycle, including those when the measurement cavity contains gas [26, 51, 66].

However, it should be noticed that although

<sup>42</sup>As was alluded to above, irrespective of whether refractometry is performed unmodulated or modulated, all realizations (including GAMOR-based systems) are based on the same fundamental principle; they measure the change in refractivity between two situations, with and without gas in a cavity, as a change in the frequency of laser light that is locked to a mode of the cavity. Hence, both unmodulated and modulated types of refractometry can be based on the same basic expressions, for the case with refractometry in general, given by the Eqs. (5) and (9), and, more suitable for the GAMOR methodology, given by the Eqs. (13) and (16) below.

this interpolation procedure is straightforward when there are no mode hops in the reference cavity and when the measurement laser, for every modulation cycle, originates from, and return to, the same mode, above assumed to be the  $m_0$  mode, this is not the case in general. The beat signal  $f$  is in such cases, because of such mode jumps, a non-continuous (i.e. a wrapped) function. In order to accommodate for also such situations, it has been found convenient to create an unwrapped (i.e. a mode-jump-corrected) beat frequency,  $f_{UW}$ , defined as

$$f_{UW} = \pm f - \left( \frac{\Delta m_m}{m_{0m}} \nu'_{0m} - \frac{\Delta m_r}{m_{0r}} \nu'_{0r} \right), \quad (13)$$

where  $\Delta m_m$  and  $\Delta m_r$  are the numbers of mode jumps the measurement and reference lasers have made from the modes  $m_{0m}$  and  $m_{0r}$  at which their empty cavity frequencies,  $\nu'_{0m}$  and  $\nu'_{0r}$  were assessed.<sup>43</sup> The  $\pm$  sign refers to the cases when  $\nu'_{0m} > \nu'_{0r}$  and  $\nu'_{0m} < \nu'_{0r}$ , respectively [37, 39].

The unwrapped empty measurement cavity beat frequency,  $f_{UW}^{(0)}$ , which represents the beat frequency the system would have provided if both lasers would have been at the modes at which the empty cavity frequencies were assessed, i.e. at  $m_{0m}$  and  $m_{0r}$ , has thus the property that it is continuous even if any of the lasers make any mode hop, and is thereby suitable for the interpolation process.

This implies that the interpolation, for modulation cycle  $k$ , can be estimated, for all times that fulfills  $t_k < t < t_{k+1}$ , as

$$\tilde{f}_{UW}^{(0)}(t_k, t, t_{k+1}) = f_{UW}^{(0)}(t_k) + \frac{f_{UW}^{(0)}(t_{k+1}) - f_{UW}^{(0)}(t_k)}{t_{k+1} - t_k} (t - t_k). \quad (14)$$

This process is schematically illustrated by the green straight line in panel c in Fig. 19 shown in section 6.4.2 below.

This implies, in turn, that, at each instant during which the filled measurement cavity assessment is evaluated during modulation cycle  $k$  (in particular

<sup>43</sup> $\nu'_{0m}$  and  $\nu'_{0r}$  are given by  $\nu_{0m}/(1 + \frac{\Theta_G}{\pi m_{0m}} + \frac{\Upsilon_C}{m_{0m}})$  and  $\nu_{0r}/(1 + \frac{\Theta_G}{\pi m_{0r}} + \frac{\Upsilon_C}{m_{0r}})$ , respectively, where, in turn,  $\nu_{0m}$  and  $\nu_{0r}$  are the measured empty cavity frequencies. Moreover,  $\Delta m_r$  accounts for a possible shift in the mode addressed in the reference cavity when gas is let into the measurement cavity. For a well-designed, stable system, this entity is often zero.

during the last part of the filled measurement cavity section of the gas modulation cycle), the shift in beat frequency between the two laser fields most suitably can be assessed as

$$\Delta f_{UW}(t) = f_{UW}^{(g)}(t) - \tilde{f}_{UW}^{(0)}(t_k, t, t_{k+1}). \quad (15)$$

This is schematically shown by the curve in panel d in Fig. 19 below.

As has been shown by Silander et al. [37], based on these expressions, the refractivity,  $n - 1$ , can then be straightforwardly and expediently expressed as a function of the shift of the unwrapped beat frequency,  $\Delta f_{UW}$ . In this case, Eq. (9) (still under the condition that the relative elongation is linear with pressure and when nitrogen is addressed)<sup>44</sup> can be written as

$$n - 1 = \frac{\frac{|\Delta f_{UW}|}{v'_{0m}}}{1 - \frac{|\Delta f_{UW}|}{v'_{0m}} + \frac{\Delta m_m}{m_{0m}} + \frac{\Theta_G}{\pi m_0} + \varepsilon'_0}. \quad (16)$$

The refractivity,  $n - 1$ , is then finally assessed as the average of  $(n - 1)(t)$ , calculated from Eq. (16) with  $\Delta f_{UW}(t)$  given by Eq. (15), over a suitable time interval of the filling measurement cavity section (for the case with 100 s long gas modulation cycles, typically for 10 s, between 40 and 50 s after the filling of the measurement cavity), schematically illustrated by the data points within the red circle in panel d in Fig. 19 below.

As is discussed in some detail below, by these procedures the influence of several types of disturbances, comprising noise, fluctuations, and drifts, can be efficiently mitigated [26, 54, 65].

It can finally be concluded that Eq. (16) provides a convenient means to assess refractivity from a variety of systems using repeated fillings and emptyings of the measurement cavity, in particular those that assess pressure on a "real-time" basis, not only when the GAMOR methodology is utilized.

<sup>44</sup>For the case when these two conditions do not hold, an equation corresponding to Eq. (16) should be exchanged to one based on Eq. (5).

## 6.4 Theoretical analysis and explication of the ability of the GAMOR methodology to mitigate the influence of disturbances

As was alluded to above, independent of whether the GAMOR methodology is used or not, assessments of refractivity (and thereby pressure) by refractometry rely, in general, on (at least) two assessments, one with and one without gas in the measurement cavity. It has been found that the two cornerstones of the GAMOR methodology<sup>45</sup> play an important role in the extent to which the assessment of refractivity is influenced by various types of disturbances the system is exposed to.

To properly assess the ability of the GAMOR methodology to reduce the influence of various types of disturbances on the assessment of refractivity, two scientific works dedicated to the concept have been published; one, regarding the ability of gas modulation to mitigate the influence of fluctuations in refractometry, was performed just prior to the initiation of the EMPIR QuantumPascal project [65], while the other, addressing the ability of the GAMOR methodology to mitigate the influence of drifts [54], was made as a part of the project.<sup>46</sup>

### 6.4.1 Ability of the GAMOR methodology to mitigate the influence of fluctuations

To provide an intuitive understanding of how the length of the gas modulation cycle<sup>47</sup> can influence

<sup>45</sup>A short time separation between these two assessments and, to assess the empty measurement cavity beat frequency at the time when the filled measurement cavity assessment is performed, the use of interpolation between two evacuated measurement cavity beat frequency assessments, one performed before and one after the filled cavity assessments.

<sup>46</sup>The reason for treating fluctuations separately from drifts was that the two types of disturbances, which appear at dissimilar time scales, affect refractometry assessments dissimilarly and they therefore need to be described in different manners (mathematically modelled as Fourier and Taylor series, respectively).

<sup>47</sup>Although, when unmodulated refractometry is performed, it is natural to see the time separation between the empty and filled measurement cavity assessments as "the gas exchange time", while, when gas modulation is utilized, the same entity alternatively is referred to as the "length of the gas modulation cycle", or simply the "gas modulation period". To be able to compare various modes of operation of refractometry (primarily unmodulated and modulated refractometry), we will henceforth denote all of them either the "length of the gas modulation cycle" or the "gas modulation period" and denoted them  $t_{mod}$ .

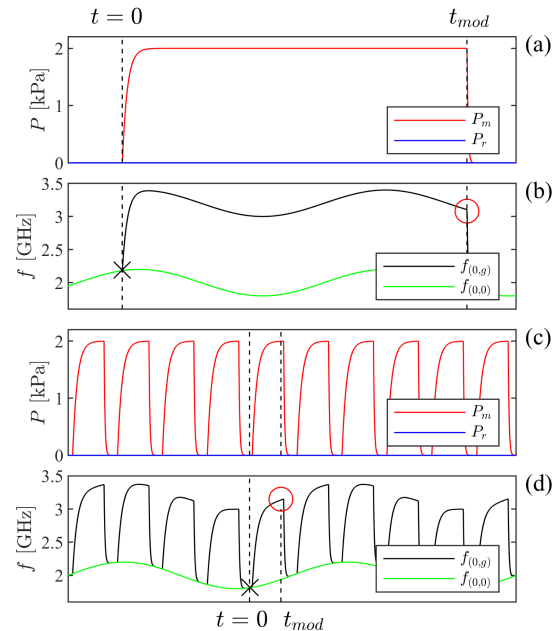
how much of a given fluctuation the detection process will pick up (or be affected by), a theoretical description was developed for the influence of fluctuations, modeled as a set of Fourier components, on refractometry in the absence and presence of the gas modulation [65].

Figure (17) displays, by the panels (a) and (c), a schematic illustration of the gas filling-and-emptying process for DFPC refractometry when assessing a pressure of 2 kPa in the absence and presence of gas modulation, respectively. The panels (b) and (d) show the developments of the associated beat frequencies in the presence of an individual Fourier component of a fluctuation,  $f_D$ . For illustrative purposes, it was assumed that the period of the Fourier component is similar to the gas modulation period in the unmodulated case. Since the latter most often is significantly longer than the modulation period when gas modulation is utilized, the period of the fluctuation can be significantly longer than the modulation period of the modulated assessment.<sup>48</sup>

The instants for the two beat frequency measurements in the panels (a) and (b) are marked by vertical dashed lines (the left and right lines represent the empty and filled measurement cavity assessments, respectively). Although there is one pair of beat frequency assessments for each modulation cycle when gas modulation is utilized, again for illustrative purposes, vertical lines have been associated to only one cycle in the panels (c) and (d). Each assessment of beat frequency, marked, for the illustrated cycle, by a circle and a cross for when the measurement cavity is filled with gas and emptied, respectively, comprises an averaging over several data points for a time that is significantly shorter than the length of the gas modulation cycle in the modulated case, typically 10 s.

The model was then used to estimate the fractions of specific Fourier components of a given fluctuation the system picks up (is affected by) as a function of its (Fourier) frequency for two different lengths of the gas modulation cycle ( $t_{mod}$ ),  $10^5$  s (corresponding to 28 hours) and  $10^2$  s, representing typical unmodulated and modulated conditions, respectively [65]. As is shown in that work, it was found that a given refractometry system indeed picks

<sup>48</sup>Note though that although Fig. (17) depicts the modulated case with a gas modulation period that is solely one order of magnitude shorter than what it is in the unmodulated case, though in reality, they often differ by three orders of magnitude or more.



**Figure 17.** Schematic illustration of the gas filling-and-emptying process and the measured beat frequencies when a pressure of 2 kPa is assessed in the presence of a single Fourier component of fluctuations for unmodulated [the panels (a) and (b)] and modulated [the panels (c) and (d)] refractometry. The panels (a) and (c) represent the pressures of the two cavities [the upper (red) curves, those of the measurement cavity; the lower (blue) curves, those of the reference cavity]. The panels (b) and (d) indicate the corresponding beat frequencies [the upper (black) curves, the actual beat frequency when the measurement cavity is filled with gas, i.e.  $f^{(g)}(t)$ , in the figure denoted  $f_{(0,g)}(t)$ ; the lower (green) curves, the empty measurement cavity beat frequency,  $f^{(0)}(t)$ , denoted  $f_{(0,0)}(t)$ ]. Note that, for display reasons, the gas modulation period for the modulated case is only one-tenth of that of the unmodulated case, although, in reality, it is significantly shorter (typically 3 orders of magnitude shorter). Reproduced with permission from Ref. [65].

up (i.e. is affected by) dissimilar amounts of fluctuations depending on the modulation condition.

Figure (18) displays, by the red and blue curves in the panels (a) and (b), the fraction of specific components of fluctuations the system picks up as a function of their Fourier frequency for the case of unmodulated detection (with a gas filling period of  $10^5$  s) and with gas-modulated detection (utilizing a modulation period of  $10^2$  s), respectively. As a means to guide the eye, the black straight lines are the envelopes of the structured responses.

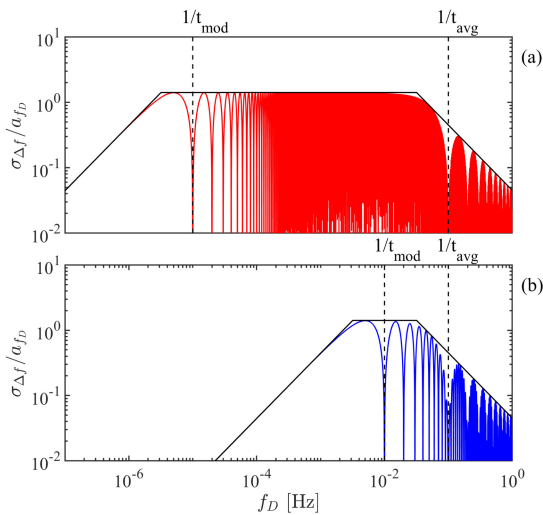


**Figure 18.** The fraction of specific components of fluctuations the system picks up as a function of its Fourier frequency,  $f_D$ , for two different lengths of the gas modulation cycle ( $t_{mod}$ ), representing [panel (a)] unmodulated detection with a gas modulation period of  $10^5$  s, and [panel (b)] with gas-modulated detection, utilizing a modulation period of  $10^2$  s. In both cases, an averaging time ( $t_{avg}$ ) of 10 s has been assumed. The black lines are the envelopes of the responses. Reproduced with permission from Ref. [65].

As can be seen from the leftmost parts of the two panels, the system will pick up only minor fractions (below unity in the figure) of the fluctuations whose Fourier frequencies are lower (smaller) than the inverse of the length of the gas filling/modulation cycle [i.e.  $< 1/(2\pi t_{mod})$ ]; as indicated by the slanted lines in the graphs, for such modulation cycles, it will only pick up a fraction  $2\pi f_D t_{mod}$  of the fluctuation. Since  $t_{mod}$  is much shorter when the system is modulated than when it is not, this implies that when a refractometry system is run under modulated con-

ditions, it will pick up significantly less of any such fluctuations than when it is run unmodulated.<sup>49</sup> This shows that, irrespective of other properties of the system, a refractometry system will always pick up less amount of fluctuations when it is run modulated than when it is run unmodulated.<sup>50</sup>

Hence, in agreement with what has been concluded about other types of modulation techniques in metrology, e.g. frequency and wavelength modulation spectrometry [67–70], the model indicates that rapid gas modulation has the ability to reduce the influence of a significant fraction of the low-frequency fluctuations [primarily those whose frequency is below  $< 1/(2\pi t_{mod})$ ] that often are the dominating ones in measurement systems (due to their anticipated  $1/f$  dependence).<sup>51</sup>

#### 6.4.2 Ability of the GAMOR methodology to mitigate the influence of drifts

The two cornerstones upon which the GAMOR methodology relies (modulation and interpolation) also contribute to a mitigation of the influence of

<sup>49</sup>For the specific case considered in Fig. (18), when being unmodulated (the uppermost panel), it will primarily be affected by (and thus pick-up) fluctuations with Fourier frequencies above  $(1/2\pi)10^{-5}$  Hz (corresponding to fluctuations whose periods are shorter than  $2\pi 10^5$  s) while, when being modulated (the lowermost panel), it will primarily solely be affected by fluctuations whose frequencies are above  $(1/2\pi)10^{-2}$  Hz (corresponding to fluctuations with periods shorter than  $2\pi 10^2$  s). The influence of fluctuations with Fourier frequencies below  $(1/2\pi)10^{-2}$  Hz (corresponding to fluctuations whose periods are longer than  $2\pi 10^2$  s) will thus be mitigated significantly more when the system is run with modulation than when it is not. For Fourier frequencies below  $(1/2\pi)10^{-5}$  Hz, this mitigation is given by the ratio of the lengths of the gas modulation cycles in the two cases, in this particular case by three orders of magnitude.

<sup>50</sup>The figure also shows that the modulation procedure reduces the influence of fluctuations with other frequency components than what the conventionally used averaging processes mitigate (which decrease the influence of fast fluctuations, i.e. the components whose Fourier frequencies are higher than the inverse of the integration time, i.e. the frequencies that are  $> 1/(2\pi t_{avg})$  [corresponding to fluctuation components whose period is  $< (2\pi t_{avg})$ ]; as is shown by the rightmost parts of the panels, in this case, the components whose period is  $< 2\pi 10$  s.

<sup>51</sup>It is worth to note that the analysis above, as well as that given in Axner et al. [65], refer to the influence of solely one of the two cornerstones of the GAMOR methodology on the assessment of refractivity, viz. (i). However, cornerstone (ii) will additionally mitigate the influence of fluctuations when the GAMOR methodology is utilized. The influence of cornerstone (ii) on the ability to mitigate the influence of disturbances is analyzed in some detail below though when the ability to mitigate the influence of drifts is scrutinized.

drifts. However, it has been found that they do not do so to the same extent for all types of drifts. Axner et al. [54] therefore provide a comparison of (both an estimate based on a theoretical analysis and an experimental assessment) the extent to which several types of refractometry methodology<sup>52</sup> are affected by various types of drift.<sup>53</sup>

#### 6.4.2.1 Qualitative description

To depict the ability of the GAMOR methodology to mitigate the influence of campaign-persistent drifts (denoted drifts of type I), and to illustrate the roles the two cornerstones of GAMOR have in this process, the response of a system exposed to this type of drift probed by the GAMOR methodology (for simplicity, in the absence of mode jumps) is schematically depicted in Fig. (19).

Panel (a) illustrates the pressure in the measurement cavity (upper red curve), which is alternately evacuated and filled with gas while the reference cavity (lower blue curve) is held at a constant pressure (in this case for simplicity chosen to be at vacuum).

For the case with a drift of type I, the frequencies of both the measurement and the reference lasers, shown in panel (b), will be affected (although to dissimilar extent). This implies that the beat frequency, assessed as the difference between the two curves in panel (b), displayed by the uppermost (black) curve in panel (c), likewise will be affected by the drifts.

The lower green line in the same panel, which

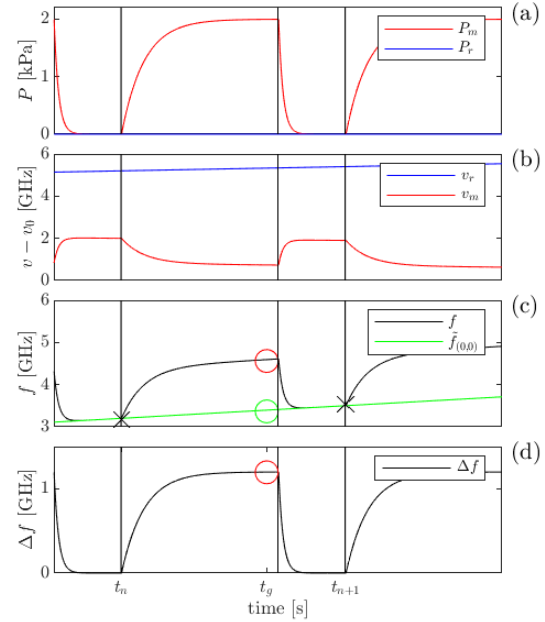


**Figure 19.** The principles of GAMOR on a system exposed to drifts of type I displayed over two modulation cycles. Panel (a) displays, by the upper red and the lower blue curves, the pressures in the measurement and reference cavities, respectively, as functions of time. Panel (b) shows the corresponding frequencies of the two lasers (for simplicity, in the absence of mode jumps and offset to a common frequency). Panel (c) illustrates, by the upper black curve, the corresponding beat frequency. The  $\times$  markers represent empty cavity beat frequency assessments while the green line, denoted  $\tilde{f}_{(0,0)}(t)$ , corresponds to the inter-cycle evacuated measurement cavity beat frequency, in Eq. (14) denoted  $\tilde{f}_{UW}^{(0)}(t)$ , constructed as a linear interpolation between the two evacuated measurement cavity assessments. Panel (d) displays the drift-corrected shift in beat frequency, denoted  $\Delta f$ , corresponding to  $\Delta f_{UW}(t)$  in Eq. (16), given by the difference between the beat frequency measured with gas in the measurement cavity,  $f_{UW}^{(g)}(t)$ , and the "baseline", given by the interpolated evacuated measurement cavity beat frequency,  $\tilde{f}_{UW}^{(0)}(t)$ . Reproduced with permission from Ref. [54].

<sup>52</sup>Unmodulated noninterpolated (UMNI) refractometry [both single-FPC (SFPC) refractometry and DFPC refractometry]; unmodulated interpolated (UMI) refractometry; modulated noninterpolated (MNI) refractometry; and GAMOR, representing modulated interpolated refractometry.

<sup>53</sup>It was found suitable to distinguish between the drifts that affect the cavity mode frequencies persistently and continuously during the entire measurement campaign, irrespective of the state of the gas modulation cycle, referred to as campaign-persistent drifts (denoted type I), from those that are reset once per gas modulation cycle by the gas modulation process (so the drift process starts over for each modulation cycle), referred to as cycle-limited drifts (referred to as type II). The type II drifts, in turn, are separated into two subcategories, viz., those that affect the refractivity of the gas in the reference and measurement cavities, (a) and (b) respectively. Drifts of the physical lengths of the cavities are thus drifts of type I. Leakages and outgassing into the reference cavity represent drifts of type I for the case the reference cavity is sealed off during the entire measurement campaign while they constitute drifts of type IIa for the case the reference cavity is evacuated once per gas modulation cycle. Leakages or outgassing into the measurement cavity are of type IIb.

has been constructed according to Eq. (14) as a linear interpolation between two evacuated measurement cavity assessments, indicated by  $\times$  markers, represents the estimated inter-cycle interpolated evacuated measurement cavity beat frequency.<sup>54</sup>

Panel (d), finally, displays, by the sole black curve, the drift-corrected shift in beat frequency,  $\Delta f(t)$ , given by the difference between the two curves displayed in panel (c), i.e. the difference between the beat frequency measured when the measurement cavity contains gas and the interpolated evacuated measurement cavity beat frequency,  $f^{(g)}(t) - \tilde{f}_{UV}^{(0)}(t)$ . The value of the drift-corrected shift in beat frequency at the position of the red circle,  $\Delta f(t_g)$ , represents the data used for the assessments of refractivity by use of Eq. (16) above.

This schematic illustration thus indicates graphically, and thereby qualitatively, that the influence of drifts can efficiently be mitigated by the interpolation procedure that constitutes one of the cornerstones of GAMOR.

#### 6.4.2.2 Quantitative analysis

To quantitatively assess the ability of GAMOR to reduce the influence of campaign-persistent drifts, such a drift of the evacuated measurement cavity beat frequency, modelled with both linear and non-linear contributions according to the Eqs. (B.1)-(B.3) in Appendix B (and further defined there), is illustrated by the uppermost curve in the center of the graph in Fig. (20).

Since, in the unmodulated case, the shift of the beat frequency used for assessment of refractivity by the Eqs. (13) - (16) is given by the difference between the beat frequency measured when there is gas in the measurement cavity at the time instant  $t_g$  and that when it is evacuated at  $t_n$ , the error in the assessment of the beat frequency is given by the shift in the evacuated measurement cavity beat frequency between these two time instants,  $f^{(0)}(t_g) - f^{(0)}(t_n)$ , referred to as  $\delta[\Delta f(t_n, t_g)]$ . This entity is represented by the long (leftmost) green vertical line in Fig. (20).

<sup>54</sup>The red and the green circles in panel (c) represent the values of the beat frequency at the time when the filled measurement cavity assessment is performed,  $f^{(g)}(t_g)$ , and the evacuated measurement cavity beat frequency, estimated by interpolation, at the same time,  $\tilde{f}^{(0)}(t_g)$ , in the figure denoted  $f(t_g)$  and  $\tilde{f}_{(0,0)}(t_g)$ , respectively.

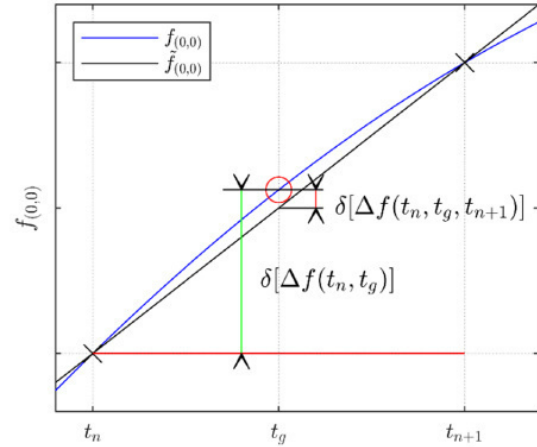


**Figure 20.** Blue solid curve (the uppermost in the center of the graph): the evacuated measurement cavity beat frequency,  $f^{(0)}(t)$  [in the figure denoted  $f_{(0,0)}(t)$ ], for modulated refractometry in the presence of drifts. The beat frequency at time at which the gas measurement is performed is marked by a red circle. The beat frequencies measured at the times of an empty measurement cavity are marked by crosses ( $\times$ ). Reproduced with permission from Ref. [54]

For the interpolated methods, such as GAMOR, the evacuated measurement cavity beat frequency is given by an estimated inter-cycle interpolated evacuated measurement cavity beat frequency,  $\tilde{f}^{(0)}(t)$ , calculated based on two evacuated cavity measurement beat frequencies [in Fig. (20) denoted  $f^{(0)}(t_k)$  and  $f^{(0)}(t_{k+1})$ , and represented by the crosses]. This interpolation, which is based on Eq. (14) and corresponds to the straight green line in Fig. (19c) above, is given by the straight slanted line in Fig. (20). The figure shows that the error made when an interpolated methodology (e.g. GAMOR) is used, which is given by the difference between the real and the interpolated evacuated cavity measurement beat frequencies, denoted  $\delta[\Delta f(t_n, t_g, t_{n+1})]$ , is given by  $f^{(0)}(t_g) - \tilde{f}^{(0)}(t_g)$ , represented by the short (rightmost) red vertical line.

As can be deduced from Fig. (20) together with the Eqs (B.1) - (B.3) in Appendix B, and as is further discussed in Axner et al. [54], this implies that while non-interpolated refractometry is mainly affected by the linear parts of the drift, given by

$$\delta[\Delta f(t_n, t_g)] = \left( \frac{\partial f^{(0)}}{\partial t} \right)_{t_g} t_{mod}, \quad (17)$$

the corresponding entity in the case with interpolation is predominantly affected solely by the first non-linear contribution to the drift, i.e.

$$\delta[\Delta f(t_n, t_g, t_{n+1})] = -\frac{1}{2} \left( \frac{\partial^2 f^{(0)}}{\partial t^2} \right)_{t_g} t_{mod}^2, \quad (18)$$

where the  $(\partial f^{(0)}/\partial t)_{t_g}$  and  $(\partial^2 f^{(0)}/\partial t^2)_{t_g}$  represent the amount of linear and first order non-linear drift of empty cavity mode frequency, respectively.

This clearly illustrates the important fact that while non-interpolated methodologies are affected by the linear part of the drifts, i.e. by the  $(\partial \nu_i^{(0)}/\partial t)_{t_g}$  entity, when interpolation is used, it is solely influenced by non-linear parts of the drift, predominately by the  $(\partial^2 \nu_i^{(0)}/\partial t^2)_{t_g}$  entity. This implies that when interpolation is used, the assessment is not influenced by the dominating linear parts of the drift. The Eqs. (17) and (18) also show that, in both cases, the amount of drift the measurements are influenced by depends on the modulation period is — the shorter the modulation period, the lesser the technique will be affected by drifts, and more so for an interpolated methodology than for a non-interpolated one.

All this illustrates the ability of the GAMOR methodology, which encompasses both short gas modulation periods and an interpolation process, to reduce the influence of drift (in this case of type I).

The interested reader is referred to Axner et al. [54] for its ability to reduce the influence of other types of drift.

## 6.5 A note on the uncertainty in assessments of refractivity

When the major influence of fluctuations and drifts have been mitigated the uncertainty of the refractivity is given by the remaining uncertainty in both a number of assessed entities, predominantly  $\Delta f$ ,  $\nu_0$ ,  $\Delta m_m$  and  $m_{0m}$ , and some system parameters, mainly  $A_R$ ,  $\Theta_G$ ,  $\gamma_c$  (or  $\gamma'_s$ ), and  $\epsilon'$  (or  $\epsilon'_0$ ), together with some virial coefficients (see section 6.8.3.5 below as well as Silander et al. [37] and Silander et al. [38]).

It should be though noticed that, for all pressures except the lowest ones (i.e. from a few kPa and

above), the leading term in the expression for the refractivity in Eq. (16) is the  $\frac{\Delta m_m}{m_{0m}}$  part of the  $\frac{|\Delta f_{UV}|}{\nu_{0m}}$  entity [denoted  $\frac{\Delta m}{m_0}$  in Eq. (5)].

It should furthermore be clear that  $\Delta m_m$  (and  $\Delta m$ ) can be assessed without any uncertainty (since it is in general a one- or two-digit integer). It should additionally be noticed that, since  $m_{0m}$  (and  $m_0$ ) represent mode numbers, they are also integers. As can be deduced from Eq. (2), the latter ones can most conveniently be assessed as the closest integer to the ratio of  $\nu'_0$  and the free-spectral-range ( $FSR$ ), i.e. as  $Int\left(\frac{\nu'_0}{FSR}\right)$ , where the  $FSR$ , according to the same equation, is defined as  $\nu(m_0 + 1) - \nu(m_0)$  and given by  $\frac{c}{2L'_0}$ . This implies that, as long as  $\nu'_0$  and  $FSR$  have sufficiently small relative uncertainties (typically both  $< \frac{1}{2m_{0m}}$ ), also  $m_{0m}$  can be assessed without any uncertainty. This implies that the leading term in the numerator in the expression for the refractivity, the  $\frac{\Delta m_m}{m_{0m}}$  part of the  $\frac{|\Delta f_{UV}|}{\nu_{0m}}$  entity (or the  $\frac{\Delta m}{m_0}$ ), in practice does not provide any uncertainty [38]. This implies, in turn, that for the case when  $\Delta f \approx 0$ , the main uncertainty in the assessment of refractivity lies in the uncertainties of  $\epsilon'_0$  and  $\nu_0$ .

As was alluded to in section 3.3.1.2 above, and as is further discussed in section 6.8.3.3 below, a procedure for how to assess  $\epsilon'_0$  with an accuracy contributing in the low parts-per-million (ppm,  $10^{-6}$ ) range has recently been developed by Zakrisson et al. [46]. This procedure is further described in section 6.8.3.3 below.

A procedure for how to assess  $\nu_0$  with an uncertainty that is below that of a conventional wavelength meter although only such a device is available at the time of the assessment is presently under development by Silander et al. Its basics and performances will be presented in an upcoming work.

When molar density or pressure are assessed, additional uncertainties originate from the molecular constants of the gas addressed (the molar polarizability and virial coefficients) and the assessment of temperature, respectively.

## 6.6 Experimental Setup

### 6.6.1 GAMOR instrumentation - General realization

A GAMOR instrumentation comprises two main parts, a refractometry system and a gas handling sys-

tem.

The refractometry systems so far realized for GAMOR have all been utilizing a DFPC [26, 27, 30, 37–41, 46, 49–52, 54–56, 65, 66]. In addition to the cavity system, they contain a number of optical, acousto-optic, and electro-optic devices used to control, modulate, and assess the frequency of the light.

The gas handling system connects the cavities with a gas supply, the device whose pressure is assessed, and a gas evacuation system. It contains a number of valves and tubing that control the filling and evacuation of the cavities in an automated and predetermined manner in such a way the system is fully autonomous; it can work unattended 24/7 for any length of time.

Over the years, several "generations" of instrumentation have been developed. Since Invar is a material that has a number of advantageous properties for refractometry (see below), and since the GAMOR methodology can mitigate the drawbacks of its disadvantageous properties (e.g. a thermal expansion coefficient that is larger than that of many types of glass), the most recent refractometry system, which has shown best performance and therefore has been used most lately, has been constructed around an Invar-based DFPC system. This system, which in short is referred to as the "Invar-based DFPC system", is briefly described below. A more detailed description is given elsewhere [39, 49].

## 6.6.2 The Invar-based DFPC system

### 6.6.2.1 Advantages of constructing a FPC system made of Invar

The most prominent reasons why Invar can be seen as an appealing material for refractometry are the following ones [49, 50]:

- (i) Invar has a *high volumetric heat capacity*. This implies that a given amount of energy (supplied by the gas) only provides a small temperature increase in the spacer material;
- (ii) It has a *high thermal conductivity*. This implies that any possible small temperature inhomogeneity created by the filling or evacuation of gas will rapidly spread in the system (significantly faster than in systems with cavity spacers made of glass materials, with larger gas volumes or with heat islands) so as to make the temperature of the DFPC-system homogeneous

in a short time, which is a prerequisite for an accurate assessment of the temperature of the gas when using short modulation cycles;

- (iii) It has a *high Young's modulus*, which gives the cavity a lower pressure induced deformation;
- (iv) It has a *low degree of He diffusivity and permeation*, significantly lower than that of ULE glass. This implies that there are virtually no memory effects when He is addressed; and
- (v) Invar can be *machined in a standard metal workshop*. This implies that more complicate geometries can be created swiftly and to a low cost.

This has allowed Invar-based FPC-systems to be constructed with a number of appealing features, e.g.:

- (vi) The cavity system can be made "*closed*". This implies that the gas does not fill a volume surrounding the spacer as is the case for an "open" system; instead it fills only one of the cavities. This restricts the amount of gas being transferred into the refractometer in a single gas filling cycle;
- (vii) Each cavity can be manufactured with a *narrow bore* (with a radius of 3 mm). This implies that the gas rapidly takes the temperature of the cavity wall (within a fraction of a second) and that each filling of gas brings in only a small volume of gas (with a spacer length of 148 mm,  $< 5 \text{ cm}^3$ ), and thereby, when 100 kPa is addressed, only a small amount of energy ( $< 0.5 \text{ J}$ ), so as to reduce the amount of *pV*-work;
- (viii) The system can be constructed *without any heat islands* (i.e. regions that are connected with low thermal conductance), which additionally adds to the ability that a small temperature inhomogeneity created by the filling or evacuation of gas will rapidly spread in the system so as to make the temperature of the DFPC-system homogeneous in a short time; and
- (ix) *The temperature of the cavity spacer* can be assessed by the use of sensors either placed in holes drilled into the cavity spacer (three Pt-100) or wrapped around the outside of the spacer (a thermocouple) whose output is *referred to a gallium fix point cell*. This implies

that the assessment of gas temperature is not affected by any possible homogeneous heating of the cavity spacer; it is only influenced by the difference in temperature between the cavity spacer at the position(s) of the sensors and that of the cavity wall.

Based on this, as was shown in Fig. 2, a GAMOR-based system based on an Invar-based DFPC refractometer, has therefore been realized and characterized [37, 49, 50].

### 6.6.2.2 The refractometry system

As was alluded to in section 3.2.4.1.2 above, the Invar-based system, shown in Fig. 2, comprises an Invar-based DFPC that is precision machined from a Ø60 mm Invar rod that has a finesse of  $10^4$  and, for the wavelength used, an FSR of 1 GHz [49].

It also comprises a number of devices that make possible an efficient and expeditious probing of longitudinal cavity modes of the DFPC. A schematic of the system is shown in Fig 21.

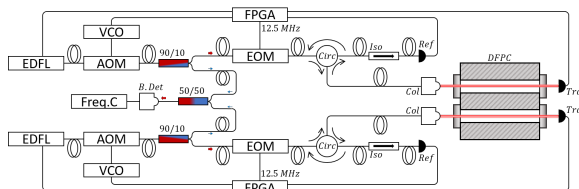


**Figure 21.** Schematic illustration of the refractometer setup. EDFL: Er-doped fiber laser; AOM: acousto-optic modulator; 90/10: 90/10 fiber splitter; EOM: electro-optic modulator; Circ: optical circulator; Iso: optical isolator; Ref: fast photodetector for the reflected light; Col: collimator; DFPC: dual-Fabry-Perot cavity; Tra: large area photodetector for the transmitted light; FPGA: field programmable gate array, VCO: voltage controlled oscillator; 50/50: 50/50 fiber coupler; B. Det: fast fiber-coupled photodetector for the beat signal; and Freq. C: frequency counter. Reproduced with permission from Ref. [52].

Each cavity is probed by the light from an Er-doped fiber laser (EDFL) at a wavelength of  $1.55 \mu\text{m}$ . Since this wavelength is in the data communication NIR region, there are plenty of fiber-connected devices available. This does not only facilitate the re-

alization of the system, it is also the basis for the sturdiness and reliability of the systems.

The light is coupled into a fiber-coupled acousto-optic modulator (AOM) that uses the acousto-optic effect to shift (by diffraction) the frequency of light using a sound wave. Its first order output, which contains the frequency up-shifted component of the laser light, is coupled to a 90/10 fiber splitter.

The 90% output from the splitter is coupled into an electro-optic modulator (EOM) that, by phase modulation, produces sidebands (at 12.5 MHz) on the monochromatic laser beam for the locking of the laser light to a cavity mode by the Pound-Drever-Hall (PDH) locking technique [71].

The output of the EOM is coupled to an optical circulator (Circ) whose first order output is fed to a custom built collimator (Col). The output of the collimator, which is mode matched to a  $\text{TEM}_{00}$  mode of the cavity, is sent to the cavity. The reflected light, which carries information for the PDH locking, is coupled back into the collimator and routed via the second output of the circulator and an optical isolator (Iso) to a fast photodetector (Ref). The light transmitted through the cavity is monitored by a large area photodetector (Tra).

Each reflection detector is connected to a field programmable gate array (FPGA) that demodulates the signal at the modulation frequency (12.5 MHz) to produce the PDH-error signal. Its slow components ( $<100 \text{ Hz}$ ) are sent to the EDFL-piezo, which provides the "slow" tuning of the frequency of the light, while the fast components ( $>100 \text{ Hz}$ ) are sent to a voltage controlled oscillator (VCO) that produces an RF-signal that drives the AOM around 110 MHz to correct for the rapid fluctuations.

To sample the beat frequency between the two cavities, the 10% outputs from the splitter in each arm are combined in a 50/50 fiber coupler (50/50). The combined light is routed to a fast fiber-coupled photodetector (B. Det) whose RF-signal is measured by a frequency counter (Freq. C). To account for mode jumps done by the automatic relocking routine, as is further discussed below, the voltages sent to the EDFL by the FPGA is monitored by an analogue input module (not in figure).

The refractometry system is described in more detail in [49].

### 6.6.2.3 The gas handling system

A schematic view of the gas handling system is given by Fig. 22. It consists of a combined inlet and gas regulating system, a combined valve control and cavity system, and a gas evacuation system.

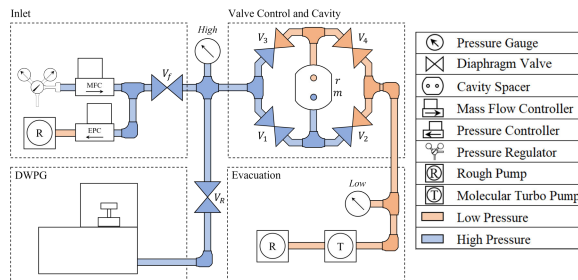


**Figure 22.** The gas handling system, comprising an inlet system, which, by sustaining a constant gas flow between the MFC and EPC, reduces the risk for contamination of the gas in the volume prior to the filling valve ( $V_f$ ), a combined valve control and cavity system, which connects the two cavities to the gas filling and evacuation systems (via valves  $V_1$ ,  $V_2$ ,  $V_3$ , and  $V_4$ ), and a gas evacuation system, which evacuates the selected parts of the valve control and cavity system. MFC: mass flow controller; EPC: electronic pressure controller; T: turbo pump; R: oil-free rough pump; High: a high pressure gauge; and Low: a low pressure gauge.

The inlet system comprises a mass flow controller (MFC) connected to a gas supply, an electronic pressure controller (EPC), and a diaphragm filling valve ( $V_f$ ) used together with the device that regulates the pressure (whose pressure is assessed), here, a dead weight piston gauge (DWPG). To reduce the risk for contamination of the gas in the volume prior to the filling valve, the output of the EPC is continuously evacuated by an oil-free rough pump resulting in a constant gas flow between the MFC and EPC.

The valve control system, which comprises four diaphragm valves connecting the two cavities to the gas filling and evacuation systems via separate paths ( $V_1$ ,  $V_2$ ,  $V_3$ , and  $V_4$ ), is placed on top of the cavity system. The valve that connects the gas system of the refractometer with the measurement cavity is denoted  $V_1$ . All five diaphragm valves are controlled by solenoid pilot valves (not in the figure) via a digital output module (not in the figure).

The evacuation system comprises a molecular turbo pump backed by an oil-free rough pump.

To estimate the pressure under scrutiny, which is needed for the assessment of mode jumps, a pressure gauge (High) is positioned between the filling valve and the combined valve control and cavity system. To monitor the residual pressure, a low pressure gauge (Low) is positioned between the combined valve control and cavity system and the gas evacuation system.

The gas handling system is described in more detail in [39].

## 6.7 A cycle-resolved illustration of the operation and performance of the GAMOR methodology

As was stated above, the gas modulation process in GAMOR comprises a series of periodic modulation cycles of the pressure of gas in the measurement cavity while the pressure in the reference cavity is held constant (often constantly evacuated through valve 4).

To illustrate the data acquisition process, the role of the mode jumps, and the unwrapped beat frequency in the assessment of pressure, Fig. 23 shows some typical cycle resolved raw data from a 200 s long gas modulation cycle, distributed over a filling and an evacuation part of the cycle, each lasting 100 s (denoted  $t_I$  and  $t_{II}$ , defined in Fig. 24), for a pressure of 30.7 kPa [39]. The three panels in Fig. 23 display, for an individual modulation cycle, the measured beat frequency,  $f(t)$ , the cavity mode numbers,  $\Delta m_i(t)$ , for the two cavities, and the corresponding unwrapped beat frequency,  $\Delta f_{UW}(t)$ , as a function of time, respectively.

The modulation cycle is initiated (at time 0) by a closing of valve  $V_2$  and, shortly thereafter, an opening of valve  $V_1$ , which, by volumetric expansion, results in an almost momentary increase of the pressure in the measurement cavity to around 85% of the set pressure. The MFC is then, for a time of 20 s (referred to as  $t_f$  in Fig. 24), until a so called set pressure is reached, filling up the system (by a constant increase of the pressure). As is shown by the panels (a) and (b) in Fig. 23, during this time, the frequency of the measurement laser changes rapidly (the beat frequency decreases as the pressure increases until the laser makes a mode jump, at which the beat frequency makes a sudden jump to a higher value).

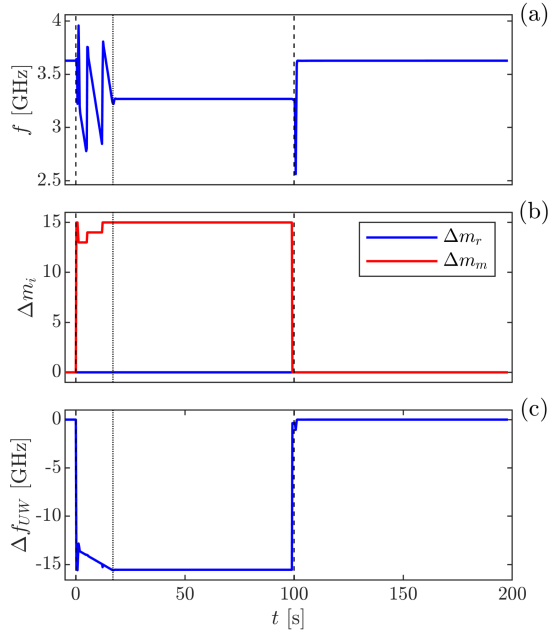


**Figure 23.** The time evolution of: panel (a); the measured beat frequency,  $f(t)$ ; panel (b); the mode numbers addressed,  $\Delta m_i(t)$  with  $i$  being either  $m$  or  $r$  representing the measurement and reference cavities, respectively; and panel (c); the corresponding unwrapped beat frequency,  $\Delta f_{UW}(t)$ , over a 200 s long modulation cycle assessing a pressure of 30.7 kPa. For a description of the various time intervals of the modulation cycle, see the figure caption of Fig. 24. Reproduced with permission from Ref. [39].

After the set pressure is reached (i.e. after ca. 20 s), the piston in the DWPG floats, which, for the remaining 80 s of the 100 s long filling part of the gas modulation cycle (denoted  $t_s$  in Fig. 24), results in a stabilization of the pressure at a constant pressure, given by the DWPG. As has been shown elsewhere, this provides sufficient time for the DWPG to produce a stabilized pressure and for the DFPC to reach a thermal steady-state [52]. Data representing the filled measurement cavity assessment,  $f_{UW}^{(g)}(t)$ , is then taken during the last 10 s of the filling part of the gas modulation cycle (i.e. between  $t = 90$  and 100 s in the Figs. 23 and 24).

The measurement cavity is thereafter evacuated

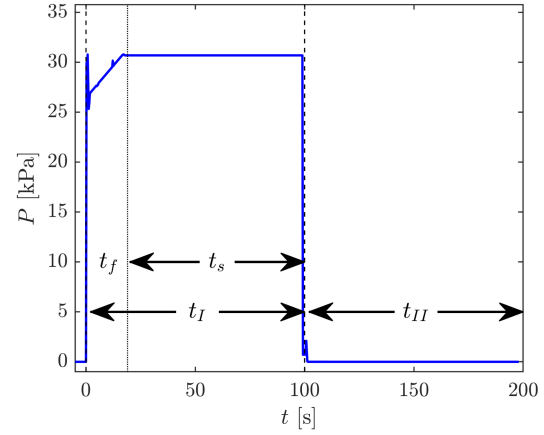


**Figure 24.** The time evolution of the assessed pressure during the 200 s long gas modulation cycle displayed in Fig. 23,  $P(t)$ .  $t_I$  represents the filling part and  $t_{II}$  the evacuation part of the gas modulation cycle, each being 100 s.  $t_f$  is the time during which the MFC is re-filling the system while  $t_s$  is the time during which the DWPG is stabilizing the pressure (i.e. when the piston is floating). Reproduced with permission from Ref. [39].

for 100 s. This takes place by closing valve  $V_1$  and opening valve  $V_2$ , which results in a fast decrease in pressure, manifested by a sudden change in both the unwrapped beat frequency and the mode number addressed (a decrease in the latter). The empty measurement cavity assessment,  $f_{UW}^{(0)}(t)$ , is performed during the last 10 s of this part of the modulation cycle.

When a full cycle is completed, the next one follows automatically.

The assessed signals in the panels (b) and (c) in Fig. 23,  $\Delta f_{UW}$  and the  $\Delta m_i$ , are then converted into pressure by use of the Eqs. (11), (12), and (16). Figure 24 shows the resulting cycle resolved pressure,  $P(t)$ . Note that although mode jumps appear as steps in the beat frequency  $f(t)$  during the first part of the filling stage [panel (a) in Fig. 23], when the changes in cavity mode numbers displayed in panel (b) [i.e. the  $\Delta m_m(t)$  and  $\Delta m_r(t)$ ] are taken into account, the shift in the unwrapped beat frequency,  $\Delta f_{UW}(t)$ , illustrated in panel (c), as well as the assessed pressure, shown in Fig. 24, are al-

most fully continuous functions with solely a few minor "kinks" during the initial part of the gas filling stage. Since the evaluation procedure is not using data points during this part of the filling stage, they do not affect the final assessments.

A more detailed scrutiny of the transient behavior of the assessed beat frequency, i.e.  $\Delta f_{UW}(t)$ , is displayed in Rubin et al. [52]. It is there shown that  $\Delta f_{UW}(t)$  takes its steady-state value within a fraction of the gas filling part of the modulation cycle, typically within 10 s.

## 6.8 Achievements of GAMOR

An important prerequisite for a measurement system exhibiting a small amount of uncertainty is to provide a high degree of precision. As is described above, the main feature of the GAMOR method is to reduce the influence of disturbances, primarily fluctuations and drifts. It is an indisputable fact that this leads to a high degree of precision. To assess to which extent the GAMOR methodology is capable of doing this, this was therefore one of the first objectives during the early development of the GAMOR methodology.

Following some first demonstrations of the ability of the methodology to improve on precision in both non-temperature stabilized [26] and temperature stabilized [27] systems, a pair of experimental verification of the predicted abilities of the GAMOR methodology to mitigate the influence of fluctuations [65] and drifts [54] were performed.

Work was then performed regarding assessment of the precision in the Invar-based DFPC system utilizing the GAMOR methodology [49, 50]. Two Invar-based DFPC GAMOR systems were then assessed for their mutual short-term ability to assess pressure [39].

Following this development, a series of works were then performed, all as a part of the "QuantumPascal" project, to make possible assessments of various physical entities with low uncertainty, addressing concepts such as the influence of thermodynamic effect associated with the filling and emptying of the measurement cavity in the Invar-based DFPC GAMOR system, i.e.,  $pV$ -work [52, 56], means to measure the gas temperature [50, 52], and development of disturbance-resistant methodologies for assessment of cavity deformation [46] and for accurate in-situ assessment of the penetration depth of mir-

rors comprising a QWS of type H [38]. In addition to this, an assessment of the extended uncertainty of the Invar-based DFPC system was performed [37].

Based on these developments it was then possible, largely within the "QuantumPascal" project, to develop transportable refractometer systems that can be used to compare pressure assessing systems at various NMIs [37, 39, 40, 55].

The results of the development of the GAMOR methodology during the last years have recently been summarized various review papers, one published in *Acta IMEKO* regarding recent advances in Fabry-Perot- based refractometry utilizing gas modulation for assessment of pressure [41], one invited published in *Spechrochimica Acta B* focused on the ability of the methodology to assess molar density [66], another, likewise invited, addressing the assessment of pressure, published as a topical review in an special issue of the journal *Journal of Optics* focusing on scientific achievements in the field of optics in Sweden [51], and yet a fourth describing the progress of the entire QuantumPascal project, recently submitted to *Acta IMEKO* [30].

### 6.8.1 Experimental verification of the predicted abilities of the GAMOR methodology to mitigate the influence of disturbances

In order to be able to develop refractometry towards improved performance, it is of importance to verify the theoretical predictions of the abilities of the GAMOR methodology to mitigate the influence of fluctuations and drifts that were predicted in the sections 6.4.1 and 6.4.2 above. Experimental investigations of these abilities have therefore been performed.

#### 6.8.1.1 Verification of the predicted ability of GAMOR to reduce the influence of fluctuations

To experimentally verify the predictions of the model for reduction of the influence of fluctuations from above, which states that the length of the gas modulation cycle plays a significant role in mitigating the influence of fluctuations in the system [65], measurements were performed under a given (but typical) set of conditions but evaluated for different cycle lengths. Figure (25) shows the standard devi-

ation of a 50 h long series of measurements of an empty measurement cavity evaluated in eight different ways, corresponding to gas modulation periods,  $t_{mod}$ , ranging from 100 s to 30,000 (8.3 h), as a function of the gas modulation period.

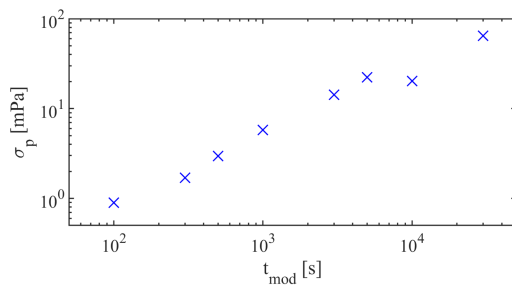


**Figure 25.** Standard deviation of a 50 h long series of measurements of an empty measurement cavity evaluated in eight different ways, corresponding to gas modulation periods,  $t_{mod}$ , ranging from 100 to 30,000 s, as a function of the length the gas modulation cycle. Reproduced with permission from Ref. [65].

The figure shows that the standard deviation decreases significantly with decreased modulation period; in this particular case, more than 50 times (from 50 to 0.9 mPa) as the length of the modulation cycle is decreased from 30,000 to 100 s. This confirms the predictions given in section 6.4.1 about the ability of GAMOR to reduce the influence of fluctuations [65].

To further confirm the alleged advantage of short gas modulation periods, and also illustrate the importance of assessing measured quantities as averages over a multitude of modulation cycles, Fig. (26) displays the Allan deviations of the data displayed in Fig. (25) with the three shortest gas modulation periods [100 s (the lowermost curve), 300 s, and 500 s (the uppermost)] as functions of averaging time.

In agreement with the data shown in Fig. (25), Fig. (26) shows that the Allan deviation of the shortest gas modulation period (100 s) is consistently smaller than those of the other cycle lengths. The data also display that the deviation depends on the averaging time. For averaging times up to around a few thousand seconds, it decreases monotonically with averaging time (thus with a white-noise dependence); from 0.9 mPa, which it takes when there is no averaging, thus for a series of individual modu-

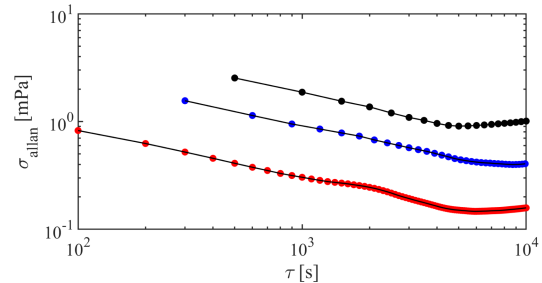


**Figure 26.** Allan deviations of the data representing the three shortest gas modulation cycle times in Fig. 4, viz., 100 s (lowermost, red markers), 300 s (blue markers), and 500 s (uppermost, black markers) as a function of averaging time. Reproduced with permission from Ref. [65].

lation cycles (each being 100 s), down to 0.15 mPa, which it takes for an averaging of 60 cycles (to an averaging time of 6000 s). This thus shows that the influence of disturbances can additionally be reduced by averaging over a number of gas modulation cycles [65].

The data displayed in Fig. (26) also show that for longer averaging times, above 5 000 - 10 000 s (i.e. 1.5 - 3 h), the Allan deviation levels off and starts to increase with averaging time. This indicates that the system is affected by drifts on such time scales. The reason why the data are not affected by drifts until such considerable times as one or three hours is that the gas modulation procedure does not only reduce the influence of fluctuations but also drifts [65].

These measurements do not only verify the predictions of the model regarding the ability of gas modulation to mitigate the influence of fluctuations given in by Axner et al. [65], but also the alleged assumption that a rapid gas modulation process, which is one of the cornerstones on which the GAMOR methodology relies, is highly beneficial for refractometry.

### 6.8.1.2 Verification of the predicted ability of GAMOR to reduce the influence of drifts

To experimentally verify the predictions of the model for the reduction of drifts from above, e.g. the Eqs (17) - (18), a set of measurements were made that was deliberately affected by drifts, viz. by use of a

system not in thermal equilibrium.<sup>55</sup>

Measurements were taken from the Invar-based refractometry system described in this work as well as elsewhere [49] with the measurement cavity being constantly evacuated while the temperature of the cavity spacer was increased from room temperature (23 °C) to the melting temperature of Ga (29.76 °C). As a result of this, the length of both cavities increased monotonically during this process.<sup>56</sup>

Figure (27) shows the error the system makes in the assessment of refractivity (expressed in terms of the corresponding pressure) as a function of the length of the gas modulation cycle (for cycle lengths ranging from 100 to 51 200 s) in the absence and presence of interpolation (by the uppermost and lowermost curve, respectively) [54].

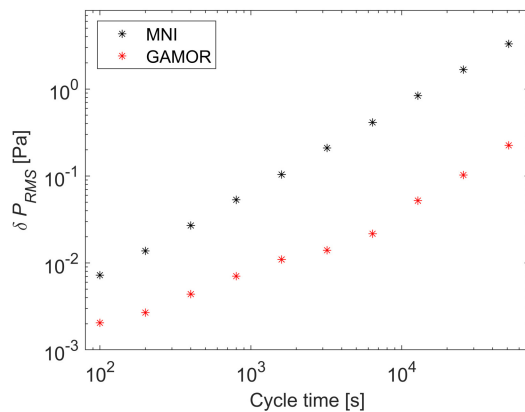


**Figure 27.** The error in the assessment of pressure as a function of the length of the modulation cycle of the Invar-based refractometry system when its temperature was increased from room temperature (23 °C) to the melting temperature of Ga (29.76 °C), evaluated by non-interpolated and interpolated (i.e. GAMOR) refractometry (the uppermost and lowermost data sets, respectively). Reproduced with permission from Ref. [54]

<sup>55</sup>This does not imply that the abilities of the various methodologies addressed to mitigate the influence of drift only appear (or are of importance) in systems with significant amounts of drift; on the contrary, they take place also in well-stabilized systems with less amounts of drifts.

<sup>56</sup>Since the changes in length of the two cavities were not identical (the heating process affected the two cavities in a slightly dissimilar manner), the beat frequency between the two laser fields drifted over time.

The data show first of all that the error in the assessment decreases significantly with decreased length of the gas modulation cycle, for the unmodulated case, from 3.3 Pa (for a gas modulation cycle length of 51 200 s) to 7 mPa (for a length of 100 s). The lower set of data (ranging from 0.2 Pa to 2 mPa) represents the corresponding cases for the GAMOR methodology [54].

These data then also indicate that the uncertainties in the assessments are consistently lower when interpolation is utilized (in the figure denoted GAMOR) than when non-interpolated methodologies (denoted MNI) are used [54].

These behaviors are in full agreement with the model presented in section 6.4.2, and thus verify its predictions. It also illustrates clearly the advantage of GAMOR (represented by the leftmost red data point in the lower set of data, 2 mPa) over conventional unmodulated refractometry (represented by the rightmost black data point in the upper set of data, at 3.3 Pa) regarding the ability to reduce the pick-up of drifts.

## 6.8.2 Demonstration of the ability of the GAMOR methodology to improve on precision

It has repeatedly been shown that the GAMOR methodology has an outstanding ability to reduce the influence of fluctuations and drifts on the assessments of refractivity to such an extent that the precision of the assessments can be significantly improved. The extent to which the methodology is capable of mitigating disturbances has therefore been scrutinized under a variety of conditions.

### 6.8.2.1 Ability of GAMOR to reduce the influence of drifts from a non-temperature stabilized system

As a part of a previous EMPIR project (JRP 14IND06 ‘Pres2Vac’), it was demonstrated that the GAMOR methodology, when applied to a DFPC refractometer utilizing a non-temperature-stabilized cavity spacer made of Zerodur, could reduce the influence of drifts more than 3 orders of magnitude (decreasing the standard deviation of a given set of assessments from 6.4 Pa to 3.5 mPa) [26].

The data in Fig. (28) show, by panel (a), that, while the temperature drifts in a non-linear manner 250 mK over a period of 24 h (uppermost curve, blue

in color, right axis), the pressure assessed by ordinary single FP cavity refractometry drifts 20 Pa (lowermost curve, red in color, left axis). The pressure assessed by the GAMOR methodology (middle curve, black in color, left axis) does not show any fluctuations on the given scale ( $\pm 15$  Pa). Panel (b) though, which displays the pressure assessed by the GAMOR methodology on an enlarged scale ( $\pm 5$  mPa), shows that the refractometer has solely picked up disturbances on the low mPa scale (with a  $2\sigma$  of 3 mPa) when the GAMOR methodology was used [26].

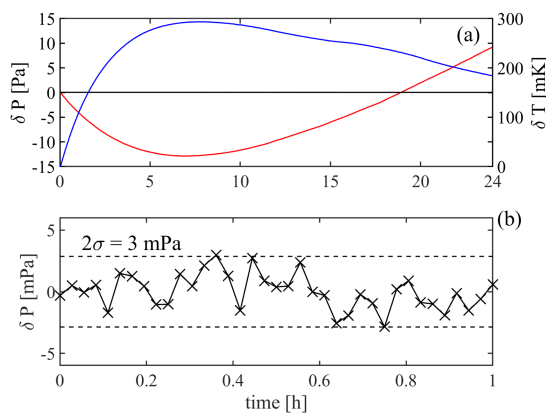


**Figure 28.** Panel (a): A 24 h long series of measurement of an empty measurement cavity evaluated by two different means: the lowermost curve (red in color) - without gas modulation, referred to as a static mode of detection, and the almost fully horizontal curve (black in color) - by use of the GAMOR methodology (both left axis). The uppermost curve (blue in color and right axis) represents the temperature. Panel (b): a zoom in of the first hour section of the data taken with the GAMOR methodology. Reproduced with permission from Ref. [26]

### 6.8.2.2 An alternative realization of GAMOR — Gas-equilibration GAMOR (GEq-GAMOR)

The GAMOR methodology can, in fact, be carried out in several ways. In contrast to the conventional one, described above, in which the measurement cavity is repeatedly filled and emptied with gas while the reference cavity is held at a constant pressure, at vacuum, denoted single cavity modulated

GAMOR (SCM-GAMOR), it was demonstrated, also as a part of the previous EMPIR project "Pres2Vac", that is alternatively possible, instead of evacuating the measurement cavity, to equilibrate the pressure in the two cavities. The alleged advantage of this methodology, which goes under the name Gas-equilibration GAMOR (GEq-GAMOR), is that the time it takes to obtain adequate conditions for the reference measurements can be shortened, whereby more time can be spent on the averaging of data when there is gas in the measurement cavity [27].

As is shown in Fig. (29), using this methodology, addressing a pressure of  $N_2$  of 4303 Pa inside a temperature stabilized Zerodur cavity, a sub-ppm ( $1\sigma$ ) precision (i.e.  $< 4$  mPa) could be demonstrated. More specifically, it was shown that the system (the red curve, the third set of data counted from above) could provide a response for short integration times (up to 10 min) of  $1.5 \text{ mPa} (\text{cycle})^{(1/2)}$ , while for longer integration times (up to 18 h), it showed an integration time-independent Allan deviation of 1 mPa (corresponding to a precision, defined as twice the Allan deviation, of 0.5 ppm), exceeding the performance of the SCM-GAMOR methodology (the blue curve, the uppermost set of data) by a factor of 2 and 8, respectively [27].

Since the GEq-GAMOR methodology could be performed with averaging times of 40 s while the ordinary SCM-GAMOR methodology utilized 10 s, this methodology demonstrated performance similar to expectations [a reduction of the white noise response by a factory of 2, given by  $\sqrt{(40/10)}$ ].

Partly based on these two early GAMOR works [26, 27], the 'Pres2Vac' project produced recommendations for the use of gas modulated optical based methods for "assessments of absolute, positive and negative pressures in the 1 Pa to  $10^4$  Pa range", both with regard to their use and a requirement of further research and development to reach the full potential of the technique in the longer term.

### 6.8.2.3 Assessment of the precision of the Invar-based DFPC system utilizing the GAMOR methodology

Utilizing the Invar-based GAMOR instrumentation described in section 6.6.2, it has been demonstrated that this system can outperform the systems based on Zerodur® and provide assessments with sub-ppm precision. Figure (30) shows a set of uninterrupted

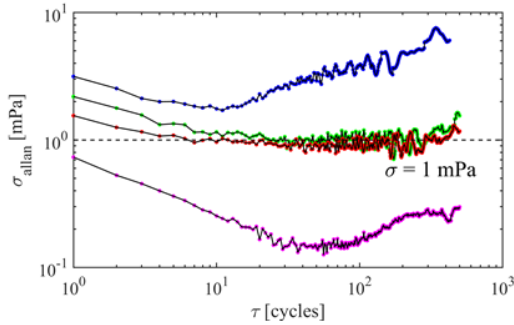


**Figure 29.** Allan deviations,  $\sigma_{Allan}$ , of data taken from a temperature regulated DFPC made of Zerodur: Blue markers (uppermost set of data): ordinary single cavity modulated GAMOR (SCM-GAMOR) [26], and red markers (third set of data counted from above): GEq-GAMOR, both taken for a set pressure of 4303 Pa. Green markers (the second set of data) represent the GEq-GAMOR data evaluated with a reduced integration time of the residual gas pressure measurement (see [27] for details). The violet markers (lowermost set of data): GEq-GAMOR, zero pressure measurement. Dashed line: an Allan deviation of 1 mPa. Reproduced with permission from Ref. [27]

measurement data taken over 24 h by the Invar-based DFPC instrumentation, presented as the difference,  $\Delta P$ , between the pressure measured by the refractometer,  $P$ , assessed from the Eqs. (11), (12), and (16), using molecular parameter values from [26], corrected by a deformation independent correction term  $\psi$  [46], and the estimated set-pressure of the DWPG,  $P_{Set}$ , for an empty measurement cavity and one at a pressure of 4303 Pa [49].

The data show, over a period of 24 h, for the empty measurement cavity data (the upper set of data, blue in color), a  $\pm 2\sigma$  spread of 0.7 mPa (corresponding to spreads in refractivity and beat frequency of  $2 \times 10^{-12}$  and 370 Hz, respectively). For 4303 Pa (the lower set of data, red in color), the data have a spread of 3 mPa (0.7 ppm) and a mean deviation of -4.7 mPa (1.1 ppm) [49].

Although the lower curve in Fig. (30) shows a noticeable amount of fluctuations, it is worth to note that the precision of the data is, in fact, excellent. This is presented, for illustrative purposes, by Fig. (31), which displays, as a function of time,

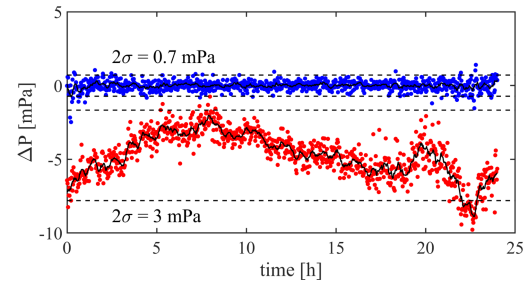


**Figure 30.** The difference between the pressure of nitrogen assessed by the refractometer (corrected, according to Ref. [46] by a deformation-independent correction term, denoted  $\psi$ ),  $P$ , and the estimated pressure supplied to the refractometer,  $P_{Set}$ , denoted  $\Delta P$ , for an empty cavity (blue set of data) and at a pressure of 4303 Pa (red set of data), respectively. The black curves represent moving averages of 10 samples. The dashed lines correspond to  $\pm 2\sigma$  of the assessed pressure difference. Reproduced with permission from Ref. [49].

this GAMOR data in seven separate panels, (a) – (g), with successively enlarged scales of the y-axis. While panel (a) displays the signal with a y-scale ranging over 8 kPa, the subsequent panels (b) – (g) display the same data with successively one order of magnitude smaller range of the y-axis: i.e., 800 Pa, 80 Pa, 8 Pa, 0.8 Pa, 0.08 Pa and 0.008 Pa, respectively. Each red data point represents an individual GAMOR cycle, while the black, dashed curves represent moving averages of 10 cycles [66].

To analyze this data in more detail, Fig. (32) displays a comparison between the Allan deviations of the GAMOR data from the Invar-based system presented in Fig. (30) (given by the blue and red markers) and a system with a Zerodur spacer (green markers, from Silander et al. [27]) [49].

This data show, as is expected of GAMOR, which is insensitive to long-term drifts of the cavity length, that the Allan deviation of data taken from an empty cavity (in which temperature drifts become irrelevant) does not show any noticeable drift (lowermost curve, blue in Fig. 32); Such measurements are solely limited by white noise, in this case at a level of  $3 \text{ mPa s}^{1/2}$ , providing a minimum deviation of 0.03 mPa (which corresponds to a deviation of the detected beat frequency of 16 Hz) at  $10^4 \text{ s}$ . This

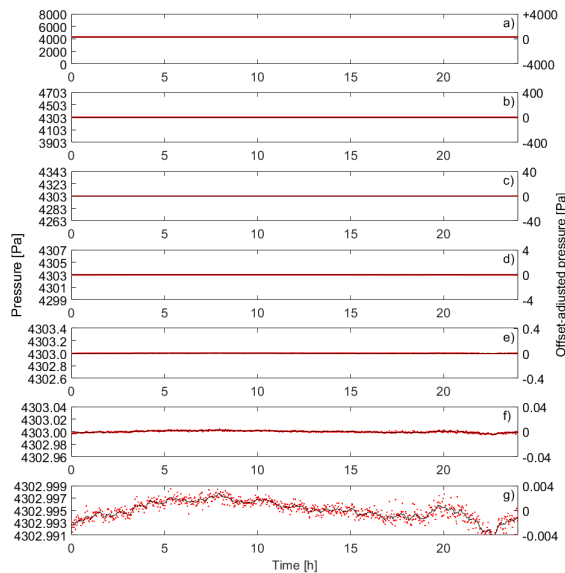


**Figure 31.** The GAMOR signal from 4303 Pa of nitrogen measured over 24 hours. The various panels (a) – (g) display the same set of data with successively smaller scales of the y-axis. Left axis: Pressure; Right axis: Offset-adjusted pressure. Panel (a) displays the response with an y-axis scale of 8 000 Pa while the subsequent panels (b) – (g) display the same data with successively one order of magnitude smaller range of the y-axis: i.e., the panels (b) – (g) cover 800 Pa, 80 Pa, 8 Pa, 0.8 Pa, 0.08 Pa and 0.008 Pa, respectively. Hence, panel (g) is an enlargement of panel (a) by six orders of magnitude. Each red data point represents an individual GAMOR cycle. The black, dashed curves represent moving averages of 10 cycles. Reproduced with permission from Ref. [66]

shows, in accordance with assumptions and predictions, that the system, within these measurement times, does not pick-up any fluctuations or drifts from an empty measurement cavity assessment [49].

The data taken at 4303 Pa (red markers), on the other hand, show, for measurement times up to 500 s, a slightly higher white noise level of  $7 \text{ mPa s}^{1/2}$ , after which flicker noise or drifts affect the system.

This implies that the 0.7 ppm spread in the low-ermost curve in the Fig. (30) is mainly attributed

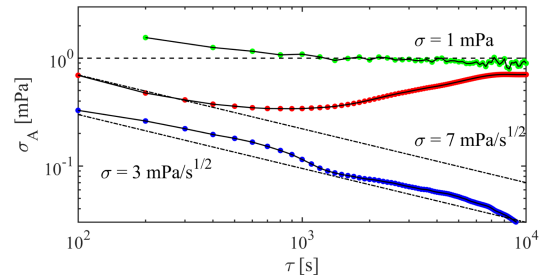


**Figure 32.** Allan deviations,  $\sigma_A$ , of pressure assessments made by the GAMOR methodology. Green markers: data earlier obtained at 4303 Pa from a Zerodur cavity [27]; Red markers: data taken at the same pressure by the Invar-based system presented in [49]; Blue markers: data taken by the Invar-based system with an empty measurement cavity; Dashed horizontal line: an Allan deviation of 1 mPa; Dash-dotted slanting lines: Allan deviations corresponding to a white noise level of 7 and 3  $\text{mPa s}^{1/2}$ , respectively. Reproduced with permission from Ref. [49].

to drifts in the temperature assessments and of a pressure gauge in the system. The mean deviation between the pressure measured by the refractometer and the set-pressure of the pressure balance at 4303 Pa of 1.1 ppm originates mainly from drifts in the temperature assessments between the instants of characterization and measurements [49].

This is a clear improvement from previous assessments based on a Zerodur cavity for which the white noise levels of the empty cavity measurement and that at 4303 Pa were 10 and 22  $\text{mPa s}^{1/2}$ , respectively (where the latter are displayed by the green markers in Fig. 32 [27]) [49].

The Allan plot analysis shows that the optimum integration time for assessment of 4303 Pa was around 1000 s (corresponding to 10 modulation cycles). Under these conditions, the system demonstrated a minimum (Allan) deviation of 0.34 mPa [which corresponds to relative deviation (or  $1\sigma$  precision) of 0.08 ppm] [49]. For longer integration times, the deviation increased (attributed to fluctuations in the temperature measurement module) before it reached a plateau of 0.7 mPa (at 7 000 s).

The optimum level of deviation of the system was found to be significantly better, and that of the plateau slightly better, than the 0.9 - 1 mPa reached

with the Zerodur cavity [27].

#### 6.8.2.4 Short-term performance of two Invar-based DFPC GAMOR systems for assessment of pressure

There is a number of applications, e.g., characterization of pressure sensors and studies of rapidly changing pressures or processes giving rise to such, for which it is of importance that the system has a fast response. Although several types of refractometers have been scrutinized over the years [10, 13, 14, 20–28, 37, 40, 41, 46, 49, 50, 72], none of them has yet been characterized with respect to its short-term behavior. It is therefore of importance to perform such characterizations. By use of two GAMOR based systems (of which one is the transportable, denoted the "Transportable Optical Pascal", abbreviated the TOP, described in section 6.8.4 below as well as in Forssén et al. [39]), it has been demonstrated that the combination of Invar-based FPC and the GAMOR methodology is suitable also for assessments of pressure shifts with short settling times.

As is shown in Fig. (33), by connecting the aforementioned stationary and the transportable GAMOR-based refractometry systems (where the former is denoted the SOP, the "Stationary Optical Pascal") to the same gas system, whose pressure was set by a common DWPG, their short-term performances could be scrutinized in some detail [39]. As the refractometers were independent, it could be concluded that deviations that are common to both systems are not inherent to any of the refractometers, but rather to the DWPG or the gas handling system. Thereby, by addressing their common response (in reality, the difference between them), it was possible to assess the short-term performances of two independent gas modulated refractometers regarding their ability to assess pressure without any influence from the DWPG or the gas handling system.

Figure (34) show, in panel (a), an enlargement of 70 s of refractometry data taken by the SOP and the TOP from 16 kPa of N<sub>2</sub> generated by a common DWPG. Panel (b) displays the same data in a correlation plot. The latter plot show that the refractometers can provide short-term precision on the 1 s time scale of  $3 \times 10^{-8}$ , which is one order of magnitude better than the corresponding stability of the pressure provided by the DWPG. This illustrates that the stability of such an assessment is not primarily lim-

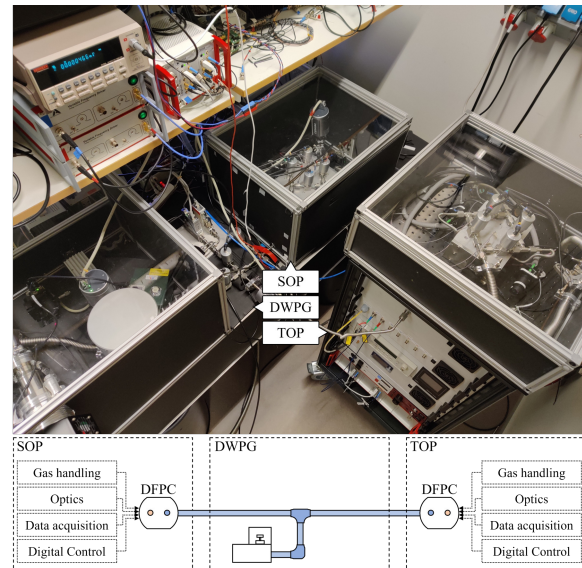


**Figure 33.** The SOP (the stationary optical Pascal) system (in the rightmost box on the optical table) and the TOP (the transportable optical Pascal) system (to the right), both connected to a common DWPG (in the leftmost box on the optical table), gas supply (between the SOP- and DWPG boxes), vacuum system (not in the figure), and computer (for control and data acquisition), together with various electronics (for the SOP, partly seen on the shelves, and, for the TOP, in the rack). The bottom part of the figure shows a schematic illustration of the two refractometers and their connection to the DWPG. Reproduced with permission from Ref. [39]

ited by the refractometer [39]. This opens up for a number of novel applications for refractometry.

#### 6.8.3 Demonstration of the ability of GAMOR-based refractometer systems to provide low uncertainty assessments

To properly assess pressure, and, in particular, if a primary standard is to be realized, it is of importance to not only have an outstanding precision, it is also necessary to certify that the assessments can be made with low enough uncertainty. To be able to achieve this, there are a number of issues that need to be addressed adequately in order for a GAMOR-

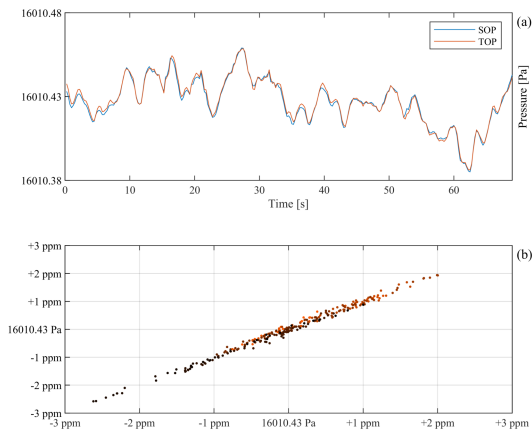


**Figure 34.** Panel a): an enlargement of 70 s of refractometry data taken by the SOP and the TOP from 16 kPa of N<sub>2</sub> generated by a common DWPG. Panel b): A correlation plot of the same data. In the latter panel, the x- and the y-axes represent the pressures assessed by the SOP and the TOP respectively. Time is represented by the color, where the first data points are marked with orange color while the last ones are in black. Reproduced with permission from Ref. [39]

based refractometer system to provide low uncertainty assessments. Of special importance are the influence of thermodynamic effects on the assessments (i.e.,  $pV$ -work) [52, 56], the ability to properly and accurately assess the gas temperature [50, 52], and assess to which extent pressure induced cavity deformation [46], mirror penetration depths [38], and the Gouy phase [38] affect assessments. To address the concept of accuracy, so as to be able to assess the total uncertainty of a pressure assessment, the influences of these concepts on the assessment of pressure by use of the Invar-based DFPC system have been addressed in some detail in a number of separate works [38, 46, 50, 52, 56].

### 6.8.3.1 The influence of thermodynamic effects ( $pV$ -work) on the assessments and the ability to assess gas temperature accurately

To accurately assess pressure, it is vital to certify that the assessments are not affected by any ther-

modynamic effects from the gas filling and emptying processes, i.e.,  $pV$ -work, and to assess the temperature of the gas accurately. The aforementioned features of the GAMOR methodology to mitigate disturbances and to provide an excellent precision (given in the sections 6.8.1 and 6.8.2) provide a number of properties of the system that vouch for both virtually no influence of any  $pV$ -work and a good ability to assess gas temperature.

As was alluded to above (in section 4.1.2.1, recent works by Rubin et al. were dedicated to scrutiny of to which extent the Invar-based DFPC system is affected by  $pV$ -work when the GAMOR methodology is applied [52, 56].

Furthermore, as was mentioned in section 4.1.2.1.1, simulations of gas dynamics showed, among other things, that, primarily due to the "reasons" (vi) and (vii) given in section 6.6.2.1, i.e. that the system is "closed" and that each cavity has been manufactured with a narrow bore (with a radius of 3 mm), the equilibration of pressure in the cavity when nitrogen is let in takes place on a time scale of ten milliseconds and that the gas adopts the temperature of the cavity wall on a time scale of less than a couple of seconds.

In addition, as was commented on in section 4.1.2.1.2) above, simulations of the transfer of heat in the system were used to estimate the characteristic time scale for the heat dissipation process. This was assessed to be in the few or ten second range. The cause for this is, in addition to the "reasons" (vi) and (vii) from above, also (i), (ii), and (viii), which state that Invar has a high volumetric heat capacity, a high thermal conductivity, and that it has been possible to construct the system without any heat islands. More specifically, since the cavity volume is small ( $< 5 \text{ cm}^3$ ), the gas transfers only a small amount of energy ( $< 0.5 \text{ J}$ ) into the system during a gas filling process. Due to the high heat capacity of Invar, this will give rise to only a minor local heating of the cavity spacer. In addition, due to the the large thermal conductivity of Invar (one order of magnitude larger than for typical glasses) and since the system is constructed without heat islands, this minor local heating will rapidly dissipate into the material and provide a small homogeneous change in temperature of the entire spacer block (in the order of 0.3 mK).

As was alluded to in section 4.1.2.1.3 above, it was estimated in that an upper limit for the influence of  $pV$ -work made by nitrogen on the Invar-based

DFPC system, is, for 100 s long modulation cycles, 0.5 mK/100 kPa (or 1.8 ppm/100 kPa) and, for 200 s long cycles, 0.4 mK/100 kPa (or 1.3 ppm/100 kPa) [52].

Moreover, as was discussed in section 4.1.2.1.5, when gas is evacuated from the cavity during the second part of the modulation cycle, a similar amount of energy is removed from the system, giving rise to a similarly sized temperature decrease of the system. The net supply of energy to the cavity from the gas filling and emptying process is therefore practically negligible [52, 56].

Moreover, since the system assesses temperature by the use of sensors placed either in holes drilled in the cavity spacer or wrapped tightly around the outside of the spacer (as shown in section 4.1.1.1), any possible homogeneous heating of the cavity spacer can be measured and will directly be accounted for. Therefore, the pressure assessments are only influenced by the difference between the temperature of the cavity walls and that of the cavity spacer at the position(s) of the sensors. It was found that, under normal conditions (for pressures up to 100 kPa and when the gas modulation periods are 100 or 200 s), this difference will, when the refractivity assessments are made, be minute, well into the sub-mK range [52, 56].

These estimates were compared with experiments. As was discussed in section 4.1.2.1.4 above, since none of these assessment performed in the 4 - 30 kPa range in [52] showed any resolvable effect from  $pV$ -work, they support the estimates of the upper limits for the influence of  $pV$ -work on the assessments of pressure. A subsequent study addressing 100 kPa [56] has shown though that the heating of the cavity spacer in reality is significantly lower than the upper limits predicted by the simulations: the measured temperature deviations was found to be about one third of the simulated upper limits. This suggests that, for the cases of 100 and 200 s long modulation cycles, deviations of 0.16 and 0.12 mK/100 kPa, corresponding to sub-ppm levels/100 kPa, should prevail, respectively.

This implies that the Invar-based DFPC system utilizing the GAMOR methodology is not expected to be significantly affected by thermodynamic processes that are associated with the exchange of gas (i.e.,  $pV$ -work). Such effects are therefore currently not a limiting factor when the Invar-based DFPC GAMOR system is used for assessments of pressure

or if it would be used as a primary pressure standard, both up to atmospheric pressure.

### 6.8.3.2 Development of a Ga fixed-temperature cell for accurate assessment of temperature.

As is shown by Silander et al. [50], and as was alluded to in section 4.1.1.1, to properly assess the temperature of the spacer block of the Invar-based DFPC refractometer, it was equipped with an automated, miniaturized gallium fixed-point cell. Utilizing repeated heating-and-cooling cycles, where each cooling part, which serves as the reference to thermocouple sensor, lasts ca. 100 h.

As was described in some detail in section 4.2.1, it was found that, during the most stable part of the Ga melting cycle, the combined ( $\pm 2\sigma$ ) stability of the fixed-point cell and thermocouple measurement was smaller than 220  $\mu$ K. An estimate of the total uncertainty in the temperature measurement system indicated that it presently amounts to 1.2 mK (4 ppm), dominated by the stability of the nanovoltmeter used for assessment of the thermocouple voltage [50].

### 6.8.3.3 Development of a disturbance-resistant methodology for assessment of cavity deformation

As was alluded to in the section 3.3.1.1, the high precision has also allowed for the realization of a novel, disturbance-resistant methodology for assessment of cavity deformation in FP-based refractometers [46]. It is based on scrutinizing the difference between two pressures: one assessed by the uncharacterized refractometer and the other provided by an external pressure reference system, at a series of (set) pressures for two gases with dissimilar refractivity, He and N<sub>2</sub> [46].

The methodology comprises a plotting of the difference between the external pressure reference and the pressure assessed by the refractometer utilizing an evaluation model that does not take deformation into account for the two gases as a function of pressure. By fitting linear functions to these responses and extracting their slopes, the cavity deformation caused by pressurization could be obtained, in terms of both a net pressure- and net refractivity-normalized relative difference in lengths of the two cavities, i.e.  $(\delta L/L)/P$  and  $\epsilon'$  [46].

A thorough mathematical description of the procedure served as a basis for the evaluation of the basic properties and features of the procedure [46]. This indicated that the cavity deformation assessments are independent of offset errors in both the reference pressure provided by the DWPG and the assessment of gas temperature, and, when the GAMOR methodology is used, that they are only weakly affected by gas leakages and outgassing into the system. This provides a robust methodology for assessment of cavity deformation with small amounts of uncertainties [46].

It was shown that when a high-precision (sub-ppm) refractometer is characterized according to the procedure, and under the condition that high purity gases are used, the deformation could be assessed with such small uncertainty that it contributes to the uncertainty in the assessment of pressure of nitrogen with solely a fraction of the present uncertainty of its molar polarizability [46]. For the case when the SOP had been refurbished and upgraded, it was found that, for the case when the molar polarizability of  $N_2$  was traced to a mechanical pressure standard, the deformation could be assessed with an uncertainty of  $1 \times 10^{-6}$ , viz. to  $1.972(1) \times 10^{-3}$  [37].<sup>57</sup> This implies, in practice, that, as long as gas purity can be sustained, cavity deformation is no longer a limiting factor in FP-based refractometer assessments of pressure of nitrogen.

#### 6.8.3.4 Development of a methodology for accurate in-situ assessment of the penetration depth of mirrors comprising a QWS of type H

When high-reflection mirrors are used, light will not solely be reflected at the front facets of the mirrors — some of the light will penetrate the coating. This implies that the optical length of the cavity will be slightly longer than the physical length.

An experimental methodology for assessment of the influence of the penetration depth of the high-reflection coatings of mirrors comprising a QWS of type H (in which the outermost layer of the coating has the highest index of refraction), which is a commonly used configuration for high-reflection mirrors, on the assessment of refractivity through the

<sup>57</sup>For the case when the molar polarizability of  $N_2$  was traced to a thermodynamic pressure standard, the corresponding value became  $1.972(2) \times 10^{-3}$ .

$\gamma'_s$  entity, defined in close proximity to the Eqs. (2) and (3), was developed and presented by Silander et al. [38]. The procedure encompasses accurate assessments of the FSR, measured by the use of induced mode jumps, and the frequency of the empty cavity mode, assessed by referencing the locked laser to an optical frequency comb, together with the use of the mode number,  $m_0$ , which, since it is an integer, can be assessed without uncertainty.

Using the presented methodology, the  $\gamma'_s$  entity for the mirrors addressed could be assessed, under the same conditions as when refractivity measurements are performed and without modifying the setup, with a relative uncertainty of 2% [to 1.728(32)]. This implies that the mirror coatings will not significantly influence the uncertainties of assessments of refractivity and pressure; they contribute to the expanded uncertainties of these entities with contributions that solely are  $< 8 \times 10^{-13}$  and (for nitrogen)  $< 0.3$  mPa, respectively [38].

This implies that the presented procedure can be applied to mitigate the influence of penetration depth of mirrors comprising a QWS of type H on the uncertainty of pressure assessed by a FPC-based system to such a level that it in many cases can be neglected.

The same work [38] also describes how the Gouy phase<sup>58</sup> should be estimated and included in the assessment of reactivity.

#### 6.8.3.5 Assessment of the uncertainty of the stationary and the transportable Invar-based FPC optical Pascals — the SOP and the TOP — for assessment of pressure

The two Invar-based FPC systems utilizing the GAMOR methodology described above (the stationary and the transportable optical Pascals, denoted the SOP and the TOP) have also been characterized with respect to their abilities to assess pressure in the 4 - 25 kPa range [37].

Based on the fact that the the influence of thermodynamic effects on the assessments (i.e., the  $pV$ -work) can be neglected [52], as was alluded to in the sections 4.1.1.1 and 4.2.1, that the construction allows for low uncertainty assessments of gas temperature [50], that the pressure induced cavity de-

<sup>58</sup>The Gouy phase is a phase advance gradually acquired by a beam around its focal region.

formation could be assessed with low uncertainty [46], and assuming that the influence of the mirror penetration depth and the Gouy phase could be neglected [38], which all are considered appropriate assumption, the expanded uncertainty of the two refractometers could be assessed to [37]:<sup>59</sup>

- for the SOP:  $[(10 \text{ mPa})^2 + (10 \times 10^{-6} P)^2]^{1/2}$ ;
- for the TOP:  $[(16 \text{ mPa})^2 + (28 \times 10^{-6} P)^2]^{1/2}$ .

It was concluded that while the uncertainty of the SOP is mainly limited by the uncertainty in the molar polarizability of  $N_2$  (8 ppm), that of the TOP is limited by the temperature assessment (26 ppm) [37].

To verify the long term stability, the systems were compared to each other over a period of 5 months. It was found that all measurements fell within the estimated expanded uncertainty ( $k=2$ ) for comparative measurements (27 ppm). This verified that the estimated error budget for the uncorrelated errors holds over this extensive period of time [37].

#### 6.8.4 Realization of transportable refractometer systems based on the GAMOR methodology

The ability of the GAMOR methodology to mitigate the influence of fluctuations and drifts has also enabled the realisation of transportable systems. A first version was realized as a part of the previous EMP-IR project (JRP 14IND06 ‘Pres2Vac’) although its performance was assessed as a part of the present ‘QuantumPascal’ project [40]. Its functionality was demonstrated at the last workshop at the National Metrology Institute at RISE, in Borås, Sweden, 2018 with sub-ppm precision (0.5 – 0.9 ppm). The system was thereafter disassembled, packed and transported on winter roads in sub zero °C temperature

1 040 km to Umeå University, where it, after unpacking and reassembling, demonstrated a similar precision (0.8 – 2.1 ppm). This shows that the system could be disassembled, packed, transported, unpacked, and reassembled with virtually unchanged performance [40].

Based on this successful realization, and addressing its identified shortcomings, a second version of a transportable refractometer system, denoted the TOP (Transportable Optical Pascal), was constructed as a part of the present QuantumPascal project. As is shown in Fig. (35), the system is constructed around a 19-inch rack which comprises all lasers, electronics, and gas connections. Its construction and functionality are described in the works by Forssén et al. [39] and Silander et al. [37].

In short, on top of the rack, there is a  $60 \times 60 \times 25$  cm encapsulated box (denoted the cavity unit) that contains an optical breadboard on which the Invar-based DFPC is placed (which in turn, is encapsulated in an aluminum enclosure, denoted the ‘oven’). As is described above (in section 6.6.2.3), this unit comprises four pneumatic valves that control the filling and emptying of gas in the two cavities during the GAMOR-cycles and a number of collimators, mirrors, and detectors that couple light into the cavities and measures the reflected and the transmitted light, respectively.

The rack comprises thereafter seven modules containing vacuum connectors, communication hub, fiber-optics, a frequency counter, two fiber lasers, and locking electronics. The rack stands on four wheels that allow the system to be easily moved within the laboratory. Details of the system are given in Forssén et al. [39].

The system, whose ( $k=2$ ) expanded uncertainty of the system was assessed to  $[(16 \text{ mPa})^2 + (28 \times 10^{-6} P)^2]^{1/2}$ , limited by the uncertainty in the temperature assessment (26 ppm) [37], has been in use for a circular comparison of existing primary standards at several National Metrology Institutes (NMIs); the measurement campaign originated from RISE and comprised PTB (Berlin), INRiM (Turin), and LNE (Paris), before it returned to RISE [55]. One of the aims of this ring comparison was to provide information about the refractometer, its mode of operation, and its performance, including its ability to withstand ordinary commercial transportation. The result of the ring comparison, which presently is ongoing, will be reported elsewhere.

<sup>59</sup>Since the mirror penetration depth and the Gouy phase were neglected in the work by Silander et al. [37], the analysis was based on Eq. (4) above, which, according to footnote 3, is based on a cavity resonance condition given in terms of the number of wavelengths the light experiences under a round trip. As is discussed in the proximity of Eq. (9), this is adequate as long as the empty measurement cavity frequency is defined as an ‘effective’ empty cavity frequency,  $\nu'_0$ , given by  $\nu_0 / (1 + \frac{\Theta_G}{\pi m_0} + \frac{\gamma'_G}{m_0})$ . This was not done within the work by Silander et al. [38] though. However, as is discussed in footnote 29 of Silander et al. [38], although this implies that the cavity mode number was incorrectly assessed by Silander et al. [37] by a single unit, when this redefinition is included in the analysis, it does not affect the assessment of the uncertainty of the instrumentation.

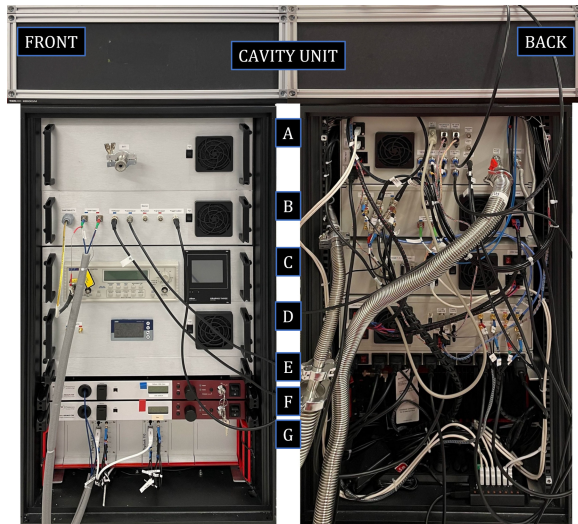


**Figure 35.** The TOP system seen from the front and rear. All lasers, electronics, and gas connections are placed within a 19-inch rack. On top of the rack, there is a  $60 \times 60 \times 25$  cm encapsulated box (denoted the cavity unit) that contains, as its base, an optical breadboard, on which the Invar-based DFPC is placed (in turn, encapsulated in an aluminum enclosure, denoted the "oven"). This unit also comprises four pneumatic valves that control the filling and emptying of gas in the cavity during the GAMOR-cycles and collimators, mirrors, and detectors that couple light into the cavities and measures the transmittance, respectively. The rack contains thereafter, from the top to the bottom, seven modules, denoted A-G, containing vacuum connectors, communication hub, fiber-optics, frequency counter, two fiber lasers, and locking electronics. The rack stands on four wheels that allow the system to be easily moved within the laboratory. Reproduced with permission from Ref. [39]

It has already been established though that once the system arrived at the host laboratory it could be unpacked in a couple of hours. Although it is, in principle, directly ready for operation, it was found advantageous to let the system thermalize overnight [55]. This is not seen as a major drawback since it gives the operator time to test and prepare the system for its task.

The experiences obtained from this ring comparison will be used for improvement of the TOP and

for future realizations of transportable systems.

### 6.9 A recipe on how to construct a GAMOR-based FPC refractometry system suitable for high precision and low uncertainty assessments

Based on the knowledge acquired about the GAMOR methodology in this project, it is possible to provide a guide on how to implement GAMOR in a DFPC-system, suitable for those that would like to implement the methodology.

To allow for "short" gas modulation cycles:

- (1) Realize a DFPC-based system with such small gas volumes that only a restricted amount of energy is brought into the cavity system with the introduction of the gas and with good thermal conductivity and no "heat islands" so that  $pV$ -work will not adversely affect the performance on the time scales utilized;
- (2) Design and construct a gas handling system that automatically can modulate the amount of gas in the measurement cavity;
- (3) Avoid using cavity materials and components in the gas handling system that have a large permeability to any of the gases to be used; and
- (4) Create a gas evacuation system (based on the cavity volume, the tube dimensions, and the pumping effect) that allows for effective evacuation of the measurement cavity during the evacuation period;

In addition:

- (5) To provide good temperature conditions, construct a temperature-stabilized environment around the cavity system, preferably with a stability in the low mK range;
- (6) To avoid accumulation of gas impurities, avoid creating a system in which gas stands still — i.e., use flowing gas where possible;
- (7) Utilize lasers that are tunable within a suitable wavelength range for which molecular data are provided or can be retrieved and for which there are suitable electro-optic (and, if needed, acousto-optic) components available so that the lasers can be easily tuned and sturdily locked to cavity modes;

- (8) Construct a system for sturdy locking the lasers to longitudinal modes of the cavities; preferably by use of the PDH technique;
- (9) Construct an optical system that allows for efficient spatial mode matching and easy optimization of the lasers to the cavity modes;
- (10) To allow for autonomous assessments over any lengths of time, and to stay within the tuning range of the lasers, but also to avoid too large frequency detunings (so as to minimize the influence of the group delay dispersion, GDD), provide means to automatically and rapidly (preferably within a second) relock the lasers (e.g., by detecting and using also the transmitted light);
- (11) Assess, with adequate accuracy, the empty cavity frequencies of the two lasers, i.e.,  $\nu_{0m}$  and  $\nu_{0r}$ ;
- (12) Design and utilize a method to assess the values of the numbers of the modes at which the empty cavity frequencies are assessed, i.e.,  $m_{0m}$  and  $m_{0r}$ , preferably with no uncertainty;
- (13) Design and utilize a method to automatically keep track of the numbers of the modes addressed in terms of deviations from  $m_{0m}$  and  $m_{0r}$ , i.e., the  $\Delta m_m(t)$  and  $\Delta m_r(t)$  entities;
- (14) Provide means to assess, in a repeated manner, the beat frequency between the two lasers, i.e., the  $f(t)$ ;
- (15) Provide means to assess the temperature of the gas,  $T(t)$ , preferably by assessing the temperature of the cavity spacer repeatedly, with a stability in the low or sub-mK range;
- (16) Create a data acquisition system that can assess all repeatedly assessed input parameters, primarily the  $f(t)$ ,  $\Delta m_m(t)$ ,  $\Delta m_r(t)$ , and  $T(t)$ , in a synchronous manner with clearly defined time stamps;
- (17) Estimate the value of the Gouy phase parameter,  $\Theta_G$ ;
- (18) Characterize (or estimate) the penetration depths of the mirrors in terms of the  $\gamma_c$  entity (or, when the mirrors are not used around their center frequency,  $\gamma'_s$ ), possibly using the methodology developed by Silander et al. [38];
- (19) Assess, from the  $\nu_{0m}$ ,  $\Theta_G$ ,  $m_{0m}$ , and  $\gamma_c$  (or  $\gamma'_s$ ) entities, the  $\nu'_{0m}$  entity for the measurement cavity;
- (20) Assess the  $\nu'_{0r}$  for the reference cavity from the corresponding entities for that cavity;
- (21) Provide means to automatically assess, by the use of Eq. (13) and the  $f(t)$ ,  $\Delta m_m(t)$ ,  $\Delta m_r(t)$ ,  $m_{0m}$ ,  $m_{0r}$ ,  $\nu'_{0m}$ , and  $\nu'_{0r}$  entities, the unwrapped beat frequency, i.e., the  $f_{UW}(t)$  entity;
- (22) To be able to implement cornerstone 2, create, based on pair-wise assessments of the "baseline" [i.e. the unwrapped beat frequency entity when both cavities are evacuated, i.e.,  $f_{UW}^{(0)}(t_{k+1})$  and  $f_{UW}^{(0)}(t_k)$ ], by interpolation, according to Eq. (14), an estimate of the empty cavity beat frequency for all time instants during a gas modulation cycle,  $\tilde{f}_{UW}^{(0)}(t)$ ;
- (23) To create the  $\Delta f_{UW}(t)$  entity, relate, at each time instant, according to Eq. (15), the unwrapped beat frequency measured with gas in the measurement cavity,  $f_{UW}^{(g)}(t)$  to the interpolated "baseline",  $\tilde{f}_{UW}^{(0)}(t)$ ;
- (24) Characterize the system with respect to its refractivity normalized pressure induced deformation,  $\varepsilon'$ , (for the case when the relative elongation is considered to be linear with pressure and when nitrogen is assessed, to  $\varepsilon'_0$ ) possibly using the methodology developed by Zakrisson et al. [46];
- (25) Assess, from the  $\Delta f_{UW}(t)$ ,  $\nu'_{0m}$ ,  $\Delta m_m(t)$ ,  $m_{0m}$ ,  $\Theta_G$ , and  $\varepsilon'_0$  entities, the refractivity,  $(n-1)(t)$ , by use of Eq. (16);<sup>60</sup>;
- (26) To certify that the assessments are not influenced by thermodynamic effects, assess the lower limit of the gas modulation period for which the assessments are not noticeably influenced by any  $pV$ -work, and use modulation times equal to or longer than this;

<sup>60</sup>For the case when not both the conditions that the relative elongation is linear with pressure and nitrogen is addressed hold, Eq. (16) should be exchanged to a corresponding one based on Eq. (5).

- (27) Assess the molar density and pressure by use of the Lorentz-Lorenz equation and an appropriate equation of state. For the case of nitrogen, and for pressures up to  $10^5$  Pa, use the Eqs. (11) and (12) with appropriate molecular parameter values from the literature;
- (28) To reduce the influence of white noise, assess, by a series of measurements, the optimum intracycle averaging time for assessment of the beat frequency under both filled and empty measurement cavity conditions; and
- (29) To optimize the system, assess the optimum modulation and detection conditions for the system (e.g., the number of modulation cycled over which the data are averaged) by analyzing the assessed pressure by an Allan variance analysis.

By this, refractivity, molar density, and pressure, can be assessed by DFPC-based refractometry in an autonomous manner with higher precision than if unmodulated refractometry would be used, and, if precision has been a sizeable part of the uncertainty, also an improved uncertainty.

## 7 Conclusions

As has been shown by the sections 3 "Pressure-induced cavity deformation in Fabry-Perot refractometry", 4 "Temperature control and assessment", 5 "Gas permeation, and 6 "Scrutiny and implementation of gas modulation in FPC-based refractometry (GAMOR) above, as well as in the specific guides "Pressure-induced cavity deformation in Fabry-Perot refractometry assessed by the use of simulations and experimental characterizations" [31], "Development of methods for control and assessment of the temperature of the gas in Fabry-Perot cavities" [32], "Guide: Information about permeation of gas into various cavity spacer materials" [33], and "Gas modulated Fabry-Perot-cavity-based refractometry (GAMOR) — Guide to its basic features, performance, and implementation" [34], the first work package, WP1, of the EMPIR 18SIB04 "QuantumPascal" project, "Towards quantum-based realisations of the pascal", "Pressure measurements based on Fabry-Pérot cavity based refractometry", has contributed significantly to the further development of FPC-based refractometry. In particular, they have led to the following conclusions.

## 7.1 Pressure-induced cavity deformation in FP-based refractometry

### 7.1.1 Deformation assessed by simulations

Simulations have indicated that the net pressure-normalized relative deformations for the types of systems addressed range from  $0.20(2) \times 10^{-12} \text{ Pa}^{-1}$ , which was achieved for the closed multi-cavity system based on sapphire components at PTB,<sup>61</sup> up to  $(-6.85(3) \times 10^{-12} \text{ Pa}^{-1})$ , which was obtained for the open single FPC system realized in a Zerodur spacer at CNAM, and to values in the  $6.7 \times 10^{-12} \text{ Pa}^{-1}$  to  $7.8 \times 10^{-12} \text{ Pa}^{-1}$  range for the closed DFPC systems realized in Invar spacers at UmU and RISE. The corresponding values of the refractivity-normalized relative deformations range similarly from  $7.5 \times 10^{-5}$  to  $290 \times 10^{-5}$ .<sup>62</sup> This implies that the amount of deformation of the systems addressed varies over range of 35. This shows that FP-systems, although being well design in many respect, still can exhibit a large variety of deformations

The simulations also revealed that solely two of the simulations could provide deformations with uncertainties that clearly are below the benchmark corresponding to an over all uncertainty in the assessment of pressure of 10 ppm (which implies that the uncertainty in  $\epsilon'$  should not exceed  $1 \times 10^{-5}$ ), viz. the DFPC Zerodur system at UmU and the multi-cavity sapphire system at PTB, which reported uncertainties in  $\epsilon'$  of  $0.7 \times 10^{-5}$ . It was also found that it was possible to assess the deformation of the Zerodur spacer system at CNAM with an uncertainty the more or less is equal to the benchmark (with an uncertainty in  $\epsilon'$  of  $1.1 \times 10^{-5}$ ). These simulations were found to largely be limited by the uncertainty in the material parameters used, e.g. the Young's modulus and the Poisson ratio.

The simulations of the NEXCERA-based system at CEM, the Zerodur system at PTB, which incorporated glued mirrors, and the Invar system, which encompasses mirrors pressed into the Invar spacer, could not provide deformation values whose uncer-

<sup>61</sup>Via  $0.76(2) \times 10^{-12} \text{ Pa}^{-1}$ , which was obtained for the closed DFPC system realized in a Zerodur spacer with mirrors mounted by optical contacting at UmU, and  $2.6(1) \times 10^{-12} \text{ Pa}^{-1}$ , which was obtained for the closed single FPC system realized in a Zerodur spacer with mirrors mounted by glue at PTB,

<sup>62</sup>This implies that the deformation contributes to the refractivity (and thereby pressure) on a level ranging from 75 ppm to 2.9 ‰.

tainties were below the benchmark;<sup>63</sup> for the NEXCERA system because of restricted options in the software to model the mirror mounting, for the Zerodur system at PTB mainly due to the glue, and for the Invar system at UmU and RISE, mainly due to difficulties with modeling of the spacer-to-mirror interface (the rim) caused by a difficulty to, in the presence of the pertinent surface roughness, sufficiently accurately model and assess the plastic deformation of the spacer material.

### 7.1.2 Development of a novel disturbance-resistant methodology for assessment of cavity deformation

It has been shown that, thanks to the sub-ppm precision of the GAMOR methodology, a novel methodology that can significantly improve on the assessment of cavity deformation has been developed [46]. This methodology utilizes two gases with dissimilar relative refractivity at a series of pressures that allows for assessments of cavity deformation that are independent of systematic pressure-independent (constant) errors in both the reference pressure and the assessment of gas temperature. In addition, since the GAMOR methodology is used, the assessments are immune to linear drifts and has a significantly reduced sensitivity to gas leakages and outgassing into the system [54]. Thus, it provides a robust assessment of cavity deformation with small amounts of uncertainties [46].<sup>64</sup>

By use of this methodology, it could be concluded that, when a high-precision (sub-ppm) refractometer (which often can be obtained when the GAMOR methodology is used) is characterized according to the procedure developed, and under the condition that high purity gases are used, the uncertainty in

<sup>63</sup>The simulations of the NEXCERA-based system at CEM provided an uncertainty that was twice the benchmark, while those of the Zerodur system at PTB provided an uncertainty that was four times above the mark. Those of the Invar systems provided an order of magnitude larger value than those of PTB.

<sup>64</sup>Regarding the characterization of this system, it could be concluded that simulations of the DFPC system experimentally addressed provided a value of the refractivity normalized cavity deformation,  $\epsilon$ , of  $2.44 \times 10^{-3}$ , while it was experimentally determined to  $1.96 \times 10^{-3}$  [46]. This discrepancy is mainly attributed to the uncertainty in the geometrical parameters of the spacer-to-mirror interface (the rim) caused by a difficulty to properly assess the shape and minuscule size of the contact area between the curved mirror and the spacer.

the deformation contributes to the uncertainty in the assessment of pressure of nitrogen to a level of 1 or 2 ppm (depending on which type of  $N_2$  pressure standard it refers to; a mechanical or a thermodynamic one, respectively), which presently solely represents a fraction of the relative uncertainty of its molar polarizability. This implies, in practice, that, as long as gas purity can be sustained, cavity deformation is presently not a limiting factor in FP-based refractometer assessments of pressure of nitrogen.

### 7.1.3 Deformation assessed by experimental means

It was found that by use of the aforementioned disturbance-resistant methodology for assessment of cavity deformation, the refractivity-normalized relative deformation of the two Invar-based DFPC systems (the SOP and the TOP) could be assessed to  $1.972(1) \times 10^{-3}$  and  $1.927(1) \times 10^{-3}$ , respectively [37]. This indicates that the deformation of the two systems could be assessed with such a low uncertainty that the deformation only contributes to assessments of pressure on the 1 ppm level.

It was also found that the pressure-normalized relative deformation of the new Zerodur-based single FP cavity refractometer at CNAM,  $\kappa$ , has so far been assessed to  $-6.70(2) \times 10^{-12} \text{ Pa}^{-1}$ , which differs from the simulated value solely by 2 % and whose uncertainty is  $2 \times 10^{-14} \text{ Pa}^{-1}$ , which is a slightly smaller than the targeted  $2.7 \times 10^{-14} \text{ Pa}^{-1}$  benchmark.

## 7.2 Temperature control and assessment

UmU, RISE, and CEM have realized and scrutinized the performance of systems for temperature assessment and control based on classical thermistors (Pt-100). CNAM has realized and investigated a system utilizing a SPRT sensor. UmU and RISE have together demonstrated a  $2\sigma$  precision of  $\pm 0.2 \text{ mK}$ , while CEM and CNAM have demonstrated a precision at the  $\pm 1 \text{ mK}$  level. For highest accuracy, UmU, RISE, and CNAM have constructed systems that are referenced to a Gallium fixed point cell, working at  $29.76 \text{ }^\circ\text{C}$ .

As was described in the sections 4.1.1.2 and 4.2.2 above, PTB has implemented a regulation of the ambient air temperature within the laboratory by three commercial water cooled systems comprising fans and radiators ( $P2P = 1 \text{ K}$ ). The assessment of the

temperature was performed by the use of four calibrated SPRTs. This system could provide resolutions will into the  $\mu\text{K}$  range.

All these findings clearly indicate that several systems are capable of reaching the targeted goal of a precision below 1 mK ( $< 3$  ppm) and an uncertainty below 3 mK ( $< 10$  ppm).

### 7.3 Permeation of gas into cavity spacer materials

Permeation of He gas in the cavity spacer material can adversely affect both the purity and the pressure of the gas as well as, potentially, the physical length of the cavity. It has been established that the permeability, diffusivity and solubility of He gas in ULE-glass is significant. It is significantly less (three to four orders of magnitude) in Zerodur, and virtually non-existent in sapphire or metals. Hence, the use of either of the latter two materials as cavity spacer is suggested if effects of gas permeation is to be minimized.

### 7.4 Gas modulation in FPC-based refractometry — the GAMOR methodology

While ordinary refractometry tends to emphasise that the most accurate assessments need to be performed under extraordinary well-controlled (i.e. disturbance free) conditions, the GAMOR methodology, whose Hallmark is that it has a capacity to mitigate the influence of various types of disturbances, is based on a recognition of the fact that virtually all types of instrumentation are affected by various types of disturbances.

Since many types of fluctuation have a  $1/f^a$  dependence (where  $a > 0$ ), the higher the frequency at which the signal is detected, the less the system is influenced by (or will pick up) fluctuations. The same is valid for drifts; the higher the frequency at which the signal is detected, the less the system is influenced by (or will pick up) a given amount of drift. Similar to various other modulated detection techniques, e.g. frequency and wavelength modulation spectrometry [67–70], the GAMOR methodology therefore strives for coding and decoding the signal at an as high frequency as possible. This is done by a modulation of the amount of gas in one of the cavities.

This is manifested through its first cornerstone, viz.

- (i) the refractivity of the gas in the measurement cavity is assessed by a frequent referencing of filled measurement cavity beat frequencies to evacuated cavity beat frequencies.

To additionally reduce the influence of disturbances (primarily fluctuations and drifts) it also incorporates a second cornerstone, viz.

- (ii) the evacuated measurement cavity beat frequency at the time of the assessment of the filled measurement cavity beat frequency is estimated by use of an interpolation between two evacuated measurement cavity beat frequency assessments, one performed before and one after the filled cavity assessments.

By this, the GAMOR methodology mitigates swiftly and conveniently the influence of various types of disturbances in refractometry systems, not only those from changes in length of the cavity caused by drifts in the temperature of the cavity spacer, but also several of those that have other origins (e.g., those from gas leakages and outgassing) [26, 27, 36, 49, 54, 65].

As described in some detail above, the GAMOR methodology has an extraordinary ability to improve on the precision of assessments of refractivity and thereby pressure. Its ability to reduce various types of fluctuations has been found to be of increasing importance the lower the addressed pressure, emphasising its role for assessments of pressures up to 100 kPa.

It also provides a number of advantages that not only simplify the assessments of refractivity and thereby pressure, it also opens up for the realization of systems based on cavity spacers in non-conventional material and transportable systems. After some initial proof-of-concept demonstrations using a cavity spacer of Zerodur [26, 27, 60], a system based on an Invar-cavity-spacer was realized [37, 49, 50]. Such a cavity spacer has a number of advantages that provides several extraordinary properties that facilitates assessments of refractive and pressure.

In addition, it has been shown that it is possible to construct an Invar-based DFPC system cavity system that, when utilizing the GAMOR methodology

with gas modulation periods of 100 s, is not significantly affected by thermodynamic processes that are associated with the exchange of gas (i.e.,  $pV$ -work) [52]. This implies that  $pV$ -work is currently not a limiting factor when the Invar-based DFPC GAMOR system is used for assessments of pressure or if it would be used as a primary pressure standard, both up to atmospheric pressure.

Moreover, it has been shown that, thanks to its sub-ppm precision, it can significantly improve on the ability to assess cavity deformation by the use of a novel methodology that not only comprises two gases with dissimilar relativity but also performs the assessment at a series of assessments [46]. It has also allowed for a methodology for accurate in-situ assessment of the penetration depth of mirrors comprising a QWS of type H to such an extent that the phenomenon presently does not have any significant impact on the extended uncertainty of the technique.

The specific features of GAMOR has also led to such excellent precision that it, for the instrumentation utilized, solely plays a minor (under optimal conditions, no) role in the total uncertainty budget of the pressure assessment. Up until today, a system that has demonstrated assessment of pressure with an expanded uncertainty ( $k=2$ ) of  $[(10 \text{ mPa})^2 + (10 \times 10^{-6} P)^2]^{1/2}$  has been demonstrated, mainly limited by the uncertainty in the molar polarizability of nitrogen (8 ppm), and only being affected to a significantly smaller degree by all other entities taken together [37].

All this indicates that the combination of a well-characterized Invar-based DFPC system (with respect to cavity distortion and mirror penetration depth), the GAMOR methodology, and a Ga fixed-point cell can provide a basis for a self-contained system that only needs a pure gas supply and accurate frequency references to realize the Pascal. This is an important step towards the dissemination of the Pascal through fundamental principles.

## 7.5 Assessment of the performance of FPC-based refractometry developed within the QuantumPascal project

As is described in some detail in the D2 report of the "QuantumPascal" project, "Report evaluating the performance of the different types of FP-based refractometers developed with respect to their precision, accuracy, working range and target relative uncertainties of 500

ppm in the range 1 Pa – 1 kPa and 10 ppm in the range 1 kPa – 100 kPa" [73], the combined conclusions from the four tasks addressed in work package 1 of the QuantumPascal project indicate that it has been possible to develop at least one instrumentation that is capable of realizing FP-based refractometry with the targeted 10 ppm relative uncertainty in the 1 - 100 kPa range [37].

For this particular instrumentation, comprising an Invar based DFPC and utilizing the GAMOR methodology [37], neither of the concepts under scrutiny in the project, viz. pressure-induced cavity deformation, temperature assessment, or finite gas permeability of the cavity spacer material, are limiting the assessment. The system is also not limited by the finite penetration depth from mirrors.

The same instrumentation has though only reported a relative uncertainty 500 ppm in the 20 Pa - 1 kPa range (expressed as 10 mPa) [37].

Entities limiting the performance at the lowest pressures were the empty cavity (beat) frequency, outgassing and leaks (since the last evacuation), and residual pressure in the measurement cavity (at the end of the evacuation part of the modulation cycle), which in the characterization by Silander et al. [37] were assessed to 7, 5, and 5 mPa respectively.

It can also be concluded that there are also other realizations of FP-refractometry, e.g. the system developed by CNAM, that have made significant and important steps towards the targeted limits of 10 ppm level for pressures in the 1 - 100 kPa range and 500 ppm in the entire 1 Pa to 1 kPa range.

Hence, as is described in some detail in the D2 report "Report evaluating the performance of the different types of FP-based refractometers developed with respect to their precision, accuracy, working range and target relative uncertainties of 500 ppm in the range 1 Pa – 1 kPa and 10 ppm in the range 1 kPa – 100 kPa" [73], since the characterization of the Invar based DFPC GAMOR utilizing system at UmU [37] was performed at an early stage in the project, and due to successful achievements from other partners, we consider it today, after a series of continuous improvements, to be possible to achieve a vacuum pressure with a significantly lower uncertainty, to which level remains to be formally assessed. An indication of this is that separate empty cavity assessments made by the Invar based DFPC GAMOR utilizing system at UmU have demonstrated assessments of vacuum pressure with a minimum deviation of 0.03 mPa

[49], which is more than two orders of magnitude below the 7 mPa that was demonstrated in Silander et al. [37].<sup>65</sup>

## 8 Recommendations

### 8.1 Pressure-induced cavity deformation in FP-based refractometry

It has been shown that that simulations indeed can be useful for assessments of deformation of well-characterized systems, i.e. those with firmly attached mirrors to the spacer.<sup>66</sup> A limitation is though that such simulations often are limited by the uncertainty in the material parameters used, e.g. the Young's modulus and the Poisson ratio.

A more feasible approach is therefore to assess deformation by an experimental means. It has been concluded that it is clearly advantageous to utilize, if possible, the novel distortion-resistant methodology developed by Zakrisson et al. [46], since it has the ability to mitigate the influence of various types of disturbance; it makes the assessments immune to linear drifts and provides a significantly reduced sensitivity to gas leakages and outgassing in the system. It has been demonstrated that by use of this methodology, the deformation of the Invar-based systems could be assessed with such a low uncertainty (well below the benchmark) that it only contribute to the final assessment of pressure on a low ppm level.

It should also be mentioned that, to decrease the required accuracy by which an experimental deformation characterization needs to be done, it could be advisory to, if possible, to construct an FPC-system with a minimum of cavity distortion. In such cases, it is plausible that it is fully adequate to assess deformation by simulations.

Moreover, to mitigate the effect of gas impurities (in particular in He), it would be beneficial to investigate the possibility to realize an experimental characterization methodology that does not rely on this gas.

<sup>65</sup>It is also anticipated that improvements in the gas handling system have provided improved figures-of-merits of the other two limiting factors, viz. the outgassing and leaks since the last evacuation and the residual pressure in the measurement cavity, again, to levels that remain to be formally assessed. By this, we consider the last hurdles to obtain the targeted 500 ppm in the 1 Pa - 1 kPa range to be within reach within a not too distant future.

<sup>66</sup>This implies, among other things, that it is recommended, For the Invar-based DFPC used by UmU and RISE, to not rely on simulations for assessment of the cavity deformation.

### 8.2 Temperature control and assessment

As is shown and discussed in the Guide "Development of methods for control and assessment of the temperature of the gas in Fabry-Perot cavities" [32], this project has indicated that there are several realizations (based on classical thermistors, Pt-100, or SPRT sensors, either calibrated or, for best long term uncertainty, in some cases in conjunction with a Gallium fixed point cell, working at 29.76 °C) that are capable of reaching the targeted goal for the assessment of gas temperature with a precision below 1 mK (< 3 ppm) and an uncertainty below 3 mK (< 10 ppm). Based on this, it can be concluded (and thereby recommended) that there are several ways future FPC-based refractometers can be realized with respect to their ability to assess temperature.

Particular concern needs though to be given to temperature fluctuations or alterations that are caused by the  $pV$ -work that originates from the filling of the cavity by the gas. The characterization of the UmU and RISE constructed Invar-based DFPC system performed by Rubin et al. [52, 56] needs to be particularly emphasised in this respect since it provides a thorough analysis of the effect of  $pV$ -work on the assessment of temperature of the gas. It also clearly points out important constructions considerations when novel FPC-based systems with a minimum of influence of  $pV$ -work are to be constructed. The use of closed FPC-systems with a narrow bore and the use of a heat-island free cavity spacer system are particularly emphasised as being of high importance. It was shown that a construction based on such recommendations can assess gas refractivity with sub-ppm influence of  $pV$ -work on timescales of sub-minute gas modulation cycles. It can also be concluded though that it is advantageous (and it is therefore recommended) to perform frequent assessments of the temperature of the cavity spacer since such can pick up any possible fluctuation of the temperature of the cavity spacer that can take place as a consequence of  $pV$ -work done by the gas.

### 8.3 Gas permeability

Since the permeation of He gas in the cavity spacer material can adversely affect both the purity and the pressure of the gas as well as the physical length of the cavity, and since permeability, diffusivity and solubility of He gas in ULE-glass is significant, it can

be concluded that, as long as He is either addressed as the measuring gas or utilized when the pressure-induced deformation is assessed, the use of ULE-glass cannot be recommended. Moreover, when the highest accuracy (i.e. the best uncertainty) is to be achieved, Zerodur should be used only when refractivity is assessed during time-wise limited measurement cycles with frequent exchanges of gas, as is done in the GAMOR methodology.

It is instead advocated that, to minimize the effect of gas permeation, cavity spacer materials that have low He solubility, e.g. sapphire or Invar, should be used.

#### 8.4 Gas modulation in FPC-based refractometry — the GAMOR methodology

For the cases where it is possible to implement the GAMOR method, it is advisable to do so. This will first of all improve on the precision of the assessments. Secondly, it enables the realization of DFPC systems based on non-conventional cavity spacer materials (e.g., Invar) that have beneficial properties regarding concepts such as temperature control and assessment and gas permeability. The technique is also advantageous in cases when entities such as pressure-induced cavity distortions or mirror penetration depths are to be assessed.

#### 8.5 Realization and implementation of state-of-the-art FPC-based refractometers

This guide has shown, by the multitude of results obtained by the various partners, that task 1 of the QuantumPascal project, "Pressure-induced cavity deformation in Fabry-Perot refractometry", has been noticeably successful. So far, however, the various experiences gained have not yet been merged into a single instrumentation, which would establish the possible current state-of-the-art performance for FPC-based refractometry. This should be the next step in the development of this pressure assessment technique.

## References

- [1] C. R. Tilford. Three and a half centuries later - the modern art of liquid-column manometry. *Metrologia*, 30(6):545–552, jan 1994. doi: 10.1088/0026-1394/30/6/001.
- [2] C M Sutton. The pressure balance as an absolute pressure standard. *Metrologia*, 30(6):591–594, jan 1994. doi: 10.1088/0026-1394/30/6/008.
- [3] S. Semenoja and M. Rantanen. Comparisons to establish a force-balanced piston gauge and a spinning rotor gauge as the new measurement standards of mikes. *Vacuum*, 73:269–274, 03 2004. doi: 10.1016/j.vacuum.2003.12.007.
- [4] J. W. Schmidt, K. Jain, A. P. Müller, W. J. Bowers, and D. A. Olson. Primary pressure standards based on dimensionally characterized piston/cylinder assemblies. *Metrologia*, 43(1):53–59, nov 2005. doi: 10.1088/0026-1394/43/1/008.
- [5] J. Hendricks and D. Olson. 1–15,000Pa Absolute mode comparisons between the NIST ultrasonic interferometer manometers and non-rotating force-balanced piston gauges. *Measurement*, 43(5):664–674, jun 2010. ISSN 02632241. doi: 10.1016/j.measurement.2009.12.031.
- [6] J. Ricker, J. Hendricks, T. Bock, K. Dominik, T. Kobata, J. Torres, and I. Sadkovskaya. Final report on the key comparison CCM.p-k4.2012 in absolute pressure from 1 pa to 10 kPa. *Metrologia*, 54(1A):07002–07002, dec 2016. doi: 10.1088/0026-1394/54/1a/07002.
- [7] M. Stock, R. Davis, E. de Mirandés, and M. J. T. Milton. The revision of the SI—the result of three decades of progress in metrology. *Metrologia*, 56(4):022001, aug 2019. ISSN 0026-1394. doi: 10.1088/1681-7575/ab0013.
- [8] M. Stock, R. Davis, E. de Mirandés, and M. J. T. Milton. Corrigendum: The revision of the SI—the result of three decades of progress in metrology. *Metrologia*, 56(4):49502, aug 2019. ISSN 0026-1394. doi: 10.1088/1681-7575/ab28a8.
- [9] K. Jousten, J. Hendricks, D. Barker, K. Douglas, S. Eckel, P. Egan, J. Fedchak, J. Flügge, C. Gaiser, D. Olson, J. Ricker, T. Rubin,

- W. Sabuga, J. Scherschligt, R. Schödel, U. Sterr, J. Stone, and G. Strouse. Perspectives for a new realization of the pascal by optical methods. *Metrologia*, 54(6):S146—S161, 2017. ISSN 16817575. doi: 10.1088/1681-7575/aa8a4d.
- [10] M Andersson, L Eliasson, and L R Pendrill. Compressible Fabry-Perot refractometer. *Applied Optics*, 26(22):4835, nov 1987. ISSN 0003-6935. doi: 10.1364/AO.26.004835.
- [11] M. L. Eickhoff and J. L. Hall. Real-time precision refractometry: new approaches. *Appl. Opt.*, 36(6):1223–1234, Feb 1997. doi: 10.1364/AO.36.001223.
- [12] N. Khélifa, H. Fang, J. Xu, P. Juncar, and M. Himbert. Refractometer for tracking changes in the refractive index of air near 780 nm. *Appl. Opt.*, 37(1):156–161, Jan 1998. doi: 10.1364/AO.37.000156.
- [13] H. Fang, A. Picard, and P. Juncar. A heterodyne refractometer for air index of refraction and air density measurements. *Review of Scientific Instruments*, 73(4):1934–1938, apr 2002. ISSN 0034-6748. doi: 10.1063/1.1459091.
- [14] L. R. Pendrill. Refractometry and gas density. *Metrologia*, 41(2):S40–S51, apr 2004. ISSN 0026-1394. doi: 10.1088/0026-1394/41/2/S04.
- [15] R. W. Fox, B. R. Washburn, N. R. Newbury, and L. Hollberg. Wavelength references for interferometry in air. *Appl. Opt.*, 44(36):7793–7801, Dec 2005. doi: 10.1364/AO.44.007793.
- [16] G. Z. Xiao, A. Adnet, Z. Zhang, F. G. Sun, and C. P. Grover. Monitoring changes in the refractive index of gases by means of a fiber optic fabry-perot interferometer sensor. *Sensors and Actuators A: Physical*, 118(2):177–182, 2005. ISSN 0924-4247. doi: 10.1016/j.sna.2004.08.029.
- [17] F. Riehle, P. Gill, F. Arias, and L. Robertsson. The CIPM list of recommended frequency standard values: guidelines and procedures. *Metrologia*, 55(2):188–200, feb 2018. doi: 10.1088/1681-7575/aaa302.
- [18] S. Häfner, S. Falke, C. Grebing, S. Vogt, T. Legero, M. Merimaa, C. Lisdar, and U. Sterr.  $8 \times 10^{-17}$  fractional laser frequency instability with a long room-temperature cavity. *Opt. Lett.*, 40(9):2112–2115, May 2015. doi: 10.1364/OL.40.002112.
- [19] Y. Y. Jiang, A. D. Ludlow, N. D. Lemke, R. W. Fox, J. A. Sherman, L. S. Ma, and C. W. Oates. Making optical atomic clocks more stable with 10-16-level laser stabilization. *Nature Photonics*, 5(9):1749–4893, 2011. doi: 10.1038/nphoton.2010.313.
- [20] J. A. Stone and A. Stejskal. Using helium as a standard of refractive index: Correcting errors in a gas refractometer. *Metrologia*, 41(3):189–197, 2004. ISSN 00261394. doi: 10.1088/0026-1394/41/3/012.
- [21] P. F. Egan and J. A. Stone. Absolute refractometry of dry gas to  $\pm 3$  parts in  $10^9$ . *Appl. Opt.*, 50:3076, 2011. doi: 10.1364/AO.50.003076.
- [22] P. Egan, J. Stone, J. Hendricks, J. Ricker, G. Scace, and G. Strouse. Performance of a dual fabry-perot cavity refractometer. *Opt. Lett.*, 40(17):3945–3948, Sep 2015. doi: 10.1364/OL.40.003945.
- [23] P. Egan, J. Stone, J. Ricker, and J. Hendricks. Comparison measurements of low-pressure between a laser refractometer and ultrasonic manometer. *Review of Scientific Instruments*, 87(5):053113, 2016. ISSN 10897623. doi: 10.1063/1.4949504.
- [24] I. Silander, M. Zelan, O. Axner, F. Arrhén, L. Pendrill, and A. Foltynowicz. Optical measurement of the gas number density in a Fabry–Perot cavity. *Measurement Science and Technology*, 24(10):105207, oct 2013. ISSN 0957-0233. doi: 10.1088/0957-0233/24/10/105207.
- [25] D. Mari, M. Bergoglio, M. Pisani, and M. Zucco. Dynamic vacuum measurement by an optical interferometric technique. *Meas. Sci. Technol.*, 25:125303, 2014. doi: 10.1088/0957-0233/25/12/125303.
- [26] I. Silander, T. Hausmaninger, M. Zelan, and O. Axner. Gas modulation refractometry

- for high-precision assessment of pressure under non-temperature-stabilized conditions. *J. Vac. Sci. Technol. A*, 36:03E105, 2018. doi: /10.1116/1.5022244.
- [27] I. Silander, T. Hausmaninger, C. Forssén, M. Zelan, and O. Axner. Gas equilibration gas modulation refractometry for assessment of pressure with sub-ppm precision. *Journal of Vacuum Science & Technology B*, 37(4):042901, 2019. doi: 10.1116/1.5090860.
- [28] Y. Takei, K. Arai, H. Yoshida, Y. Bitou, S. Telada, and T. Kobata. Development of an optical pressure measurement system using an external cavity diode laser with a wide tunable frequency range. *Measurement: Journal of the International Measurement Confederation*, 151:107090, 2020. ISSN 02632241. doi: 10.1016/j.measurement.2019.107090.
- [29] Y. Yang and T. Rubin. Simulation of pressure induced length change of an optical cavity used for optical pressure standard. *Journal of Physics: Conference Series*, 1065:162003, aug 2018. doi: 10.1088/1742-6596/1065/16/162003.
- [30] T. Rubin, I. Silander, C. Forssén, J. Zakrisson, E. Amer, D. Szabo, T. Bock, A. Kussicke, C. Günz, D. Mari, R. M. Gavioso, M. Pisani, S. Pasqualin, D. Madonna Ripa, Z. Silvestri, P. Gambette, D. Bentouari, G. Garberoglio, M. Lesiuk, M. Przybytek, B. Jeziorski, J. Setina, M. Zelan, and O. Axner. ‘Quantum-based realizations of the pascal’ status and progress of the empir-project: QuantumPascal. *Acta IMEKO, in press*, x(x):xxx-xxx, 2022. ISSN xxx. doi: xxx.
- [31] J. Zakrisson, I. Silander, C. Forssén, M. Zelan, T. Rubin, A. Kussicke, Z. Silvestri, A. Rezki, C. Garcia-Izquierdo, and O. Axner. Pressure-induced cavity deformation in fabry-pérot refractometry - characterization and recommendations. *Report on the A1.1.4 activity in the EMPIR project 18SIB04, "QuantumPascal"*, 2022.
- [32] T. Rubin, A. Kussicke, M. G. Gonzalez, Z. Silvestri, A. Rezki, J. P. Wallerand, M. Zelan, C. Forssén, I. Silander, J. Zakrisson, and O. Axner. Development of methods for control and assessment of the temperature of the gas in fabry-pérot cavities. *Report on the A1.2.3 activity in the EMPIR project 18SIB04, "QuantumPascal"*, 2022.
- [33] T. Rubin, J. Setina, and A. Kussicke. Guide: Information about permeation of gas into various cavity spacer materials. *Report on the A1.3.4 activity in the EMPIR project 18SIB04, "QuantumPascal"*, 2022.
- [34] I. Silander, J. Zakrisson, C. Forssén, M. Zelan, and O. Axner. Gas modulated fabry-perot-cavity-based refractometry (gamor) — guide to its basic features, performance, and implementation. *Report on the A1.4.3 activity in the EMPIR project 18SIB04, "QuantumPascal"*, 2022.
- [35] C. Koks and M. P. van Exter. Microcavity resonance condition, quality factor, and mode volume are determined by different penetration depths. *Opt. Express*, 29:6879, 2021. doi: 10.1364/OE.412346.
- [36] O. Axner, I. Silander, T. Hausmaninger, and M. Zelan. Drift-free fabry-perot-cavity-based optical refractometry—accurate expressions for assessments of gas refractivity and density. e-print arXiv:1704.01187v2, 2017.
- [37] I. Silander, C. Forssén, J. Zakrisson, M. Zelan, and O. Axner. Optical realization of the Pascal—Characterization of two gas modulated refractometers. *J. Vac. Sci. Technol. B*, 39:044201, 2021. doi: /10.1116/6.0001042.
- [38] I. Silander, J. Zakrisson, V. Silvia de Oliveira, C. Forssén, A. Foltynowicz, M. Zelan, and O. Axner. In situ determination of the penetration depth of mirrors in Fabry-Perot refractometers and its influence on assessment of refractivity and pressure. *Optics Express*, 30(14):25891–25906, 2022. ISSN 1094-4087. doi: 10.1364/OE.463285.
- [39] C. Forssén, I. Silander, J. Zakrisson, O. Axner, and M. Zelan. The short-term performances of two independent gas modulated refractometers for pressure assessments. *Sensors*, 21(18), 2021. ISSN 1424-8220. doi: 10.3390/s21186272.

- [40] C. Forssén, I. Silander, D. Szabo, G. Jönsson, M. Bjerling, T. Hausmaninger, O. Axner, and M. Zelan. A transportable refractometer for assessment of pressure in the kPa range with ppm level precision. *Acta IMEKO*, 9(5):287–292, 2020. ISSN 2221870X. doi: 10.21014/ACTA\_IMEKO.V9I5.986.
- [41] M. Zelan, I. Silander, C. Forssén, J. Zakrisson, and O. Axner. Recent advances in Fabry-Perot-based refractometry utilizing gas modulation for assessment of pressure. *Acta IMEKO*, 9(5):299–304, 2020. ISSN 2221870X. doi: 10.21014/ACTA\_IMEKO.V9I5.988.
- [42] A. D. Buckingham and C. Graham. The Density Dependence of the Refractivity of Gases. *Proceedings of the Royal Society A: Mathematical, Physical and Engineering Sciences*, 337(1609): 275–291, mar 1974. ISSN 1364-5021. doi: 10.1098/rspa.1974.0049.
- [43] M. Jaeschke, H. M. Hinze, H. J. Achtermann, and G. Magnus. PVT data from burnett and refractive index measurements for the nitrogen—hydrogen system from 270 to 353 K and pressures to 30 MPa. *Fluid Phase Equilibria*, 62(1-2):115–139, jan 1991. ISSN 03783812. doi: 10.1016/0378-3812(91)87010-7.
- [44] H. J. Achtermann, G. Magnus, and T. K. Bose. Refractivity virial coefficients of gaseous CH<sub>4</sub>, C<sub>2</sub>H<sub>4</sub>, C<sub>2</sub>H<sub>6</sub>, CO<sub>2</sub>, SF<sub>6</sub>, H<sub>2</sub>, N<sub>2</sub>, He, and Ar. *J. Chem. Phys.*, 94(8):5669–5684, apr 1991. ISSN 0021-9606. doi: 10.1063/1.460478.
- [45] P. Egan, J. Stone, J. Scherschligt, and Allan H. Harvey. Measured relationship between thermodynamic pressure and refractivity for six candidate gases in laser barometry. *Journal of Vacuum Science & Technology A*, 37(3):031603, 2019. ISSN 0734-2101. doi: 10.1116/1.5092185.
- [46] J. Zakrisson, I. Silander, C. Forssén, M. Zelan, and O. Axner. Procedure for robust assessment of cavity deformation in Fabry–Pérot based refractometers. *J. Vac. Sci. Technol. B*, 38:054202, 2020. doi: 10.1116/6.0000375.
- [47] P. M. C. Rourke. Perspective on the refractive-index gas metrology data landscape. *J. Phys. Chem. Ref. Data*, 50:033104, 2021. doi: 10.1063/5.0055412.
- [48] J. Zakrisson, I. Silander, C. Forssén, Z. Silvestri, D. Mari, S. Pasqualin, A. Kussicke, P. Asbahr, T. Rubin, and O. Axner. Simulation of pressure-induced cavity deformation – the 18SIB04 QuantumPascal EMPIR project. *Acta IMEKO*, 9(5):281–286, 2020. ISSN 2221870X. doi: 10.21014/ACTA\_IMEKO.V9I5.985.
- [49] I. Silander, C. Forssén, J. Zakrisson, M. Zelan, and O. Axner. Invar-based refractometer for pressure assessments. *Optics Letters*, 45(9):2652–2655, 2020. ISSN 0146-9592. doi: 10.1364/ol.391708.
- [50] I. Silander, C. Forssén, J. Zakrisson, M. Zelan, and O. Axner. An invar-based Fabry-Perot cavity refractometer with a gallium fixed-point cell for assessment of pressure. *Acta IMEKO*, 9(5):293–298, 2020. ISSN 2221870X. doi: 10.21014/ACTA\_IMEKO.V9I5.987.
- [51] C. Forssén, I. Silander, J. Zakrisson, M. Zelan, and O. Axner. An Optical Pascal in Sweden. *Sensors*, 24:033002, 2022. doi: 10.1088/2040-8986/ac4ea2.
- [52] T. Rubin, I. Silander, M. Bernien, C. Forssen, J. Zakrisson, M. Hao, P. Kussicke, .and Asbahr, M. Zelan, and O. Axner. Thermodynamic effects in a gas modulated Invar-based dual Fabry-Perot cavity refractometer. *Metrologia*, 59:035003, 2022. doi: 10.1088/1681-7575/ac5ef9.
- [53] J. Zakrisson and O. Axner. Partial report on the a1.1.2 activity in the quantumpascal project. *Unpublished*, 2021.
- [54] O. Axner, C. Forssén, I. Silander, J. Zakrisson, and M. Zelan. Ability of gas modulation to reduce the pickup of drifts in refractometry. *J. Opt. Soc. Am. B*, 38(8):2419–2436, Aug 2021. doi: 10.1364/JOSAB.420982.
- [55] C. Forssén, I. Silander, J. Zakrisson, E. Amer, D. Szabo, T. Bock, A. Kussicke, T. Rubin, D. Mari, S. Pasqualin, Z. Silvestri, D. Bentouari, O. Axner, and M. Zelan. Circular comparison of

- conventional pressure standards using a transportable optical refractometer. *Acta IMEKO, in press*, x(x):xxx-xxx, 2022. ISSN xxx. doi: xxx.
- [56] T. Rubin, I. Silander, J. Zakrisson, M. Hao, C. Forssén, P. Asbahr, M. Bernien, A. Kussicke, K. Liu, M. Zelan, and O. Axner. Thermodynamic effects in a gas modulated Invar-based dual Fabry-Pérot cavity refractometer addressing 100 kPa of nitrogen. *Acta IMEKO, in press*, x(x):xxx-xxx, 2022. ISSN xxx. doi: xxx.
- [57] R. W. Fox. Temperature analysis of low-expansion fabry-perot cavities. *Opt. Express*, 17(17):15023–15031, Aug 2009. doi: 10.1364/OE.17.015023.
- [58] M. Zelan, I. Silander, T. Hausmaninger, and O. Axner. Fast Switching Dual Fabry-Perot-Cavity-based Optical Refractometry for Assessment of Gas Refractivity and Density - Estimates of Its Precision, Accuracy, and Temperature Dependence. *arXiv: 1704.01185v2*, apr 2017.
- [59] H. Fang and P. Juncar. A new simple compact refractometer applied to measurements of air density fluctuations. *Review of Scientific Instruments*, 70(7):3160–3166, jul 1999. ISSN 00346748. doi: 10.1063/1.1149880.
- [60] I. Silander, T. Hausmaninger, M. Bradley, M. Zelan, and O. Axner. Fast Switching Dual Fabry-Perot Cavity Optical Refractometry - Methodologies for Accurate Assessment of Gas Density. *arXiv:1704.01186v2*, apr 2017.
- [61] J. H. Hendricks, G. F. Strouse, J. E. Ricker, D. A. Olson, G. E. Scace, J. A. Stone, and P. F. Egan. Photonic article, process for making and using same, January 2015.
- [62] E. Hedlund and L. R. Pendrill. Improved determination of the gas flow rate for UHV and leak metrology with laser refractometry. *Measurement Science and Technology*, 17(10):2767–2772, oct 2006. ISSN 0957-0233. doi: 10.1088/0957-0233/17/10/031.
- [63] E Hedlund and L R Pendrill. Addendum to ‘Improved determination of the gas flow rate for UHV and leak metrology with laser refractometry’. *Measurement Science and Technology*, 18(11):3661–3663, nov 2007. ISSN 0957-0233. doi: 10.1088/0957-0233/18/11/052.
- [64] A. Picard and H. Fang. Three methods of determining the density of moist air during mass comparisons. *Metrologia*, 39(1):31–40, feb 2002. doi: 10.1088/0026-1394/39/1/5.
- [65] O. Axner, I. Silander, C. Forssén, J. Zakrisson, and M. Zelan. Ability of gas modulation to reduce the pickup of fluctuations in refractometry. *Journal of the Optical Society of America B*, 37(7):1956–1965, 2020. ISSN 0740-3224. doi: 10.1364/josab.387902.
- [66] O. Axner, I. Silander, C. Forssén, J. Zakrisson, and Zelan. M. Assessment of gas molar density by gas modulation refractometry: A review of its basic operating principles and extraordinary performance. *Spectrochim. Acta B*, 179:106121, 2021. doi: 10.1016/j.sab.2021.106121.
- [67] J. A. Silver. Frequency-modulation spectroscopy for trace species detection: theory and comparison among experimental methods. *Appl. Opt.*, 31:707–717, 1992. doi: 10.1364/AO.31.000707.
- [68] D. S. Bomse, A. C. Stanton, and J. A. Silver. Frequency modulation and wavelength modulation spectroscopies: comparison of experimental methods using a lead-salt diode laser. *Appl. Opt.*, 31:718–731, 1992. doi: 10.1364/AO.31.000718.
- [69] J. M. Supplee, E. A. Whittaker, and T. Lenth. Theoretical description of frequency modulation and wavelength modulation spectroscopy. *Appl. Opt.*, 33:6294–6302, 1994. doi: 10.1364/AO.33.006294.
- [70] P. Kluczynski and O. Axner. Theoretical description based on fourier analysis of wavelength-modulation spectrometry in terms of analytical and background signals. *Appl. Opt.*, 38(27):5803–5815, Sep 1999. doi: 10.1364/AO.38.005803.
- [71] R. W. P. Drever, J. L. Hall, F. V. Kowalski, J. Hough, G. M. Ford, A. J. Munley, and H. Ward. Laser phase and frequency stabilization using an optical resonator. *Applied*

*Physics B Photophysics and Laser Chemistry*, 31 (2):97–105, jun 1983. ISSN 0721-7269. doi: 10.1007/BF00702605.

- [72] Z. Silvestri, D. Bentouati, P. Otał, and J. P. Wallerand. Towards an improved helium-based refractometer for pressure measurements. *Acta IMEKO*, 9:303, 2020. doi: /10.21014/ACTA\_IMEKO.V9I5.989.
- [73] M. Zelan, O. Axner, C. Forssén, I. Silander, J. Zakrisson, A. Rezki, Z. Silvestri, J. P. Wallerand, A. Kussicke, T. Rubin, C. Garcia-Izquierdo, and S. M. Gonzalez. Report evaluating the performance of the different types of fp-based refractometers developed with respect to their precision, accuracy, working range and target relative uncertainties of 500 ppm in the range 1 pa – 1 kpa and 10 ppm in the range 1 kpa – 100 kpa. *The D2 report on the A1.5.3 activity in the EMPIR project 18SIB04, "QuantumPascal"*, 2022.

## Appendix

### A. Derivation of expressions for the refractivity in FP-based refractometry in the presence of mirrors comprising a QWS of type H and the Gouy phase

Following [35], the round-trip resonance condition of the  $m^{\text{th}}$   $TEM_{00}$  mode of a FP cavity with DBR mirrors can be written as

$$2k_{in}(L_0 + \delta L) + \phi_1 + \phi_2 - 2\Theta_G = 2\pi m, \quad (\text{A.1})$$

where  $k_{in}$  is the wave vector of the light in the cavity,  $L_0$  the distance between the front facets of the two DBRs coatings of the mirrors,  $\delta L$  the pressure induced cavity deformation,  $\phi_1$  and  $\phi_2$  the reflection phases of the two DBR equipped mirrors,  $\Theta_G$  the (single pass) Gouy phase, and  $m$  an integer, representing the number of the longitudinal mode the laser addresses.

For the case with two identical mirrors, as is assumed here, it is convenient to assume that  $\phi_1 = \phi_2 = \phi$ .

#### A.1. For working ranges centred on the mirror center frequency

Assuming that the laser frequency is close to the design frequency,  $\nu_c$ , where the non-linear contributions to the phase can be neglected, it is possible to express  $\phi$  as  $(\partial\phi/\partial\omega)(\omega - \omega_c)$ . It is customary to define  $(\partial\phi/\partial\omega)$  as the delay an optical pulse experiences upon reflection from a DBR when its spectrum fits well within the stop-band of the coating, commonly referred to as the group delay and generally denoted  $\tau_c(n)$ , where the subscript  $c$  indicates that it refers to the mirror center frequency and  $n$  is the index of refraction of the gas in front of the mirror (which, in this case, is in the cavity). This implies that it is possible to express  $\phi$  in terms of the natural frequencies,  $\nu$  and  $\nu_c$ , as  $2\pi\tau_c(n)(\nu - \nu_c)$ .

Since  $k_{in}$  in general is given by  $n(\omega/c)$ , this implies that Eq. (A.1) can be expressed as

$$2n(L_0 + \delta L)\nu + 2c\tau_c(n)(\nu - \nu_c) = c \left( m + \frac{\Theta_G}{\pi} \right). \quad (\text{A.2})$$

As is shown by Silander et al. [38], solving this for  $\nu$  [assuming  $\Theta_G$  and  $\tau_c(n)$  to be independent of the frequency of the light, which is a most reasonable assumption for the cases when the laser frequency makes recurring mode jumps whereby the maximum shift in frequency is the free-spectral-range, FSR, of the cavity] gives

$$\nu = \frac{c \left[ m + \frac{\Theta_G}{\pi} + 2\tau_c(n)\nu_c \right]}{2 \left[ n(L_0 + \delta L) + c\tau_c(n) \right]} = \frac{cm \left[ 1 + \frac{\Theta_G}{\pi m} + \frac{n\gamma_c(n)}{m} \right]}{2n \left[ L_0 + \delta L + 2L_{\tau,c}(n) \right]}, \quad (\text{A.3})$$

where we in the last step have introduced  $\gamma_c(n)$ , formally defined by  $\frac{2\tau_c(n)\nu_c}{n}$ , and  $L_{\tau,c}(n)$ , given by  $\frac{c\tau_c(n)}{2n}$ , where the latter represents the frequency penetration depth of a single mirror [ $2L_{\tau,c}(n)$  thus represents the elongation of the length of the cavity experienced during scans due to the penetration of light into the mirror coatings].

For a mirror coating of type H,  $\tau_c(n)$  is given by  $\frac{n}{n_H - n_L} \frac{1}{2\nu_c}$ , where  $n_H$  and  $n_L$  are the indices of refraction for the coating layers with highest and lowest index of refraction, respectively [35]. This implies that, for this type of coating, both  $\gamma_c(n)$  and  $L_{\tau,c}(n)$  are purely material-dependent, but index-of-refraction-independent, parameters, that therefore henceforth can be written as  $\gamma_c$  and  $L_{\tau,c}$ , given by  $\frac{1}{n_H - n_L}$  and  $\frac{c\gamma_c}{4\nu_c}$ , respectively.

This implies that the frequency of the mode of the cavity the laser addresses in the absence of gas (i.e. the  $m_0^{\text{th}}$  mode),  $\nu_0$ , can be written as

$$\nu_0 = \frac{cm_0 \left( 1 + \frac{\Theta_G}{\pi m_0} + \frac{\gamma_c}{m_0} \right)}{2 \left( L_0 + 2L_{\tau,c} \right)}. \quad (\text{A.4})$$

Hence, when gas is filled into the cavity, the laser will shift its frequency an amount,  $\Delta\nu$ , defined as  $\nu_0 - \nu$ , given by

$$\Delta\nu = \nu_0 - \frac{cm \left(1 + \frac{\Theta_G}{\pi m} + \frac{n\gamma_c}{m}\right)}{2n \left(L_0 + \delta L + 2L_{\tau,c}\right)}. \quad (\text{A.5})$$

Making use of the expression for the frequency of the mode of the cavity the laser addresses in the absence of gas, i.e. Eq. (A.4), it is possible, by use of Eq. (A.5), to write an expression for the relative shift in frequency of the laser light when gas is filled into the cavity, i.e.  $\frac{\Delta\nu}{\nu_0}$ , as

$$\frac{\Delta\nu}{\nu_0} = 1 - \frac{1}{n} \frac{m \left(1 + \frac{\Theta_G}{\pi m} + \frac{n\gamma_c}{m}\right)}{m_0 \left(1 + \frac{\Theta_G}{\pi m_0} + \frac{n\gamma_c}{m_0}\right)} \frac{1}{1 + \delta L/L'}, \quad (\text{A.6})$$

where we have introduced the notation  $L'$  for the effective length of the empty cavity comprising coated mirrors experienced during a scan, given by  $L_0 + 2L_{\tau,c}$ .

Solving this expression for  $n - 1$  gives

$$n - 1 = \frac{\frac{\Delta\nu}{\nu_0} \left(1 + \frac{\Theta_G}{\pi m_0} + \frac{\gamma_c}{m_0}\right) + \frac{\Delta m}{m_0} - \frac{\delta L}{L'} \left(1 - \frac{\Delta\nu}{\nu_0}\right) \left(1 + \frac{\Theta_G}{\pi m_0} + \frac{\gamma_c}{m_0}\right)}{\left(1 - \frac{\Delta\nu}{\nu_0}\right) \left(1 + \frac{\delta L}{L'}\right) \left(1 + \frac{\Theta_G}{\pi m_0} + \frac{\gamma_c}{m_0}\right) - \frac{\gamma_c}{m_0}}. \quad (\text{A.7})$$

where  $\Delta m$  is the shift of the mode number, given by  $m - m_0$ .

Noting that  $\frac{\delta L}{L'}$ , to first order, is linear with pressure (and thereby refractivity), it is convenient to introduce  $\epsilon'$  as the refractivity-normalized relative elongation of the FSR of the cavity due to the presence of the gas, defined as  $\frac{\delta L}{L'} \frac{1}{n-1}$ . By doing this, it can be noted that the last term in the numerator, which is proportional to  $\frac{\delta L}{L'}$ , has a linear dependence on refractivity, i.e. it is proportional to  $(n - 1)$ . Merging this term with the left hand side of the expression implies that it is possible to derive an expression for the refractivity that is given by

$$n - 1 = \frac{\frac{\Delta\nu}{\nu_0} \left(1 + \frac{\Theta_G}{\pi m_0} + \frac{\gamma_c}{m_0}\right) + \frac{\Delta m}{m_0}}{1 - \frac{\Delta\nu}{\nu_0} \left(1 + \frac{\Theta_G}{\pi m_0} + \frac{\gamma_c}{m_0}\right) + \frac{\Theta_G}{\pi m_0} + n\epsilon' \left(1 + \xi_c\right)}, \quad (\text{A.8})$$

where we have introduced the entity  $\xi_c$ , defined as  $\xi_c = \left(1 + \frac{\Theta_G}{\pi m_0} + \frac{\gamma_c}{m_0}\right) \left(1 - \frac{\Delta\nu}{\nu_0}\right) - 1$ . It is worth to note that Eq. (A.8) is, for the case with mirror coatings comprising a QWS of type H, mathematically identical to Eq. (A.1).

Since, for all practical purposes,  $\xi_c \approx \frac{\Theta_G}{\pi m_0} + \frac{\gamma_c}{m_0} - \frac{\Delta\nu}{\nu_0} \approx \left(\frac{\Theta_G}{\pi} + \gamma_c - 1\right) \frac{\Delta\nu}{\nu_0}$ , for standard types of cavities (with a length of some tens of cm and with mirrors with curvatures of 0.5 m, for which  $\frac{\Theta_G}{\pi} < 1$  and  $\frac{\Delta\nu}{\nu_0}$  maximally is in the mid  $10^{-6}$  range, and for a typical QWS for which  $0.5 < \gamma_c < 2$ ),  $n\epsilon'\xi_c$  is maximally in the  $10^{-9}$  to the low  $10^{-8}$  range, thus significantly smaller than unity. This implies that it is possible to neglect the influence of  $\xi_c$  in the expression for the refractivity above and write it as

$$n - 1 = \frac{\frac{\Delta\nu}{\nu_0} \left(1 + \frac{\Theta_G}{\pi m_0} + \frac{\gamma_c}{m_0}\right) + \frac{\Delta m}{m_0}}{1 - \frac{\Delta\nu}{\nu_0} \left(1 + \frac{\Theta_G}{\pi m_0} + \frac{\gamma_c}{m_0}\right) + \frac{\Theta_G}{\pi m_0} + n\epsilon'}. \quad (\text{A.9})$$

Moreover, as is shown by Eq. (SM-15) in the supplementary material to Zakrisson et al. [46], under the condition that  $\frac{\delta L}{L_0}$  can be written as  $\kappa P$ , and by using an equation of state and the Lorentz-Lorenz expression, it is possible to conclude that  $\epsilon'$  is an entity that has a very weak dependence on refractivity (for low pressures it acts as a constant and for higher it is weakly dependent on the refractivity) that can be written as  $\epsilon'_0 [1 + \xi_2(T)(n - 1)]$ , where  $\epsilon'_0$  is given by  $\kappa RT \frac{2}{3A_R}$  and  $\xi_2(T)$  is given by a combination of density and refractivity virial coefficients.

This implies that Eq. (A.9) can be expressed as

$$n - 1 = \frac{\frac{\Delta v}{\nu_0} \left(1 + \frac{\Theta_G}{\pi m_0} + \frac{\gamma_c}{m_0}\right) + \frac{\Delta m}{m_0}}{1 - \frac{\Delta v}{\nu_0} \left(1 + \frac{\Theta_G}{\pi m_0} + \frac{\gamma_c}{m_0}\right) + \frac{\Theta_G}{\pi m_0} + \varepsilon'_0 + (n - 1)\varepsilon'_0 [1 + \xi_2(T)]}. \quad (\text{A.10})$$

Although this is a recursive equation in  $n - 1$ , the recursivity is very weak for most gas species. For nitrogen, for example, it has been estimated by Zakrisson et al. that, at a temperature of 296.15 K,  $\xi_2(T)$  takes a value of -1.00(4) [46]. This implies that the  $\xi_2(T)$  term fully cancels the unity term in the non-linear  $(n - 1)\varepsilon'_0 [1 + \xi_2(T)]$  term in the denominator. For temperatures close to, but not exactly at, this,  $\xi_2(T)$  differs solely slightly from -1.00(4). Since, for the Invar-based cavity system used in this work [49], for which  $\varepsilon'_0$  has been found to be ca.  $2 \times 10^{-3}$ , and for the case when nitrogen is addressed,  $(n - 1)\varepsilon'_0$  is solely  $0.54 \times 10^{-6}$  at 100 kPa, this implies that the  $(n - 1)\varepsilon'_0 [1 + \xi_2(T)]$  term can, also for a range of temperatures around 296 K, and as long as pressures of nitrogen up to 100 kPa are addressed, safely be neglected. In this case, Eq. (A.10) can be written more succinctly as

$$n - 1 = \frac{\frac{\Delta v}{\nu_0} \left(1 + \frac{\Theta_G}{\pi m_0} + \frac{\gamma_c}{m_0}\right) + \frac{\Delta m}{m_0}}{1 - \frac{\Delta v}{\nu_0} \left(1 + \frac{\Theta_G}{\pi m_0} + \frac{\gamma_c}{m_0}\right) + \frac{\Theta_G}{\pi m_0} + \varepsilon'_0}. \quad (\text{A.11})$$

Since  $\varepsilon'_0$  is a constant (index of refraction independent) entity, this implies that, by use of the  $\varepsilon'$ -concept,  $n - 1$  can, when nitrogen is addressed, be expressed in terms of a recursive-free expression. This facilitates significantly the assessment of refractivity from measurement data.

It is worth to note that the step that brings Eq. (A.10) into Eq. (A.11) is not appropriate when He is addressed, since  $\xi_2(T)$  for He takes a value of -15.208(1) (at 296.15 K). In this case, Eq. (A.10) needs to be used instead of Eq. (A.11).

## A.2. For working ranges not centred on the mirror center frequency

As is shown in Silander et al. [38], when the mirrors are not used around their mirror center frequency, the reflection phase should preferably be expressed in terms of a Taylor series expanded around the center frequency of the working range, denoted  $\nu_s$ . In this case, the cavity mode frequencies and refractivity given above, i.e. the Eqs. (A.3), (A.4), (A.9) - (A.11), can be used as long as the  $L_{\tau,c}$  and  $\gamma_c$  are replaced by  $L_{\tau,s}$  and  $\gamma'_s$ , which are given by  $\frac{c\tau_s(n)}{2n}$  and  $\gamma'_s \left(1 + \frac{1+\chi_0}{1+\chi_1} \frac{\Delta\nu_{cs}}{\nu_s}\right)$ , where, in turn,  $\tau_s(n)$  is the GD at the center frequency of the light,  $\gamma_s$  is given by  $\frac{2\tau_s(n)\nu_s}{n}$ ,  $\Delta\nu_{cs}$  represents the frequency difference between the mirror center frequency and the center of the working range, i.e.  $\nu_c - \nu_s$ , while  $\chi_0$  and  $\chi_1$  represent the relative contributions of the group delay dispersion (GDD) and the next higher order dispersion term in the Taylor expansion of the phase shift of the reflection of light at the front facets of the mirrors respectively, given by Table 1 in the Supplementary material in Ref. [38].

## A.3. Comparison with previously used nomenclature

Although Eq. (A.11) is fully adequate in virtually all situations when nitrogen is addressed (irrespective of whether any modulated methodology is used or not), it is alternatively possible to rewrite it in a form that resembles the expressions previously given in the literature to express refractivity when the influences of the mirror penetration depth and the Gouy phase are neglected, as, for example, was done in the Refs. [36, 26, 27].<sup>67</sup> By defining an "effective" empty cavity frequency,  $\nu'_0$ , given by  $\nu_0 / \left(1 + \frac{\Theta_G}{\pi m_0} + \frac{\gamma'_s}{m_0}\right)$ , it is possible to write Eq. (A.11) for working ranges not centred on the mirror center frequency in a more succinct form, viz. as

<sup>67</sup>Such an expression has often been written as

$$n - 1 = \frac{\overline{\Delta\nu} + \overline{\Delta q}}{1 - \overline{\Delta\nu} + \varepsilon}, \quad (\text{A.12})$$

$$n - 1 = \frac{\overline{\Delta\nu} + \overline{\Delta m}}{1 - \overline{\Delta\nu} + \frac{\Theta_G}{\pi m_0} + \varepsilon'_0}, \quad (\text{A.13})$$

where  $\overline{\Delta\nu}$  now is defined as  $\overline{\Delta\nu} = \Delta\nu/\nu'_0$  and  $\overline{\Delta m}$  is defined as  $\frac{\Delta m}{m_0}$ .

A comparison between the Eqs. (A.12) and (A.13) shows that the presence of mirror penetration depth and Gouy phase can be seen as a shift of the empty cavity laser frequency (transforming  $\nu_0$  to  $\nu'_0$ ) and that the Gouy phase additionally provides a contribution in the denominator, similar to the distortion. In addition, it also shows that the relevant quantum number is  $m$  (as defined above) and not  $q$  (as used in the simplified expressions given in [36, 26, 27]), where the latter one is related to the former by  $q = m + \frac{\Theta_G}{\pi} + n\gamma'_s$ . This implies that also when the influences of the penetration depth and the Gouy phase are taken into account, it is possible to make use of the simplified expressions of the refractivity for which efficient evaluation procedures have been worked out when the GAMOR methodology is used, i.e. the Eq. (A.12), with a minimum of alterations (by shifting the empty cavity laser frequency from  $\nu_0$  to  $\nu'_0$  and by interpreting  $\varepsilon$  as  $\frac{\Theta_G}{\pi m_0} + \varepsilon'_0$  where  $\varepsilon'_0$  is defined as  $\frac{\delta L}{L'} \frac{1}{n-1}$ ).

---

where  $\overline{\Delta\nu}$  is defined as  $\overline{\Delta\nu} = \Delta\nu/\nu_0$ ,  $\overline{\Delta q}$  is a shorthand notation for  $\Delta q/q_0$ , where  $\Delta q$  is the number of mode jumps the measurement cavity laser has performed as a consequence of filling of the cavity while  $q_0$  is the number of the mode addressed in the empty measurement cavity where the two  $q$  and  $q_0$  mode numbers are defined through the relations  $\nu = \frac{qc}{2n(L_0 + \delta L)}$  and  $\nu_0 = \frac{q_0 c}{2L_0}$ , respectively, and where  $\varepsilon$  is defined as  $\frac{\delta L}{L_0} \frac{1}{n-1}$ .

## B. Nomenclature and definitions of drifts

To assess the ability of GAMOR to reduce the influence of specific types of drifts, it has been found convenient to model the drift of the mode addressed in cavity  $i$ , i.e.  $\nu_i^{(0)}(t)$ , in terms of a Taylor series centered around the time instants at which a given refractometry assessment is made (i.e. at  $t_g$ ) as

$$\begin{aligned} \nu_i^{(0)}(t) = & \nu_i^{(0)}(t_g) + \left( \frac{\partial \nu_i^{(0)}}{\partial t} \right)_{t_g} (t - t_g) + \\ & \frac{1}{2} \left( \frac{\partial^2 \nu_i^{(0)}}{\partial t^2} \right)_{t_g} (t - t_g)^2 + \dots, \end{aligned} \quad (\text{B.1})$$

where  $(\partial \nu_i^{(0)} / \partial t)_{t_g}$  and  $(\partial^2 \nu_i^{(0)} / \partial t^2)_{t_g}$  represent the amount of linear and first order non-linear drifts of the mode addressed, respectively.

Since the beat frequency is given by the difference in frequency of the two cavity modes addressed, for the case with empty cavities by  $\nu_r^{(0)}(t) - \nu_m^{(0)}(t)$ , this implies that there will be drifts also of the empty measurement cavity beat frequency,  $f^{(0)}(t)$ . Following the nomenclature above, this can be written as

$$\begin{aligned} f^{(0)}(t) = & f^{(0)}(t_g) + \left( \frac{\partial f^{(0)}}{\partial t} \right)_{t_g} (t - t_g) + \\ & \frac{1}{2} \left( \frac{\partial^2 f^{(0)}}{\partial t^2} \right)_{t_g} (t - t_g)^2 + \dots, \end{aligned} \quad (\text{B.2})$$

where

$$\begin{aligned} f^{(0)}(t_g) = & \nu_r^{(0)}(t_g) - \nu_m^{(0)}(t_g) \\ \left( \frac{\partial f^{(0)}}{\partial t} \right)_{t_g} = & \left( \frac{\partial \nu_r^{(0)}}{\partial t} \right)_{t_g} - \left( \frac{\partial \nu_m^{(0)}}{\partial t} \right)_{t_g} \\ \left( \frac{\partial^2 f^{(0)}}{\partial t^2} \right)_{t_g} = & \left( \frac{\partial^2 \nu_r^{(0)}}{\partial t^2} \right)_{t_g} - \left( \frac{\partial^2 \nu_m^{(0)}}{\partial t^2} \right)_{t_g}. \end{aligned} \quad (\text{B.3})$$